UNIVERSITÀ DEGLI STUDI DI PADOVA

Sede Amministrativa: Università degli Studi di Padova

Dipartimento di Tecnica e Gestione dei sistemi industriali (DTG)

CORSO DI DOTTORATO DI RICERCA IN:
Ingegneria Meccatronica e dell'Innovazione Meccanica del Prodotto
CURRICOLO: Meccanica dei Materiali
CICLO XXXV

DEVELOPMENT AND OPTIMIZATION OF POROUS STRUCTURES FOR EFFICIENT THERMAL ENERGY STORAGE USING PHASE CHANGE MATERIALS (PCMs) FOR REFRIGERATED TRANSPORT APPLICATIONS

Coordinatrice: Ch.ma Prof.ssa Daria Battini, *Università degli Studi di Padova* (UNIPD)
Supervisore: Ch.mo Prof. Simone Mancin, *Università degli Studi di Padova* (UNIPD)
Co-Supervisore: Ch.mo Prof. Kamel Hooman, *Delft University of Technology* (TUDelft)

Dottorando: Michele Calati

"The true laboratory is the mind,
where, behind illusions,
we uncover the laws of truth."

Cit. J. C. Bose

Index

List of Figures

List of Tables

Nomenclature

Abbreviations

ATP	Accord du Transport Perissable
CFD	Computational Fluid Dynamics
COP	Coefficient of Performance
EC	European Commission
EU	European Union
FAO	Food and Agriculture Organization
FEM	Finite Element Method
GHG	Greenhouse Gas
GWP	Global Warming Potential
HR	Heat of Respiration
HTF	Heat Transfer Fluid
HVAC	Heating, Ventilation and Air Conditioning
ICT	Information and Communication Technologies
IMU	Ice-Making Unit
IN	Isotherme Normal
IR	Isotherme Renforcè
ISO	International Organization for Standardization
LCA	Life Cycle Assessment
LCCP	Life Cycle Climate Performance
LNG	Liquefied Natural Gas
LTES	Latent Thermal Energy Storage
MCU	Mobile air-Cooling Unit
PCCSU	Phase Change Cold Storage Unit
PCM	Phase Change Material
PCTSU	Phase Change Thermal Storage Unit
PET	Poly-Ethylene Terephthalate
PRESTO	PREssure STaggering Option
PU	Poly-Urethane
RH	Relative Humidity
RMF	Reflective Multi-Foil
RT	Rubitherm ®
SAP	Super Absorbent Polymer
SDG	Sustainable Development Goal
SIMPLE	Semi Implicit Method for Pressure Linked Equation
TES	Thermal Energy Storage
TEWI	Total Equivalent Warming Impact
UN	United Nations
UNI	Ente nazionale italiano di unificazione
VIP	Vacuum Insulation Panel

Parameters

a	absorptance	[-]
B	constant	[-]
c_p	Heat Capacity	[J kg^{-1} K^{-1}]
C_v	constant	[-]
$D_{i,m}$	Mass diffusivity of species i-th	[$m^2 \cdot s^{-1}$]
D_T	Thermal diffusion coefficient	[$m^2 \cdot s^{-1}$]
E	variable	[min]
E	energy per mass density	[J kg^{-1}]
F	external force	[N]
f	constant	[-]
G	solar irradiance	[W m^{-2}]
G	Generation of turbulent kinetic energy	[$kg \cdot m^{-1} \cdot s^{-3}$]
g	gravitational acceleration	[m s^{-2}]
g	constant	[-]
h	enthalpy per mass density	[J kg^{-1}]
J_i	Diffusion flux of species i-th	[$mol \cdot m^{-2} \cdot s^{-1}$]
k	thermal conductivity	[W $m^{-1}K^{-1}$]
k	Turbulent kinetic energy	[$m^2 \cdot s^{-2}$]
L	Latent Heat	[J kg^{-1}]
M	meridiane	[-]
n	day of the year	[-]
p	static pressure	[Pa]
S	source term	[W m^{-3}]
S_{ct}	Turbulent Schimdt number	[-]
T	temperature	[K]
t	Time	[s]
v	velocity	[m s^{-1}]
u	velocity	[m s^{-1}]
Y_i	Local mass fraction of species i-th	[-]

Greek Symbols

α	heat transfer coefficient	[W m^{-2} K^{-1}]
α	altitude	[°]
α	Inverse effective Prandlt number	[-]
β	tilt angle	[°]
β	constant	[-]
γ	azimuth angle	[°]
δ	solar declination	[°]
ϵ	thermal expansion coefficient	[K^{-1}]
ε	Rate of energy dissipation	[$m^2 \cdot s^{-3}$]
θ	angle of incidence	[°]

μ	dynamic viscosity	[Pa·s]
μ_t	Turbulent viscosity	[kg·m^{-1}·s^{-1}]
ρ	density	[kg m^{-3}]
τ	shear stress tensor	[Pa m^{-3}]
φ	liquid fraction	[-]
ϕ	latitude	[°]
ω	solar angle	[°]

Abstract

The aim of this research work is to develop and investigate an innovative solution for the cold storage to be implemented in the refrigerated transportation sector.

In particular, the first section offers a general overview of the different PCMs involved in cold latent thermal storages from sub-zero to higher temperatures, a short brief of the refrigerated transport sector to date, and a detailed analysis of PCM integration in refrigerated vehicles and portable boxes. From this introductive section, the main future challenges for the refrigerated transport sector and possible research paths to fill the existing gaps in the literature and facilitate the deployment of LTES in refrigerated transport systems can be identified.

The second section involves the numerical and experimental results collected during the research period. In particular, the first part shows how the numerical model for the proposed innovative LTES system was developed and validated. Then, the results obtained when simulating a daily operation route by considering several different parameters are shown. Moreover, the final part investigates the possibility of integrating a refrigerating unit based on a low-GWP refrigerant (R290, propane), by underlining the potentialities and criticalities for a further employment.

Finally, it can be concluded that a promising cost effective and environmentally friendly solution for the refrigerated transport sector can be effectively found. The numerical models developed and proposed in this work thesis can be further adopted to study and develop an integrated LTES system by optimizing the charging and discharging phases and evaluating the thermal and risk performances.

1. Introduction

It has been estimated that more than 820 million people are malnourished worldwide [1]. In September 2015, the United Nations drew up the seventeen 2030 Sustainable Development Goals (SDGs) [2].

Figure 1.1 Seventeen 2030 sustainable development goals.

As shown in Fig. 1.1, among the different goals, the second position is the “Zero Hunger” UN program. It can be easily assumed that to reach Goal#2, food losses and food wastages should be prevented. The Food and Agriculture Organization (FAO) [3] evaluated the food wastages and losses in one-third of the total amount of food produced annually, around 1.3 billion ton. In particular, 630 million ton are lost while 670 are wasted [4]. It must be stressed that those numbers are strongly dependent on the countries: for the developed countries a greater contribution is given by the food wastage, while poor or developing countries the food loss component is the prevalent figure. As reported in [4] the food loss is related to a lack of desirable conditions during the first stages of the cold chain, from the producer to the retailer. On the contrary, the food wastage is defined as the edible food being discarded and rejected at the seller and/or customer level.

The cold chain develops from perishable harvested products to the final consumer. It consists of a series of subsequent activities which ensure that fresh foodstuffs are maintained at an adequate temperature throughout the supply chain [2]. The main stages that can be found along the cold chain can be resumed in food harvesting, preconditioning, transport, bulk storage,

retail, domestic, and food service [4]. The food losses and wastage add up to $940 billion financial loss per year [5]. Besides, they contribute to the emissions of 4.4 Gton of $CO_{2,eq}$ per year [4]. As stated by Evans et al. [6], if considering both direct and indirect effects, 2.5% of global greenhouse gas (GHG) emissions are due to the cold chain imperfections. The cold chain, in facts, usually adopts refrigeration systems based on high-GWP (Global Warming Potential) refrigerants. It also exploits grid electricity from fossil-fuels or off-grid generation based on diesel equipment [4]. More importantly, the entire refrigeration sector accounts for about 30% of the global energy consumption [7]. Moreover, the world's population is continuously increasing [4] as is the need for welfare. Hence, the European Commission (EC) has been pushing the EU-27 countries in developing solutions aiming at 40% reduction in GHG emissions by 2030 [8]. As reported by Jouhara et al. [9], by adopting energy storage technologies, the goals proposed in the EU's "20-20-20" program and in the EC's "Energy Roadmap 2050" can be achieved. In this context, the development and management of a sustainable, effective, and efficient cold chain is becoming more and more crucial. Therefore, with the scope of reducing energy consumption and ensuring an adequate temperature level for the products, among the different Thermal Energy Storage (TES) available, researchers have been considering the introduction of LTES systems to replace the traditional designs along the cold chain. The LTES system takes advantage of the high energy density which can be stored through the phase change process from liquid to solid (or vice versa) at an almost constant temperature [10].

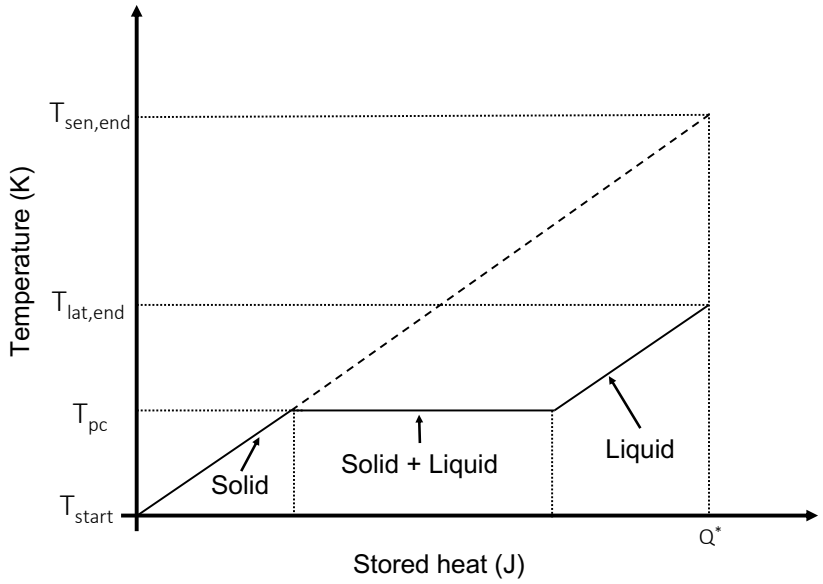

Figure 1.2 Comparison between sensible and latent thermal energy storage systems during melting.

Fig. 1.2 demonstrates the great advantage of the use of LTES systems based on PCMs compared with those using a sensible one. The two systems start at the same temperature, but, when the latent system (continuous line) reaches the phase change threshold (T_{pc}) the melting process begins, and the heat storage occurs at an almost constant temperature. Following the completion of the phase change process, liquid PCM stores sensible heat as Fig. 1.2 depicts. To store the same amount of heat, Q*, the sensible system (inclined dotted line) ends up at a final temperature $T_{sen,end}$ which is noticeably higher than that for a PCM ($T_{lat,end}$). It is clear that a lower system temperature can extend the longevity of the equipment since it can potentially be subjected to lower thermal stresses. This, in turn, lowers the risk of damage and minimizes maintenance costs while improving the system safety and reliability.

The LTESs have already found application in many different contexts as reviewed by Mobedi et al. [10]. These applications range from high temperature industries (electricity generation and waste heat recovery, [11]), medium temperature applications, from thermal management of electronics and electric vehicle batteries to buildings ([12], [13], [14]and, finally, low and very-low temperature applications such as HVAC systems ([15], [16], Botcher in [10]) or applications for the cold chain. An ideal PCM should have a suitable phase change temperature along with high thermal conductivity and latent heat. It should have low volume expansion and large density in order to limit the system size. The PCM should also be compatible with other materials with no toxicity and flammability [17].

Along the cold chain, the LTESs involving PCMs have already been studied for implementation in commercial and household refrigerating appliances, display cabinets, cold rooms. LTES systems have also started to attract attention for the refrigerated transport sector. Yusufoglu et al. [18] incorporated different PCMs near the evaporator of two types of refrigerators. They obtained improvement in evaporating and condensing temperatures of 2-4 °C for all the PCM types. Optimizing the on/off compressor times, the LTES prototypes reached energy consumption savings of around 9%. The authors also conducted economic and environmental analyses, stating that the use of PCMs in refrigerators is financially profitable for the users while helping the environment. Ezan et al. [19] placed a PCM (water) slab of different thicknesses (from 2 to 10 mm) on the rear side of a roll-bond evaporator of a vertical beverage cooler. They affirmed that the cooling performance was enhanced in presence of PCM prolonging the compressor "off" duration. Furthermore, during the off interval, the PCM limited the sudden temperature increase thereby maintaining the air inside the refrigerated space at a tolerable range. Pirvaram et al. [20] developed a household refrigerator inserting eutectic PCMs in proximity of a wire-and-tube condenser. The PCM led to a condenser

temperature reduction which resulted in the COP enhancement. The cascade arrangement of two PCMs with different melting temperature (29 and 32 °C) permitted the compressor work-on-time to be reduced to 27.6% of total work time (instead of 32.7% for the traditional refrigerator). The authors reported an energy consumption saving of 13%. Gin et al. [21] evaluated the effects of door openings, defrosting cycle and loss of electrical power in a vertical freezer. 2.2 kg of PCM (aqueous ammonium chloride, -15.7 °C) were distributed on the internal cabinet walls, inside aluminum plates. In terms of energy consumption, no differences (without or with PCM cases) were found under steady conditions. However, considering door opening effect, the new solution spared 7-8% of the total energy consumption. When analyzing the occurrence of a loss of power, the great benefit of the developed LTES can be appreciated. The new freezer worked for 11 h until the maximum allowable temperature (-3 °C) was reached whereas the conventional design could only work for 4.4 h before reaching the limit. That is, the new configuration outperformed the traditional one as it maintained operable conditions for a longer period; 2.5 times longer compared with the traditional vertical freezer. Liu et al. [22] studied the performance of an air-cooled household refrigerator with cold PCMs (0.41 °C melting temperature for cold chamber with -18.98 °C for freezing chamber). They investigated different control modes to report that under the original control mode, the solution with PCM saved 18.6% of energy compared with the reference case. Besides, a 13.6% reduction in the compressor on-time ratio was observed. On top of energy savings, the developed LTES prototype led to better food quality. Orò et al. [23] investigated the thermal performance of a commercial freezer by inserting stainless steel panels encapsulating PCM (-18 °C melting temperature) on the shelves. It was reported that in case of power failure (3 h), the LTES assured a 4-6 °C lower temperature inside the cabinet compared with the traditional design. The PCM prolonged the time the frozen products were maintained at tolerable temperature levels. An 8.6 m^2 cold room based on PCM modules was designed and built by Viking Cold Solutions company [24] for freezing. The TES plates were mounted on top of the stored cargo in the direct path of the airflow generated by the evaporator fans. The LTES system led to an energy consumption reduction of 35% compared to the original setting and the energy consumed during the peak heat load interval reduced by 43%. A warehouse storage for ice cream was numerically studied by Schalbart et al. [25]. They investigated different PCM locations (at the walls, ceiling, close to evaporators, close to products) and reported temperature fluctuations of about ±0.01 °C with PCM in the storage tank against ±1 °C in the situation without PCM over the same period. With the PCM at the ceiling, a difference of ±0.76 °C was

reported. The lower temperature differences, the lower the crystal size, with a consequent improvement of the product quality.

In view of the above, given the promising results with the implementation of LTES in refrigerating appliances, researchers have considered introducing them in the refrigerated transport sector. Among the diverse stages along the cold chain, the refrigerated transportation plays an important role as it encompasses initial phases, just after the food harvesting, up to the final ones when it reaches the market. As reported in [26], the retail value of the transported good is about $1200 billion. Nevertheless, it has been forecasted that a growth of 2.5% road cargo transport is expected by 2030 [27]. Thus, as affirmed by De Micheaux et al. [28] the delivery of perishable freight can be considered as the most energy-consuming type of road food transportation. Currently, the refrigerated transportation is regulated by the ATP (*Accord du Transport Perissable*) agreement [29] which defines the standards for refrigerated vehicles. This sector involves 1.2 million refrigerated containers (so called "reefers") and 4 million refrigerated road vehicles [2] of different sizes. The refrigerated road fleet is for the most part equipped with diesel engines which run inefficient mechanical vapor compression cycles for refrigeration [26]: their coefficient of performance (COP) usually ranges from 0.5 to 1.5 [30]. According to Li et al. [31], diesel engines consume 1 to 5 liters per hour and that only a quarter of the fuel consumed results into effective work due to engines' low efficiency. It must be stressed that considering the entire amount of energy consumed during the distribution, 40% of it can be ascribed to the food refrigeration [27].

Hence, it is essential for the refrigerated product transportation to move towards solutions which can contemporarily ensure the quality, freshness, and safety of food while meeting the regulations set for the reduction of polluting emissions. In view of the above, the implementation of LTES in the refrigerated transport sector has gained more and more attention by the scientific community.

The aim of this research work is to develop and investigate an innovative solution for the cold storage to be implemented in the refrigerated transportation sector.

In particular, the first section offers a general overview of the different PCMs involved in cold latent thermal storages from sub-zero to higher temperatures, a short brief of the refrigerated transport sector to date, and a detailed analysis of PCM integration in refrigerated vehicles and portable boxes. From this introductive section, the main future challenges for the refrigerated transport sector and possible research paths to fill the existing gaps in the literature and facilitate the deployment of LTES in refrigerated transport systems can be identified.

The second section involves the numerical and experimental results collected during the research period. In particular, the first part shows how the numerical model for the proposed innovative LTES system was developed and validated. Then, the results obtained when simulating a daily operation route by considering several different parameters are shown. Moreover, the final part investigates the possibility of integrating a refrigerating unit based on a low-GWP refrigerant (R290, propane), by underlining the potentialities and criticalities for a further employment.

2. Thermal storage based on Phase Change Materials for refrigerated transport and distribution applications along the cold chain

2.1 Materials for LTES

The PCM is the main constituent of a LTES system and, as already briefly stated in Section#1, the great benefit of employing a LTES system derives from the exploitation of the latent heat during the liquid-solid phase change transition (and, reverse) of the PCM. Nevertheless, the Energy Storage family also includes [9]: electrochemical and battery, pumped hydro, magnetic, chemical and hydrogen, flywheel, thermochemical, compressed air, liquefied air, and thermal energy storages. Among the thermal ones, sensible and latent storage systems are set as subcategories. Considering LTES, according to their chemical composition, three macro-PCM-categories can be identified:

- *Organic*: organic compounds, paraffins, and fatty acids,
- *Inorganic*: salt hydrates and metallics,
- *Eutectic*: obtained by creating a new PCM starting from at least two different materials. Depending on the nature of the pure constituents, they can be classified as organic-organics, organic-inorganics, or inorganic-inorganics.

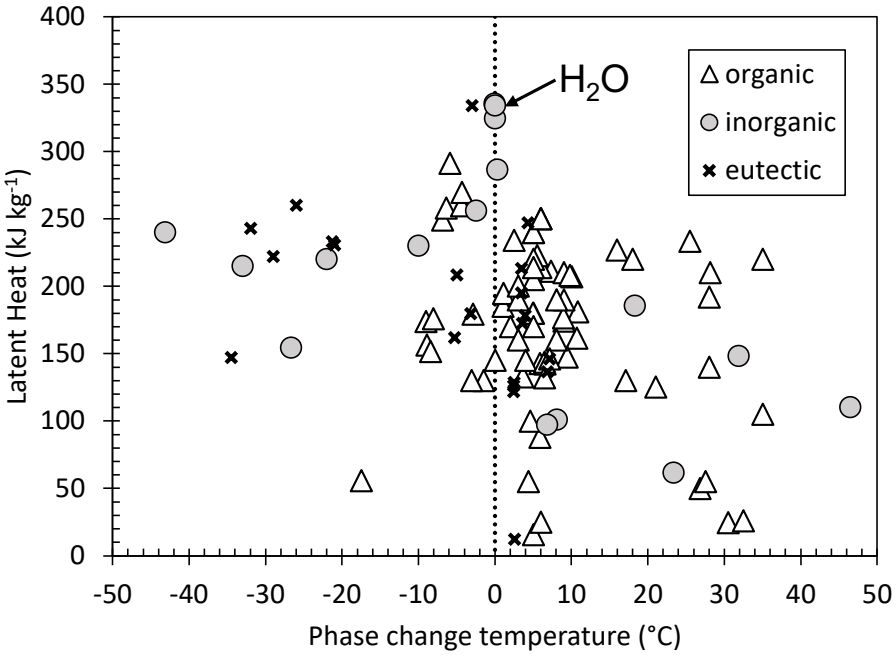

Figure 2.1 Latent heat as function of the melting temperature of the PCMs reported in Table 1.

In Fig. 2.1, the latent heat at a determined phase change temperature for all the PCMs listed in Table 2.1 is plotted. Table 2.1 was generated by considering the following search algorithm: {[(phase change material) OR (latent cold storage)] AND (cold chain)} + {[(phase change material) OR (latent cold storage)] AND [(refrigerated vehicle) OR (refrigerated truck) OR (refrigerated transport)]} which resulted in about a hundred works.

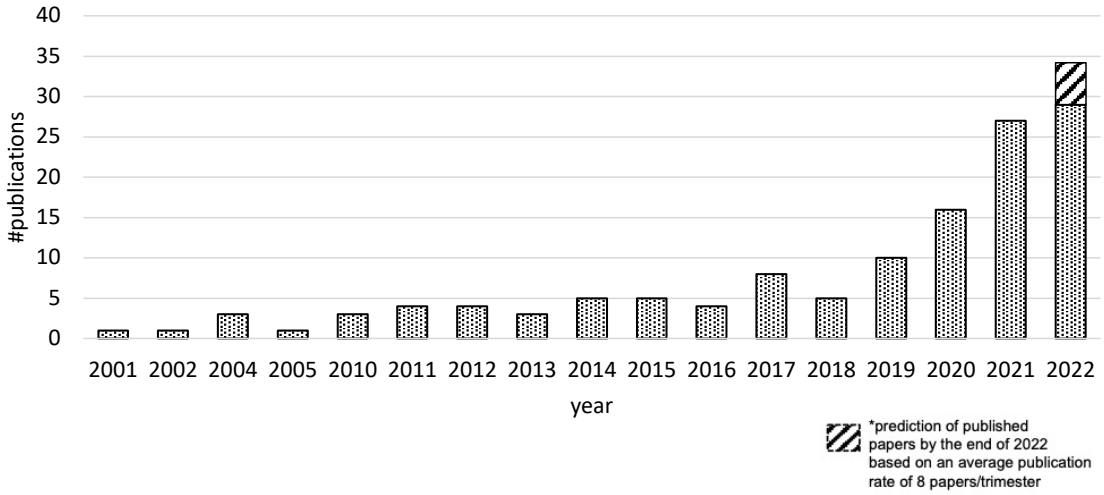

Figure 2.2 number of publications per year (updated to Nov 15th, 2022).

As depicted in Fig. 2.2, where the annual distribution of published papers from 2000 to 2022 is shown, this topic has gained greater attention in the latest years. In fact, most of the works have been published over the last six years. Among the papers resulted from the search, the ones that clearly declared the thermo-physical properties of the PCM have been listed in Table 1. To arrange Table 1, the following assumptions were made:

- When there was negligeable difference between melting and solidification temperatures, an average value was reported.
- When only melting or solidification temperature was reported in the work, only the relative column was filled.
- When there was negligeable difference between melting and freezing latent heat values, a unique representative average value was reported.
- When it was not explicitly declared, the thermal conductivity was supposed to be the solid phase and listed in the relative column.

Table 2.1 PCMs main thermo-physical properties for the cold chain

Authors	PCM name	Typology	Supplier	Melting Temperature, **Tm** (°C)	Freezing Temperature, **Ts** (°C)	Latent heat of phase change, **L** (J kg^{-1})	Thermal conductivity, **k** (W m^{-1} K^{-1})	
							solid	**liquid**
[32]	aqueous-glycol 50%	inorganic		-43.16	-48.16	240000	2.25	0.35
[33]	organic compound	organic		-6.9		249000		
[34]	25PCM (microencapsulated PCM, MPCM6D) in a water-based pulp solution (5 %w/v)	organic	Microteklabs, USA	4.34	-1.66	55000	0.0913	0.0913
	50PCM (microencapsulated PCM, MPCM6D) in a water-based pulp solution (5 %w/v)	organic	Microteklabs, USA	5.84	-1.66	88000	0.0819	0.0819
	100PCM (microencapsulated PCM, MPCM6D) in distilled water	organic	Microteklabs, USA	5.84	-2.66	142700		
[35]	RT-2	organic	Rubitherm, DE	-1.5	-1.5	130000	0.25	0.2
	RT-4	organic	Rubitherm, DE	-3.1	-3.1	130000	0.25	0.2
	water-glycol 10%	eutectic		-3	-3	334000	2.18	0.58
[36]	erythritol tetra myristate ester	organic		10.82	4.76	181000 (m); 174450 (f)	0.16	0.16
	erythritol tetra laurate ester	organic		-9.03	-12.86	173840 (m); 170760 (f)	0.14	0.14
	erythritol tetra myristate ester+EG (wt5%)	organic		10.67	4.64	161390 (m); 150520 (f)	0.18	0.18
	erythritol tetra laurate ester+EG (wt5%)	organic		-8.94	-12.14	156430 (m); 145490 (f)	0.2	0.2
[37]	RT5	organic	Rubitherm, DE	6.52	5.26	142230		
[38]	n-tetradecane	organic	Aladdin, CHN	7.3	4.2	211000		
[39]	n-hexadecane	organic		15.92	13.37	226800		
	n-octadecane	organic		25.48	24.59	233430		
[40]	RT5HC	organic	Rubitherm, DE	6	5	250000	0.2	0.2
[41]	paraffin	organic		6	2	214000		
				9	6	174000		
				9	7	190000		
				9	8	210000		

				10	9.9	207000		
[42]	Microencapsulated PCM (MPCM) in water, slurry	-		28	27	167000	0.31	0.14
[43]	octadecane	organic	Sigma-Aldrich, USA	28.1		210000		
[44]	NaCl-Na2SO4 ternary salt in water	eutectic		-21.5		180000		
	NaCl-KCl ternary salt in water	eutectic		-23		260000		
	NaCl-NaNO3 ternary salt in water	eutectic		-26.5		100000		
[45]	octanoic acid lauric acid + expanded graphite 7wt% (OA-LA/EG)	organic		3.6		132800	1.275	
[46]	dodecane	organic		-8.09		175900	0.14	0.14
	dodecane/EG 16wt%			-8.46		151700	2.2745	2.2745
[47]	octaonic acid myristic acid (MA)	eutectic		7.13		146100	0.2971	0.2971
	octaonic acid myristic acid + expanded graphite 7wt% (OA-MA/EG)	eutectic		6.8		136300	0.9975	0.9975
[48]	OM11, fatty acid based ester	organic	M/s Pluss Advance Tecnhologies, Ltd., India	9.4		147490		
[49]	23wt% MgCl2-H20 eutectic salt solution + 1wt% MWCNTs	eutectic		-34.54		146960	0.5344	
[50]	eutectic salt	eutectic		-5.02		208300	0.67	
	eutectic salt + modified expanded graphite (MEG)	eutectic		-5.3		161800	8.9	
[51]	decanoic-caprylic acid (DA-CA)	eutectic	Aladdin, CHN	2.42		126300	0.271	
	decanoic-caprylic acid (DA-CA) + MWCNT-OH	eutectic		2.45		128700	0.338	
	decanoic-caprylic acid (DA-CA) + Fe2O3	eutectic		2.51		122300	0.371	
	decanoic-caprylic acid (DA-CA) + Cu	eutectic		2.43		121800	0.321	
[52]	decyl alcohol myristyl alcohol (DA-MA) eutectic mixture 87:13	eutectic		3.9		178200	0.277	
	(DA-MA) eutectic mixture + expanded grapihte (DA-MA/EG) 14:1	eutectic		3.55		172300	0.942	
[53]	n-dodecane	organic	Aladdin, CHN	-6.41		258120		
	n-tridecane	organic	Aladdin, CHN	-2.92; -17.52		179390 (m1); 55760 (m2)		
	n-tetradecane	organic	Aladdin, CHN	8.92		276510		
	n-dodecane micro capsules			-8.96		110530		
	n-tridecane micro capsules			-4.9; -18.19		63670 (m1); 30390 (m2)		
	n-tetradecane micro capsules			6.65		116190		

[54]	Water sodium solution polymer (SP) 0.5wt% solution	inorganic		0		324350		
[55]	RT5HC	organic	Rubitherm, DE	6	5	250000	0.2	0.2
[56]	decyl alcohol (DA)	organic	Sinopharm Chemical Reagent Co., Ltd., CHN	5	2.6	205000	0.162	
	DA + expanded graphite (EG)			1	1.7	185000	1.854	
	DA/MgO/EG			1.1	2.4	194600	1.873	
[57]	SSD	inorganic		31.89	12.71	148200 (m); 55440 (f)		
	SBCKN	inorganic		8.07	4.2	101100 (m); 54590 (f)	0.25	
	SBCKN/EG 5wt%			5.92	5.67	99350 (m); 66390 (f)	0.43	
[58]	paraffin	organic		28	26.6	192000		
	MicroPCMs (paraffin) in PU-based shell. Paraffin 68wt%	organic		27.1	25.6	130000		
	MicroPCMs (paraffin) in PU-based shell. Paraffin 25wt%	organic		26.8	25.7	50000		
[59]	PEG400	organic	Sigma-Aldrich Inc.	4.6	-15.3	100000		
	PEG600	organic	Merck Chemical Ltd.	21	7.7	125000		
	HNTPEG400 (Hallosyte Nano Tubes)			1.3	-27.8	22000		
	HNTPEG600 (Hallosyte Nano Tubes			13.9	-8.3	24000		
[60]	5%D-glucose-NaCl solution	organic		-4.39		259900	0.5267	
	5%glycine-NaCl solution	organic		-5.94		291150	0.584	
	5%D-sorbitol-NaCl solution *only 5% concentrations are reported here. The authors also investigated 7.5, 10, 12.5, 15 % for each PCM typology)	organic		-4.33		269700	0.5435	
[61]	1-dodecanol-tetradecane binary eutectic mixture 26.3:73.7 (BEM)	eutectic		3.43	4.17-2.58	213000		
	BEM/EG 7%wt			3.45	7.02-2.14	195000	3.206	
[62]	decyl alcohol (DA) – lauryl alcohol (LA)	eutectic		-3.2		179700	0.2869	
	DA-LA/MWCNT-OH/SDBS 0.15wt%			-3.1		178400	0.3323	
[63]	Sodium sulfate decahydrate (SSD)	inorganic		23.36	12.56	61630 (m); 46600 (f)		
	SSD-BCKN3 (borax 3wt%, CMC 3wt%, KCl 5wt%, NH4Cl 20wt%)	inorganic		6.8	6.1	97050 (m); 69000 (f)	0.264	
	SSD + (borax, CMC, KCl, NH4Cl) in diff wt%							
[64]	OP5E (paraffin, PA)	organic	Ruhr Energy Technology, CHN	5-6		240000	0.2	

	PA/MWCNTs/SDBS (1wt% MWCNT, 2:1 MWCNT:SDBS)			5.5		222700	0.3723	
[65]	n-tetradecane (TD) PNCT-HXL-TD (foam stable composite PCM, 35wt%) PNCSi-HXL-TD (foam stable composite PCM, 40wt%)	organic		9.78 7.71 7.52	1.96 0.4 1	208000 73000 82500		
[66]	LTPCM water core and ethylcellulose (EC) (Low Temperature PCM Microcapsules)	inorganic		0.3; 7.6	3.5	286510	0.4655	
[67]	RT5	organic	Rubitherm, DE	5	7	156000	0.2	0.2
[68]	water	inorganic						
[26]	inorganic salt-water solution	inorganic		-26.7	-30.6	154400		
[69]	C-18	inorganic	Climsel	-18		306000	0.6	
	E-21	inorganic	Cristopia	-21		233000		
[70]	Energain	organic	DuPont					
[71]	inorganic salt-water solution	inorganic		-26.7	-30.6	154400		
[72]	Microencapsulated n-tetradecane in PU foam, 13.5wt%	organic	Microteklabs, USA	6		24860	0.03279	
[73]	E-26	eutectic	PCM products Ltd.	-26		260000	0.58	
[74]	RT27	organic	Rubitherm, DE	27.5		55000	0.2	
	RT28HC	organic	Rubitherm, DE	28		140000	0.2	
	RT31	organic	Rubitherm, DE	30.5		24350	0.2	
	RT35	organic	Rubitherm, DE	32.5		26000	0.2	
	RT35HC	organic	Rubitherm, DE	35		105000	0.2	
	RT42	organic	Rubitherm, DE	41		30000	0.2	
	RT44HC	organic	Rubitherm, DE	43		94500	0.2	
	RT47	organic	Rubitherm, DE	45		20000	0.2	
	C48	inorganic	Climsel	46.5		110000	0.2	
[75]	RT35HC	organic	Rubitherm, DE	35		220000	0.2	
[76]	RT28HC	organic	Rubitherm, DE	30	27	250000	0.2	
	RT31	organic	Rubitherm, DE	33	27	165000	0.2	
	PT27	organic	PureTemp LLC, USA	27		263000	0.15	0.25

	PT28	organic	PureTemp LLC, USA	28.1		254000	0.15	0.25
	PT29	organic	PureTemp LLC, USA	28.6		202000	0.15	0.25
	A27	organic	Phase Change Materials Products Ltd., UK	27		250000	0.22	
	A28	organic	Phase Change Materials Products Ltd., UK	28		265000	0.21	
	A29	organic	Phase Change Materials Products Ltd., UK	29		230000	0.21	
	A30	organic	Phase Change Materials Products Ltd., UK	30		230000	0.21	
	A31	organic	Phase Change Materials Products Ltd., UK	31		230000	0.21	
[27]	C18 Inertek 29	inorganic		18.3	14.2	185400		
	microencapsulated PCM in PU (C18 Inertek 29), 40wt%			18.1	14	49000		
	microencapsulated PCM in PU (C18 Inertek 29), 50wt%			18.3	14.3	60000		
[77]	RT35HC	organic	Rubitherm, DE	35		220000	0.2	
	RT5HC	organic	Rubitherm, DE	5		240000	0.2	
[78]	RT18HC	organic	Rubitherm, DE	18		220000		
[79]	E-26	eutectic	PCM products Ltd.	-26		260000	0.58	
	E-29	eutectic	PCM products Ltd.	-29		222000	0.64	
	E-32	eutectic	PCM products Ltd.	-32		243000	0.56	
[80]	RT3HC	organic	Rubitherm, DE	3		190000	0.2	
	RT5	organic	Rubitherm, DE	5		180000	0.2	
	RT8HC	organic	Rubitherm, DE	8		190000	0.2	
[81]	RT5	organic	Rubitherm, DE	4.96	4.84	180000	0.2	
[82]	water	inorganic						
[83]	RT2HC	organic	Rubitherm, DE	3	1	200000	0.2	
	RT4	organic	Rubitherm, DE	5	3	170000	0.2	
	RT5HC	organic	Rubitherm, DE	6	5	250000	0.2	
[84]	SP-24	inorganic	Rubitherm, DE	-22	-23	220000	0.6	

[85]	Acqueous salt solution	inorganic		-10		230000	2.2	2.2
		inorganic		-33		215000	0.6	0.6
[86]	OP5E	organic	Ruhr New Material Technology Co., CHN	6	5	235000	0.2	
[87]	RT0	organic	Rubitherm, DE	0		145000	0.2	0.2
	RT2HC	organic	Rubitherm, DE	2		170000	0.2	0.2
	RT3HC	organic	Rubitherm, DE	3		160000	0.2	0.2
	RT4HC	organic	Rubitherm, DE	4		145000	0.2	0.2
	RT5HC	organic	Rubitherm, DE	5		220000	0.2	0.2
	RT8HC	organic	Rubitherm, DE	8		160000	0.2	0.2
[88]	RT5	organic	Rubitherm, DE	6.46		143740	0.159	
	RT5-modified (fumed silica + graphene)	organic		6.49		131860	0.247	
[89]	Tetradecane-Lauryl Alcohol-Expaned graphite	eutectic		4.3		247100	0.9657	
[90]	SP-50	inorganic	Rubitherm, DE	-52	-48	190000	0.6	
[91]	Sodium polyacrylate -0.1wt% MWCNT-water			-0.037		335400	0.9021	
[92]	n-octanoic acid-myristic acid composite	organic		7.1		146100	0.2832	
	Potassium sorbate-water composite	inorganic		-2.5		256200		
[93]	Eutectic salt	eutectic	Shanghai Wenkang Co. Ltd, CHN	-80		82320		
[94]	E-21	eutectic	Cristopia	-21.3		233000	0.5	
[95]	E-21	eutectic	Cristopia	-21.3		233000	0.5	
[96]	Sodium chloride, glycerol solution, water	eutectic		-30		175300		
[97]	water	inorganic		0		334000		
	Potassium sorbate	inorganic		-2.5		256000		
	Tetradecane + docosane	organic		2.5		234000		
	Tetradecane	organic		5		214000		
[98]	BPCMG: Brine (KCl + NH_4Cl) in super absorbent polymer (SAP) gel	eutectic		-21		230620	0.589	

From Fig. 2.1, it can be noticed that most of the cold PCMs falls into the organic category. Between -10 °C and 10 °C most of the PCMs can be found, with latent heat values ranging from 150 to 250 kJ kg^{-1}. Very low temperatures (under -20 °C) seem to be exclusive prerogative of inorganic and eutectic compounds.

Nevertheless, selection of suitable PCM candidates for a given application should be performed by trying to take into consideration specific criteria in accordance with the PCM properties, as illustrated by Fig. 2.3.

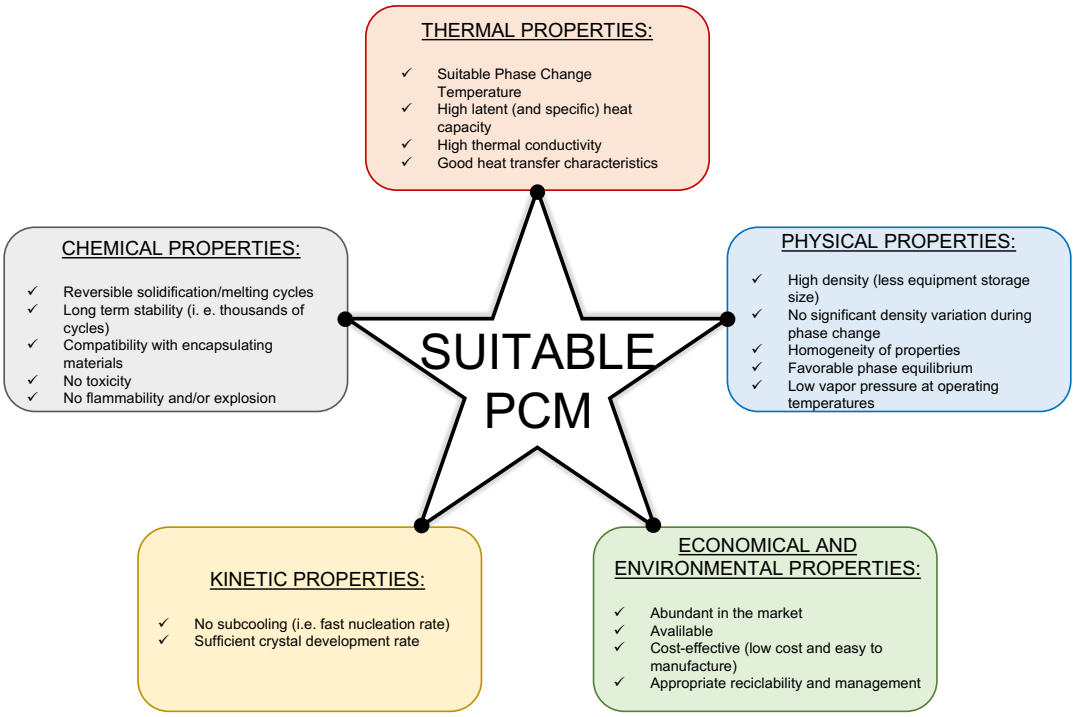

Figure 2.3 Selection criteria for the suitable PCM. Adapted from [99].

Regardless of the different nature of PCM, the ideal one should exhibit an appropriate phase change temperature and a high latent heat value. It should have a high thermal conductivity to improve the heat transfer during the charging/discharging processes. A high-density value is desired since it implies a reduction of the system size (i. e. the same storable mass with a lower occupied volume). The volume change during the phase change should be prevented. The PCM should present homogenous properties, having low vapor pressure at operating conditions. For what concerns the PCM chemical composition, it should perform reversible solidification and melting cycles, being long-term stable at the same time. Moreover, the PCM should be compatible with its TES material, nontoxic, and nonflammable. During the solidification phase, the subcooling phenomenon should be avoided and a good crystal development rate is

required. From an economical and environmental aspect, the PCM should be abundant and available in the market at a reasonable price. If possible, the ideal PCM should be recyclable, in order to make this technology environmentally friendly and sustainable, and easy-to-manage with insignificant decommissioning cost for the system.

As anticipated, a PCM matching all these requirements cannot be found [17] thereby a choice based on a trade-off is inevitable. Therefore, based on what reported in Table 1 and [9], [17] the advantages and disadvantages of the PCM classes are listed in Fig. 2.4.

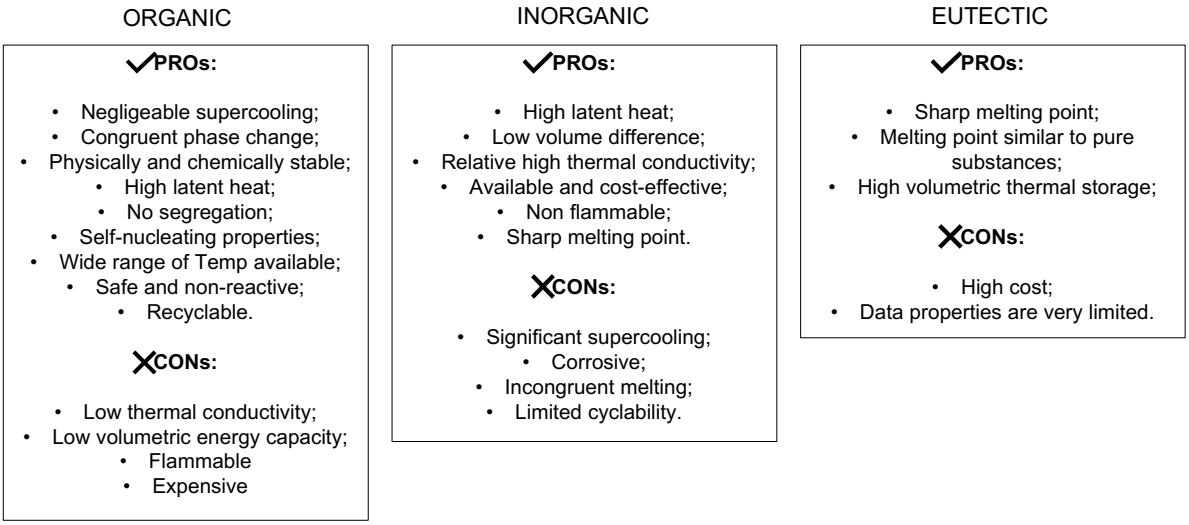

Figure 2.4 Advantages (PROs) and disadvantages (CONs) of PCM classified by chemical composition.

From what reported in Fig. 2.4 and Table 2.1, it can be noticed that the main concerns regarding the adoption of PCM based LTES are related to limited thermal conductivity (most of the values range from 0.1 to 1 W m^{-1} K^{-1}), the subcooling phenomenon during the solidification process, an incongruent melting which can result in phase segregation, possible leakage occurring during the melting process, long-term stability, and corrosion. Moreover, the negative effects on human health and the environmental and economic aspects must be carefully managed. Thus, in subsequent sections, the main challenges associated with proposed solutions are reported.

2.1.1 Low thermal conductivity

As stated by Nie et al. [100], a high thermal conductivity is necessary, in order to limit the required time to complete the phase change process. The PCM thermal conductivity can be

enhanced with the insertion of high thermal conductivity additives, as composite ones [64] or capsules [101], or they can be devoted to the extension of the heat transfer area [12].

PCM nanocomposites are a very common strategy to solve the thermal conductivity issue. Liu et al. [64] added 1wt.% multi wallet carbon nanotubes (MWCNTs) into OP5E which is a paraffin based PCM with a phase change temperature between 5 °C and 6 °C. The authors reported that the thermal conductivity increased from 0.20 to 0.37 W m^{-1} K^{-1}, with negligeable reduction of the melting enthalpy. By inserting 0.1wt.% MWCNTs in a water-sodium solution based PCM, a 19.17% increase in the thermal conductivity was reported [91], reaching the value of 0.90 W m^{-1} K^{-1}. The insertion of 1.5wt% silver-titania hybrid nanocomposite into ethyl trans-cinnamate (6.8 °C melting temperature) led to 52% of thermal conductivity augmentation (figuring out at 0.54 W m^{-1} K^{-1}). Besides, the immersion of metal foams in PCMs have been proposed to enhance the thermal conductivity. For example, Xiao et al. [102] by immersing copper foam in paraffin obtained a 15 times thermal conductivity increase. By obtaining microcapsules consisting of 50wt% calcium carbonate ($CaCO_3$) shell and n-octadecane PCM, Yu et al. [103] reported a significant thermal conductivity improvement of about 725% compared with pure PCM, reaching 1.26 W m^{-1} K^{-1}. For additional survey works, the reader may refer to Nie et al. [100]. Foam-fin combinations were tested by Liu et al. [104]

2.1.2 *Subcooling*

The subcooling phenomenon may occur during the solidification process. It implies the need of cooling the PCM at a temperature lower than its freezing point to let the solidification process to start, which results in a loss in system efficiency. Once the process is triggered, the PCM temperature jumps to the nominal phase change temperature and the solidification continues as expected. This phenomenon can be ascribable to a low rate of nucleation or a slow rate of nuclei growth [105]. As reported in Fig. 2.4, the subcooling effect is particularly significant for inorganic PCMs, whilst almost negligeable for organic ones. Aiming at overcoming the subcooling issue, the addition of nucleating agents has demonstrated to be an effective solution. Zhang et al. [106] let the degree of subcooling drop from 14.5 K to 0.8 K by employing SiO_2 nanoparticles into PCM-in-water emulsion. Wang et al. [107] added 2 wt.% of graphene nanoparticles to OP10E in water to drop the subcooling of the PCM from 9.9 K to 0 K.

2.1.3 Phase segregation

The phase segregation occurs when two or more phases constituting the PCM can be noticed, separately, after a complete phase change process. This phenomenon is significantly evident for inorganic salt hydrates PCM [108]. This problem may be overcome using thickening agents or gelling [109]. The former increases the viscosity of the PCM whilst its melting point remains almost the same. The gelling agents inhibit the phase separation by forming a 3D matrix inside the PCM. However, the heat capacity is negatively affected by the addition of thickening agents [110]. Cabeza et al. [111] reported heat capacity reductions of up to 35%.

2.1.4 Leakage

The PCM leakage is preeminently due to the volume expansion occurring during the transition from solid to liquid. As reported by Nie et al. [100], the PCM should be entrapped in container through microencapsulation or be immersed in a matrix. Since the microencapsulation is still not a cost-effective technique and due to the difficulties facing during the process of selecting and designing the appropriate material in accordance with the application, the addition of matrix has been adopted as a feasible mean to prevent leakage. By immersing capric-nonanoic acid mixture (6.84 °C melting point) into a 90wt.% expanded graphite matrix, leakage was inhibited by Wang et al. [112]. In general, polymeric matrixes require up to 30 wt.% whilst ceramic ones up to 70% to eliminate the leakage to occur [100]. Additional reviewed works on leakage prevention can be found in [100].

2.1.5 Long-term stability

The long-term stability of the thermo-physical PCMs properties is essential for their use in a real application. Therefore, several authors have analyzed the PCM stability after a certain number of melting-solidification cycles. Xu et al. [91] evaluated the step cooling curve of water and 1vol.% sodium polyacrylate PCM at the beginning and after 100 cycles. It was found that the two curves mostly overlap, suggesting good stability. The authors, also, calculated, through a differential scanning calorimeter, the latent heat value after 100 cycles obtaining negligeable differences. Nie et al. [88] developed a new composite phase change material for a portable box for cold chain applications. The composite PCM consisted of the paraffin RT5, with the addition of fumed silica and graphene. The authors investigated the cyclability of the pure and composite PCMs, finding that the two PCMs presented good thermal stability, as reported in Table 2.2.

Table 2.2 Thermo-physical properties of PCM after 0-100-200 cycles [88].

Sample	Cycles	Melting Temperature (°C)	Freezing Temperature (°C)	Latent Heat (kJ kg^{-1})	Supercooling degree (K)
Pure PCM	0	6.46	2.82	143.74	3.64
	100	6.54	2.41	142.67	4.13
	200	6.57	2.57	141.50	4.00
Composite PCM	0	6.49	3.26	131.86	3.23
	100	6.57	3.17	130.72	3.40
	200	6.65	3.11	128.99	3.43

2.1.6 Corrosion

The preliminary evaluation of the corrosive effect of the PCM on the construction material is essential to design a latent thermal storage system. As stated by Nie et al. [100], several studies on the effects of salt solutions and eutectic-based ones for low temperature application on different metals have been carried out. However, no definitive solutions in overcoming the corrosion have been achieved. Orò et al. [113] investigated the compatibility of PCM (from -21 °C to 15.4 °C melting temperature) with different metals (copper, aluminum, stainless steel 316 (SS316), and carbon steel) and four polymers to find the most appropriate container. By focusing only on metallic materials, SS316 is considered the most suitable for a cold storage application. An interesting work was conducted by Ferrer et al. [114]. Five specimens of different material (aluminum, SS316, SS304, carbon steel, and copper) and four different PCMs (inorganic mixture, ester, two fatty acid eutectics) were used. It was reported that aluminum is suitable for the ester and for the eutectic PCMs, whilst SS316 and SS314 can be adopted for all kinds of PCM. The corrosion test was also conducted by Farrell et al. [115] who analyzed PlusICE E17 (17 °C melting temperature) and Climsel C18 (18 °C melting temperature) on copper, aluminum, and copper-aluminum alloy materials. Significant mass losses were detected for the copper sample, whilst no mass loss was found for the alloyed sample. The design with aluminum performed well for E17.

2.1.7 Health, environmental and economic aspects

A complete review on the toxicity evaluation and health hazards of different types of PCMs has been proposed by Chandel and Agarwal [116].

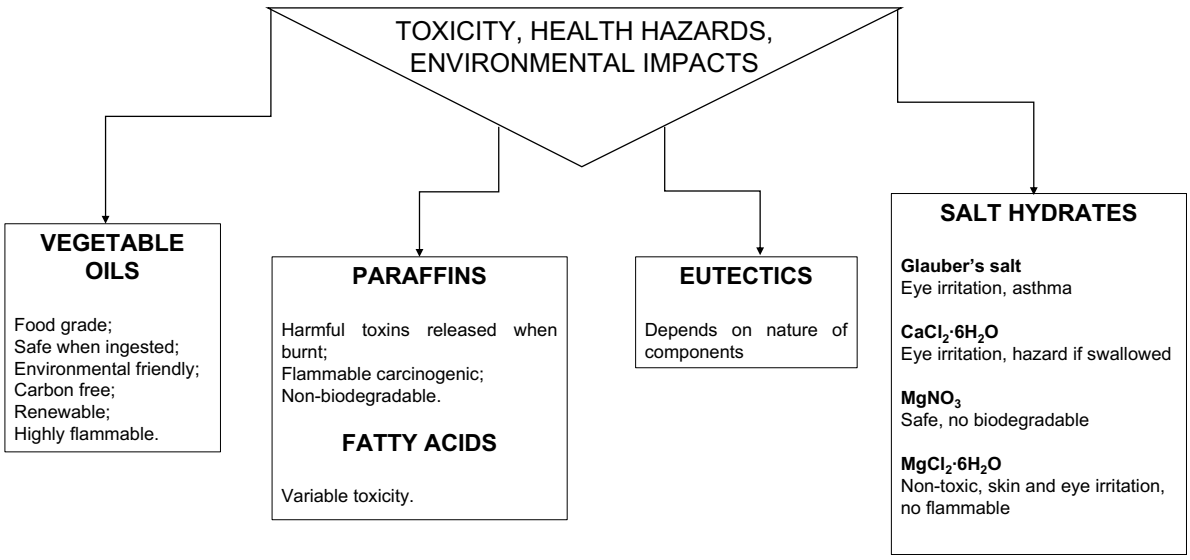

Figure 2.5 Toxicity, health hazards and environmental impacts of different PCMs.

In Fig. 2.5, the main results obtained in [116] are summarized. As seen, different impacts on the human health and environment safety may derive from different kinds of PCMs. Among the organic ones, it has been observed that vegetable oils are safer than paraffins, and they can also be considered a green technology due to their environmental sustainability. However, they generally have melting points that cannot match cold storage application requirements [116], though some exceptions can be found in the market (CrodaTherm 9.5 [117]). Fatty acids present an annoying odor which limits their exploitation. Salt hydrates can be hazardous with reported issues such as eye irritation and asthma.

To conduct a comparative analysis of the environmental impacts of an already existing technology versus an innovative LTES one, a Life Cycle Assessment (LCA), in accordance with the International Standard ISO 14040 [118], is necessary. As reported in David et al. [119], after having defined the goal and scope of the analysis, the inventory analysis, life cycle impact assessment and interpretation phase are followed. It is required the evaluation of the environmental impacts by considering the application in its complexity. Therefore, the needed energy and materials, transport means, maintenance, and disposal (re-use) must be taken into consideration.

The goal and scope definition phase involves the clearly statement of what it is wanted to demonstrate by performing the LCA. At this stage, the system boundaries, the functional units, and which categories have impacts on the analysis must be declared and clarified. The inventory phase prescribes the analysis of all the required input data (energy, materials) and it returns outputs in terms of the amount of solid, liquid, gas released into the environment.

During the impact assessment phase, the data coming from the precedent stage are converted into damage indicators. Finally, all the results are analyzed during the interpretation phase, and this lets to make the final decision. In Fig. 2.6, the scheme of a LCA for a building PCM-based application is shown.

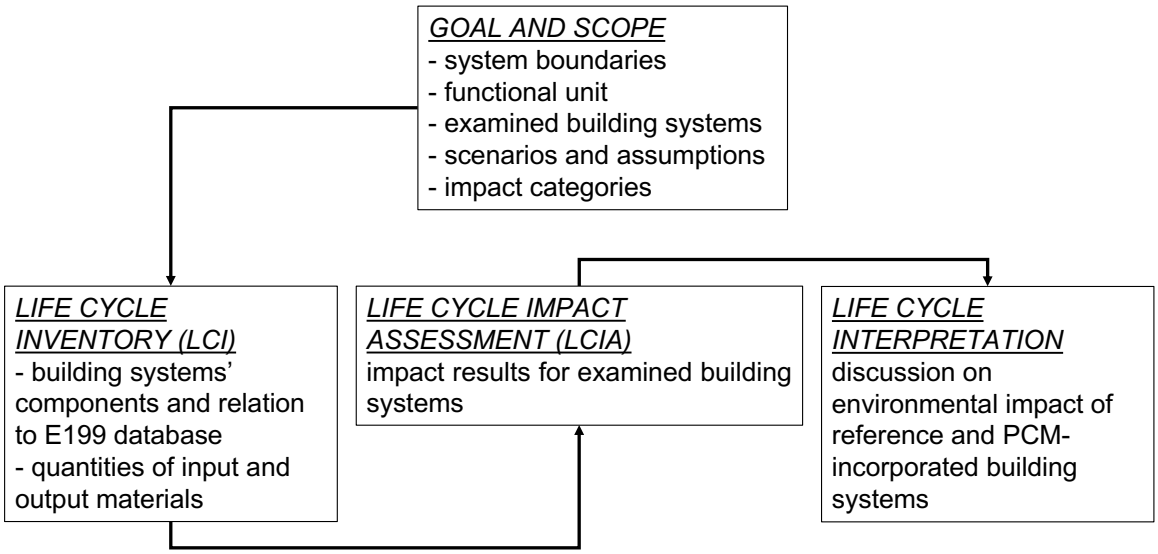

Figure 2.6 LCA for a building PCM-based application. Adapted from [120]

In parallel with the evaluation of the environmental consequences of the adoption of a latent thermal storage, a Life Cycle Cost Analysis [121] is needed. In particular, the analysis prescribes the estimation of agency, user, and environmental costs. The agency costs are related to the necessity of finding an intermediary who can solve problems associated to conflicts of interest, conflicts of relation between stakeholders or management problems. The user cost concerns the use of a fixed capital asset, which is the loss in the asset's value due to its use. Finally, environmental costs are intended to represent the potential deterioration of natural assets due to economic activities.

2.2 Refrigerated transport along the cold chain

As Fig. 2.7 indicates, a typical cold chain consists of different activities (usually in series) that ensure the temperature control for the safe management of perishable products. It involves, essentially, the products harvesting, storage, and transportation. The latter is particularly significant because it plays a fundamental role during the very diverse steps along the supply chain.

To achieve the goal of maintaining the correct temperature at different stages, diverse typologies of transport can be found: there can be inland transportation, very long-distance or

intercontinental transport involving air, sea or rail transportations, or city logistics for a short-haul distribution.

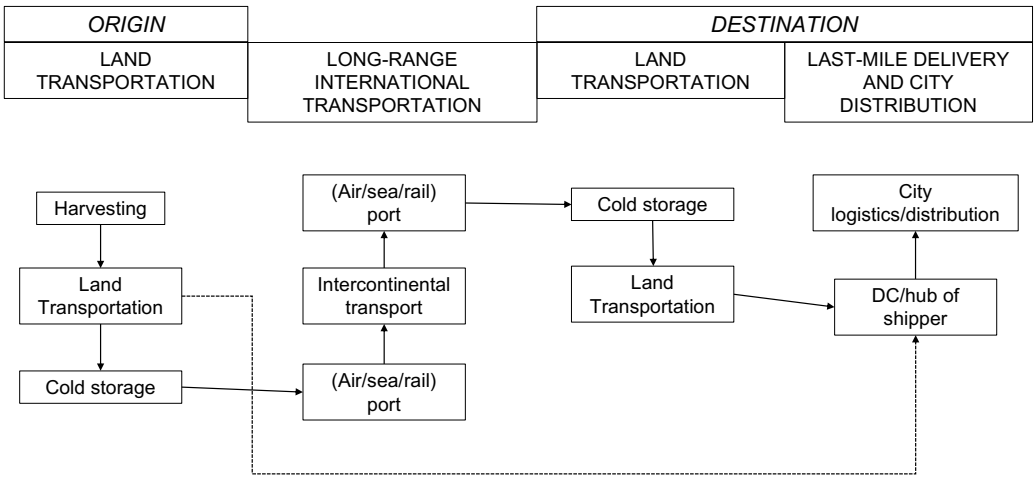

Figure 2.7 Cold chain stages. Adapted from [122]

It is clear that different modalities deal with different costs and environmental impacts. Therefore, the sustainability and carbon footprint are two aspects that must be deeply taken into consideration for the choice of the most suitable means of transportation.
In Table 2.3, the carbon emission and cost of the typologies of transport composing the cold chain are shown.

Table 2.3 Emission and costs of different transport modalities [122]

Transport typology	**Emission** (gCO_2 ton^{-1} km^{-1})	**Cost** ($ ton^{-1} km^{-1})
Sea Transport	3 (container), 0.6 (bulk)	0.01 (dry cargo) to 0.025 (reefer)
Air Transport	218 (short-haul), 159 (long-haul)	0.8-1.5
Inland waterways	50.62	0.09
Rail	139.8	0.2
Truck	15.6	0.12

Since the main focus of this work is on the road transportation, no additional details on the other transport methods will be given.
The road transport is the most adopted way for inland freight transport [122]. In 2013, 75% of the entire freight transported along the European countries involved road transport [122]. Moreover, this number can reach 95% if considering only agri-food transportation. As stated

by Tassou et al. [30], primary, secondary, and tertiary distribution can be detected. The primary distribution involves the transport from the food factory to the regional distribution centers and it is mainly served by large articulated vehicles (up to 44 ton). This transport method is also used for secondary distribution, that is from regional distribution centers to shops. Finally, rigid vehicles (up to 32 ton) are employed for tertiary distribution (to small shops).
The international carriage of perishable food products is regulated by the international ATP agreement [29] which aims at setting rules and standards for the temperature-controlled means of transport. In the next section, details of the ATP agreement will be enucleated.

2.2.1 ATP Agreement

The insulated equipment of a transport vehicle consists of rigid insulating walls or doors which limit the heat transfer between the external environment and the refrigerated cell. If a transport mean is *isotherme normal* I_N, normally insulated equipment, its global heat transfer coefficient K (W m^{-2} K^{-1}), defined as the ratio between the heat flow and the temperature difference between inner and outer vehicle body and the heat transfer surface areas, should not be greater than 0.70 W m^{-2} K^{-1}. On the contrary, an *isotherme renforcè* vehicle I_R, heavily insulated equipment, should have a K value less than or equal to 0.4 W m^{-2} K^{-1}. Moreover, if the width of the transport equipment exceeds 2.5 m, the insulation wall thickness cannot be thinner than 45 mm. The need of an I_R or I_N vehicle depends on the nature of the transported goods (if frozen, chilled, positive temperature).
The equipment can also be subdivided into *refrigerated* or *mechanically refrigerated* ones. The former deals with all the transport means which adopt a cold source to maintain the temperature inside the cell at a suitable level, with an average outside temperature of 30 °C. They can be of class A, if the temperature inside the vehicle body is lower than 7 °C, class B if lower than -10 °C, class C if lower than -20 °C, and class D if lower than 0 °C. For what stated above, it is clear that classes B and C must be of I_R type ($K \leq 0.4$ W m^{-2} K^{-1}). The mechanically refrigerated equipment, instead, concern all the transport means which use a refrigeration system (an own one or served jointly with other units of transport equipment by such an appliance). They are classified into 6 different classes (from A to F) depending on their ability in ensuring a desired temperature value inside the refrigerated body (T_i) with an external temperature of 30 °C:

- Class A: 0 °C ≤ T_i ≤ 12 °C
- Class B: -10 °C ≤ T_i ≤ 12 °C, $K \leq 0.4$ W m^{-2} K^{-1}
- Class C: -20 °C ≤ T_i ≤ 12 °C, $K \leq 0.4$ W m^{-2} K^{-1}

- Class D: $T_i \leq 0$ °C
- Class E: $T_i \leq -10$ °C, $K \leq 0.4$ W m^{-2} K^{-1}
- Class F: $T_i \leq -20$ °C, $K \leq 0.4$ W m^{-2} K^{-1}

Other classifications are related with *heated* and *refrigerated and heated* equipment [29].
The ATP standard also gives provisions on how to check the status of the different equipment for compliance with the standards [29]. The equipment conformity should be checked before starting its service, periodically (at least 2 times per year) and when required by the competence authority. The check of the insulation capacity of the equipment when in service consists of an inspection to establish the durability stated by the manufacturer, the general design of the insulating envelope, the method as to how the insulation has been applied, the condition and the thickness of the walls, and the condition of the insulated compartment. Experts may also require additional documents.
The test to confirm the validity of the refrigeration equipment results in the issue of a valid ATP capacity report. Note that considering the temperature limit imposed by the specific class and the corresponding heat flow Q to be extracted to ensure the limit when an external temperature of 30 °C is fixed, 1.35 times Q is required to endorse the refrigeration equipment installed on a refrigerated vehicle. If, instead, the refrigeration equipment is tested alone, it should provide a cooling capacity 1.75 times higher than the calculated Q in order to receive the ATP certificate. The ATP certificate covers both the insulation body and the refrigeration equipment.

2.2.2 Refrigerated vehicles overview

Depending on what cold chain stages the refrigerated transport is involved in, different solutions can be adopted (containers, trailers, semi-trailers, trucks, vans [30]). The refrigerated vehicles are about 4 million. The market share consists of 55% of vans, 25% of semi-trailers and 20% of trucks [2].
It must be stressed that diverse sizes of the insulation and refrigeration equipment of the refrigerated vehicle, result in specific performance, energy/fuel need and pollutant emissions, consequently.

2.2.2.1 Wall insulation

As reported in [123], when dealing with the design factors affecting the insulation design, despite of the specific typology of the refrigerated vehicle, the subsequent points must be taken into consideration:

- *Exterior conditions*: the extreme outer temperature, relative humidity, solar effect and wind effect.
- *Targeted interior conditions*: psychrometric variables (temperature and relative humidity).
- *Insulation materials properties*: moisture permeability, moisture retention, heat transfer properties, chemical and physical stability, structural limit, economical aspect.
- *Infiltration*: air and moisture due to door openings or cruising speed.
- *Trade-off between* operating requirements and designing cost.
- *Construction constraints*: exterior dimensions and minimum tare weight imposed by regulation or international agreement; for traditional European semi-trailer rigid box the external dimensions are 13.56 m x 2.6 m x 2.75 m (length, width, height) [30];
- *Others*: accidents or shock during the travel which can potentially deteriorate insulation ability.

Regarding the insulation wall thickness, trailers and trucks usually require 25 to 65 mm foam insulation material (Poly-Urethane foam, $k = 0.022$ W m^{-1} K^{-1}) when carrying fresh cargos, or 35 to 100 mm when dealing with frozen ones [123]. By considering 2 traditional europallets (1000 mm x 1200 mm) inserted side by side, it can be deduced that the thickness results in a numerical value, in most of the cases, no higher than 45-50 mm [30]. PU-foam is preferred due to its intrinsic hydrophilicity and relative low cost, with contemporary good mechanical properties [123]. A metal sheet is usually adopted for the exterior insulation wall surfaces of the vehicle in order to prevent air and moisture infiltration. On the other side, vapor barriers wrap the interior insulation of body surfaces. The inner layer presents protections against pallet-trucks and forklifts during loading/unloading operations. A typical material suitable to act as vapor barrier can be the aluminum foil, properly sealed at joints [123]. As reported in different works [70] [30] the insulation foam ageing is an important factor to be considered as it significantly impacts the thermal performance of the insulation material. On average, a typical value of 5% per year for loss in insulation capacity is reported. More specifically, between 3% to 5% annual increase in thermal conductivity of the insulator has been observed

[30]. That is, an increase of 55% in energy consumption (and carbon dioxide emissions, consequently) after nine years of operation. Besides the manufacturing process can affect the insulation performance of the insulation wall, mainly by affecting the global heat transfer coefficient *K* through the wall. *K* values from 0.82 to 1.24 W m^{-2} K^{-1} have been observed in [124] for similar refrigerated vans.

2.2.2.2 Refrigeration equipment

Depending on the way energy is supplied to the refrigerated equipment, two categories can be identified: *self-powered systems* usually adopted for large size vehicles (trucks, trailers) and *vehicle-powered systems* (typically for vans or small trucks) [123]. In either case, the cooling unit relies on vapor compression technology.

When dealing with self-powered refrigeration systems, four other sub-categories can be listed. The first involves the adoption of an own heat engine for the mechanical power, i.e. an autonomous unit from the vehicle. Open-shaft compressor is connected to the engine while fans and blowers are triggered by a belt-and-pulley system [123]. In such a system, the cooling capacity modulation can be achieved either by a specific control of the speed or by switching the engine on and off. The second sub-category include the systems which require electrical power to operate. The compressor, condenser, evaporator fans motors are fed by an engine-driven generator. The advantage of adopting an electrical system is the possibility of limiting the losses due to belt transmission. The trailer refrigeration systems present the cooling unit which is usually mounted on the top, with the evaporator and fans facing the inside of the refrigerated body. The entire system consists of a diesel engine connected to a battery-charging alternator while mechanically and/or electrically driven systems are also existing. The self-powered large truck systems are very similar to trailer ones. To reduce the polluting emissions particle filters and catalysts can be used [123].

Focusing on vehicle-powered systems two main sub-categories can be identified: the vehicle alternator unit system and direct belt one [30]. These categories are usually related to small trucks or vans. With the former, the electrical alternator is driven by a belt. The alternator feeds the all-electric-vehicle-powered system and is driven either by either the crankshaft or the engine power take-off. To regulate the change in the engine speed, a static converter may be adopted, which maintains a constant direct current voltage [123]. The other vehicle-powered transport means for local delivery of refrigerated products relies on the engine using a belt and pulley system. All other refrigeration components are electrically driven. One of the main

disadvantages of adopting such a system is that the performance is strictly related to the vehicle engine's speed, independent from the cooling capacity needs.

As already stated, different refrigeration technologies deal with different transport means which, in turns, are linked to different carbon dioxide emissions. A comprehensive work on CO_2 emission per carried pallets per kilometers of several refrigerated road transport vehicles was assessed by Tassou et al. [30], by discriminating between chilled or frozen carried foodstuffs, single- or multi-drop, and multi-temperature, as reported in Table 2.4. It must be highlighted that emissions for refrigerant leakage are not considered here.

Table 2.4 CO_2 emissions (gCO_2 $pallet^{-1}$ km^{-1}) for different refrigerated vehicles [30]

Vehicle	No Ref.	Chilled (single-drop)	Chilled (multi-drop)	Frozen, multi-temperature (single-drop)	Frozen, multi-temperature (multi-drop)
Medium rigid	88	106	109	112	115
Large rigid	85	102	105	108	111
City articulated	56	69	70	73	75
32 ton articulated	51	61	63	65	67
38 ton articulated	48	58	59	61	63

2.2.3 How to improve the refrigerated transport sustainability

As affirmed by Behdani et al. [122] the transport cold chain sustainability improvement could be achieved by pursuing two different goals: the enhancement of energy consumption (and, the minimization of the emissions, consequently) of the different refrigerated vehicles or improving the logistics processes.

For the efficiency enhancement of the distribution in global networks, different ICT technologies have been proposed [122]. Focusing on the first goal, and, more specifically on the reduction of pollutant emissions, Lee et al [125] demonstrated that 42-61% less GHGs were generated by an electric truck compared with a traditional diesel-driven one. In particular, when considering the frequent stops and low average speed scenario, energy consumption reductions

of 32-54% were achieved. Nevertheless, for a city-suburban scenario (less stops, higher velocities), the energy consumption was reduced from 5 to 34% and, consequently, GHGs emissions dropped from 19 to 43%. The transition to full electric transport means seems a promising solution even if some drawbacks have firstly to be overcome, such as batteries-life duration, charging points and cost of technology. As reported by Tassou et al. [30], cryogenic cooling systems and eutectic systems may improve the environmental sustainability of refrigerated transport. Phase Change Materials, as already stated in the introductive section, have been attracting more and more attention to be employed as a more sustainable alternative in refrigerated transport. In the next section, a detailed and comprehensive review of the PCM integration in refrigerated vehicles will be presented.

Regardless of the refrigerated transportation system, several procedures may be followed, and different performance indicators may be defined and adopted to evaluate the environmental impact [31]. In details, three approaches are fully described [31]: the Total Equivalent Warming Impact (TEWI), the Life Cycle Assessment (LCA) and the Life Cycle Climate Performance (LCCP). The different approaches, however, lead to an estimation for the direct and indirect emissions. Nevertheless, as stated by Li et al. [31] due to the extremely different operating conditions a refrigeration system may face, the LCCP is more trustable and meaningful to estimate the environmental performance impact (and can potentially reduce it). Moreover, knowing the energy consumption inputs, LCA and LCCP approach should result in the same solution, if the focus in only on greenhouse gas emissions.

Therefore, the key points of the transport LCCP calculation procedure developed and proposed in [31] are here reported. This methodology can be used as reference for further analysis to create a new transport LCCP model for every specific refrigerated transport application by following a similar approach.

Before starting the LCCP calculation, the procedure described in [31], prescribes to estimate the energy/fuel consumption by the adoption of the Thermo King Fuel Simulator (Fig. 2.8(a)). To address this goal, a Simulink model in Matlab environment is developed. In particular, as shown in Fig. 2.8(a), it consists of a “Box Model” which lets to obtain the necessary cooling load to maintain the system at a determined temperature. At this level, some input data are needed, such as box dimension, the material property for the insulation layer and ambient as well as the box temperature. An intermediate result is the evaluation of the heat losses through the box. The solar radiation and door openings can also be taken into account. As a subsequent step, there is the “Control Model” which deals with the control of the engine speed, fan speed, and refrigeration capacity, consequently. Finally, strictly connected to the control model, the

"Plant Model" can be found which predicts the system energy efficiency due to those particular conditions. Once the energy/fuel consumption response is obtained, the proposed transport LCCP calculation can be assessed, as depicted in Fig. 2.8(b). One can now estimate the direct and indirect emissions of the refrigeration system, by adopting the following equation (Eq. (2.1)) [31]:

$$TransportLCCP = (R + R_p)\{Y(L + L_{sa}) + E\} + Y\sum(C_f F + C_k K) + Y\sum F_t C_f + \sum C_m M + \sum C_m M_r \quad \text{Eq. (2.1)}$$

.

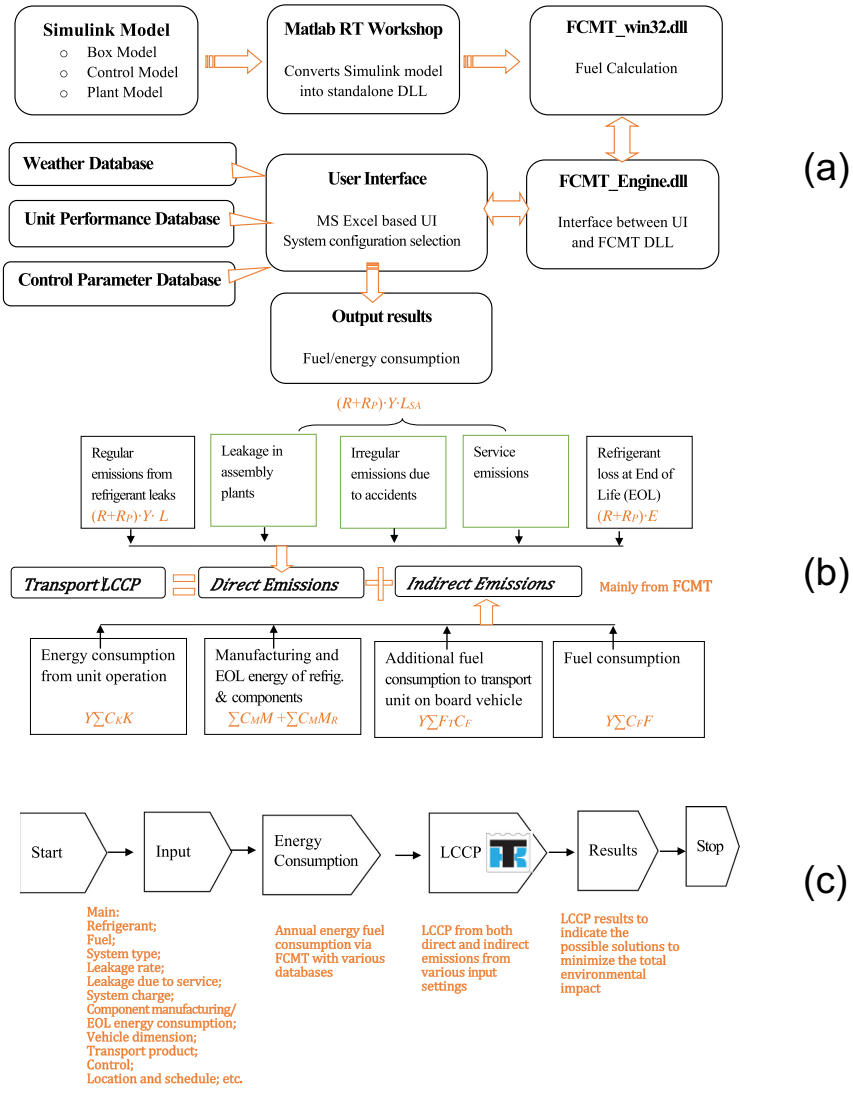

Figure 2.8 (a) Thermo King Fuel Simulator, (b) Transport LCCP, (c) Transport LCCP flowchart. Adapted from [31].

In Fig. 2.8 (b) the physical explanation of each term can be appreciated. For the sake of brevity, details are not provided here as they can be found in [31]; a flow chart is presented in Fig. 2.8(c) instead.

2.3 PCMs in refrigerated transport applications

In this section, the works involving the adoption of PCM for innovative refrigerated transport applications are explained in detail (Table 2.5).

In particular, from the reviewed works, three different approaches have been identified and critically discussed.

The first one regards the enhancement of the insulation wall by the insertion directly into the insulation material or the employment of PCMs in proximity of the insulation layer. The second one relates to the application of PCM in the refrigeration unit which can be alternatively set inside or outside the refrigerated space, and the last one involves the use of eutectic plates.

The effect of other parameters affecting the heat transfer performance have also been analyzed, such as the presence of the food load, the external temperature, and the door openings. Whether the latent thermal energy storage systems were designed to act as an active or passive cooling source, or if the new system required an additional active refrigeration unit have also been highlighted.

Table 2.5 Works regarding PCM integration into refrigerated transport applications

Authors	PCM (Melt/Solid Temperature (°C))	PCM location	Vehicle	Type of products	Product load (Y/N)	Exp/Num	Active (A) /Passive (P) cooling	Temp ext	Door opening (Y/N)	Economic analysis (Y/N)	Savings (Compared with no PCM)
[67]	RT5 (5/7)	Insulation wall	Truck	Food, positive temperature Temp target inside cell: 4 °C	N	E	A	Profile	N	N	*Single day* avg -18.3% of Heat Flux (W/m^2) avg -12.3% of Heat Flows (kWh) *Monthly* avg -29.1% of Heat Flux avg -16.3% of Heat Flow
[70]	Energain (21/16)	Insulation wall	Van	Refrigerated products Temp target inside cell: 0 °C	N	E+N	A	10 °C, 30 °C	N	N	Day-time (4 h at 30 °C): -25% energy consumption
[72]	n-tetradecane (6)	Insulation wall	Generic	Perishable products	N	E	-	- 1000 W	N	N	In PU-PCM foams, the temperature increase is slower than only PU
[74]	RT27 (27.5), RT28HC (28), RT31 (30.5), RT35 (32.5), RT35HC (35), RT42 (41), RT44HC (43), RT47 (45), C48 (46.5)	Insulation wall	Container	Chilled food Temp target inside cell: 0 °C	N	E	A	Profile (UNI 10349) Solar radiation (UNI 10349)	N	N	max heat peak load reduction: -20.87% max delay in peak: 3 h max energy rate reduction: -4.74%
[75]	RT35HC (35)	Insulation wall	Container	Chilled foods Temp target inside cell: 0 °C	N	E + N	A	Indoor: 19 °C diff ext-int Indoor: solar lamp 1000 W/m^2 Outdoor: profile	N	N	*Indoor:* 1-2 °C reduced internal surface *Outdoor:* max reduction peak heat transfer rate 8.57%, max peak delay 4:30 *Numerical:* peak heat load reduction: 20%, total energy reduction: 4.7%
[27]	C18 Inertek 29 (18)	Insulation wall	Generic	Food, positive temperature Temp target inside cell: 2 °C	N	E + N	A	Profile: 10 °C to 30 2h, 30 4h, 30 to 10 2h	N	N	Energy transferred to the cold space max reduction: 4%

[84]	SP-24 (-24)	Insulation wall	Truck	Frozen food	N	E + N	P (num)	Exp: 22 °C Num: 30 °C	N	N	*Exp:* 1 wall containing 6 mm of PCM let the air in refr space to reach 12 °C about 6 h later than reference. 10 mm, about 40 h *Num:* in truck refr space, temp maintained at -22 °C for more than 20 h
[76]	RT28HC (28), RT31 (31), PT27 (27), PT28 (28), PT29 (29), A27 (27), A28 (28), A29 (29), A30 (30), A31(31)	Insulation wall	Semi-Trailer	Frozen food Temp cell: -10 °C	N	N	A	Profile: from 27 to 31 °C	N	Y	Up to 34.4% refrigeration loads reduction Benefit cost-ratio above 1 Payback time < 3 years Greenhouse gas emission savings of more than 2700 $kgCO_2$/year.
[68]	Water (0)	Cold Storage Unit (CSU) in refr space	Truck	-	N	E	P	-	N	N	-
[26]	Inorganic salt acqueous solution (-26.7/-30.6)	Phase Change Termal Storage Unit (PCTSU) outside refr space	Truck	Frozen food (meat and fishery) Temp target inside cell: -18 °C	N	E	P	30 °C	N	Y	up to 86.4% cost reduction, if the charging process is completed during the off-peak period, and COP refr unit = 1.5
[69]	Climsel C-18 (-18) Cristopia E-21 (-21)	Thin container in refr space	Van	Frozen food	Y About 40 kg of M-packs	E	P	25 °C	N	N	*No-food load scenario*: C-18 let the air to be lower than 0 °C for 6.5 h, E-21 for 8 h, no PCM 1.5 h *food load scenario*: C-18 let the air to be lower than 0 °C for 15.6 h, E-21 for 21.5 h, no PCM 11.5 h
[71]	Inorganic salt acqueous solution (-26.7/-30.6)	Phase Change Termal Storage Unit (PCTSU) outside refr space	Van, Truck, Trailer	Frozen food (meat and fishery) Temp target inside cell: -18 °C	N	N	P	Profile	Y 36 s (30+6), every 30 min. 0-10-20 door openings	N	
[77]	RT5HC (5)	PCM air heat exchanger, inside refr room	Generic	Perishable products Temp target inside cell: 0-8 °C	N	E	A	32 °C	N	N	Power consumption reduction: 16%, on/off compressor cycles: 6 against 13

[80]	RT3HC (3), RT5HC (5), RT8 (8)	Baffle type panels, inside refr room	Truck	Perishable products	N	N	A	Profile	Y 10 cycles (60 min close, 15 min open)	N	Max reduction in energy consumption during opening-door period: 61% (RT3HC)
[81]	RT5 (4.96)	cold TES plates, inside refr space	Container	Perishable products (fruit, veget)	Y	E	P	Profile (13 to 35 °C)	Y 1 time	Y	Energy consumption reduction: 86.7%, operating cost reduction: 91.6%, emission reduction: 78.5%
[96]	Sodium chloride, glycerol solution, water	PCCSU (phase change cold storage unit), Inside refr space	Truck	Frozen products	N	E+N	P	Profile (avg 29 °C)	Y (10 door openings per day)	Y	Energy cost reduction: From 15.4 to 91.43%
[82]	Water (0)	MCU (mobile air cooling unit), inside refr space	Truck	Fresh food	N	E	P	27 °C	N	N	-
[73]	E-26 (-26)	Eutectic plates	Container	Fresh and frozen foods	N	N	P	-	N	N	-
[79]	E-26 (-26), E-29 (-29), E-32 (-32)	Eutectic plates	Truck	Frozen food	N	E	P	Profile	N	N	-
[126]	not specified (-18)	Eutectic plates	Truck	agricultural products	N	N	P	25 °C	N	N	-
[127]	Generic (-29)	Eutectic Plates	Truck	Frozen food Temp target inside : -20 °C	Y	N	P	20 °C	Y 60 s	N	-

2.3.1 PCM in the insulation wall

A pioneering study on the effect of the integration of the PCM inside the insulation wall of a traditional refrigerated truck was conducted by Ahmed et al. [67].

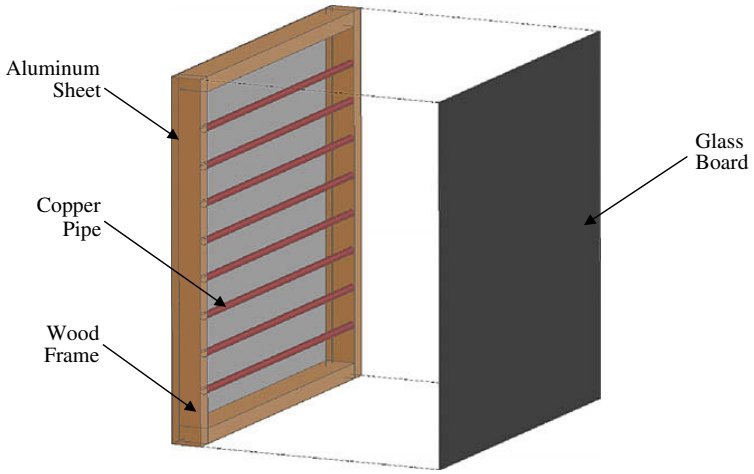

Figure 2.9 New PCM-based insulation wall [67]

As depicted in Fig. 2.9, the authors developed an in-house-made insulation wall by inserting eight copper pipes consisting of PCM into an 8.89 cm traditional polyurethane foam layer. By means of a computer program simulating the real operations, the paraffin-based RT5 PCM having a melting temperature at around 7 °C and with a latent heat value of 156 kJ kg^{-1} was selected to be the most suitable option. The authors considered the refrigerated cell to be set at a temperature close to 4 °C. Different operating conditions were studied such as a single-day operation and month-long one. The values of external temperature, relative humidity, wind and pressure information were acquired and stored by a weather station connected to a computer. The incident solar radiation was also monitored and recorded. To evaluate the effectiveness of the newly-developed insulation wall, two identical small rooms of 1.22 m x 1.22 m x 1.22 m were constructed aiming at simulating a truck trailer refrigerated cell. One room (defined by the authors "Control Unit") made of the traditional insulation, i.e. without PCM, whilst the other (the "PCM Unit") equipped with the new PCM-based walls. An active system consisted of a heat exchanger inside each room linked to a unique external chiller was developed to ensure the internal temperature to be maintained at a target value of 4 °C. For the single-day operation scenario interesting results were obtained. For what concerns the heat flux transmitted through the insulation walls, remarkable reductions were obtained for the southern, eastern, and top surfaces (from 29.7% to 42.4%) and both reduction and delay of the peak heat

transfer. By considering the entire room, a global reduction of 18.3% in heat flux was calculated which resulted in a 12.3% reduction in the transmitted heat. Similar results were reported when considering the month-long operation scenario, that is 29.1% heat flux reduction, and 16.3% reduction in the heat entering the room. The PCM-based system lowered the temperature swing, and this can be potentially beneficial for the operating life of the cooling unit. Positive impacts can also be related to energy conservation and less emissions from the diesel-driven refrigeration unit of a standard refrigerated truck.

Glouannec et al. [70] also conducted experimental and numerical investigations of the heat transferred through a novel insulated PCM-based insulation panel for vans. The authors developed an 86 cm tall and 16.2 cm long insulation layer. The insulation wall consisted of an external body (0.1 cm), an air gap of 10 cm, a fiberglass of 0.1 cm, a poly-urethane foam layer of 5.8 cm and the inner face made of 0.2 cm of Polyester+fiberglass. To that wall, adopted as reference case, 1 cm of aerogel and 0.2 cm of reflective multi-foil (RMF) were added to investigate the "Case 1". Moreover, to the reference case, 0.5 cm of Energain layer was added to analyze the effect of PCM integration inside the insulation layer ("Case 2"), as shown in Fig. 2.10.

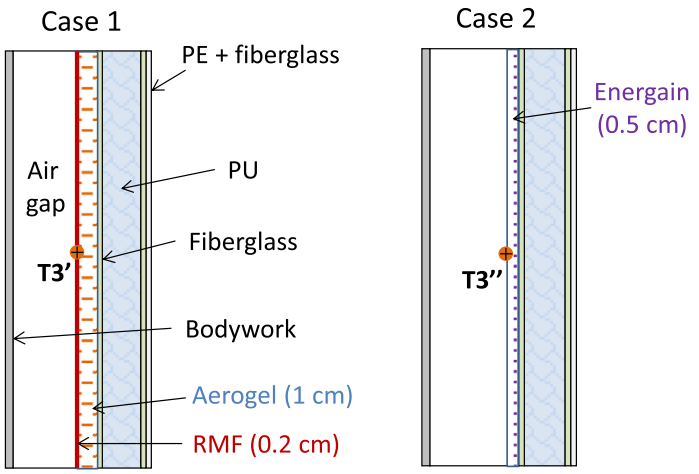

Figure 2.10 New designed insulation walls, with Aerogel+RMF (case 1), with Energain (case 2) [70]

The reference layer and the ones equipped with RMF or PCM layer were used, alternately, as a wall of an insulated small enclosure (0.5 cm^3) put inside a climate chamber. This latter was set at the external temperature (10 °C or 30 °C, depending on night and day scenarios, respectively) while an active refrigeration system assured the cooling inside the insulated enclosure to maintain the temperature at 0 °C. The authors calculated the heat flux densities

for the first 4 h when the temperature of the chamber was fixed at 10 °C (i. e. simulating the night scenario) and for the next 4 h when temperature was set to 30 °C. A reduction of 36% of the consumed energy for the case 1 was obtained. Besides, the PCM reduced the energy consumption by 25% compared with the base case. In case 1, the authors also considered the effect of the solar irradiation. By means of sunlamps, a value of 460 W m^{-2} was set during the fourth and sixth hours. The heat transfer coefficient, calculated according to the ATP agreement [29], could be increased up to 43%. The aerogel+RMF can reduce the heating effect due to the solar radiation by 27%.

Different from [70]'s concept, Zdun and Uhl [84] proposed the addition of a commercial SP-24 PCM layer, with thickness from 6 mm to 10 mm, to the inner face of an 8.6 cm Poly-Urethane foam insulation layer, as shown in Fig. 2.11.

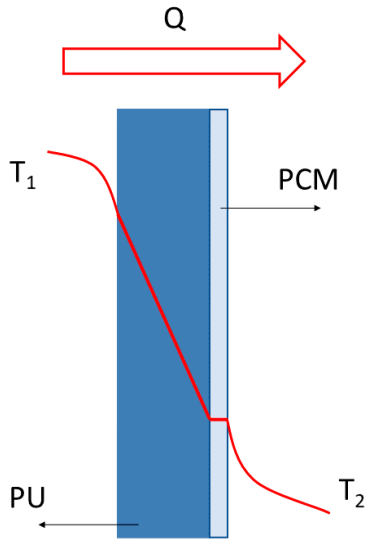

Figure 2.11 Insulation wall proposed by [84]

The proposed innovative wall substituted one of the walls of a climatic room having 1 m^3 of cold space inside. The experiments started at about -24 °C, being cooled down by a refrigeration unit, in order to ensure the PCM solidification (freezing temperature: -24 °C), to simulate the initial cooling stage of the refrigerated transport. This stage, which resulted in continuous on/off cycles of the refrigerated unit, lasted for 24 h and 40 h for the 6 mm and 10 mm layer, respectively. Once the target condition was reached, the refrigeration unit was completely turned off and only the ability of the PCM of acting as a passive cold source was monitored. The temperature evolution along time of the inner air was recorded to evaluate the overall performance. In particular, the time required to reach 15 °C in the cold space was selected as the monitoring variable for comparison purpose. By setting an external temperature

of 22 °C, the 6 mm PCM layer reached the critical value about 6 h later than the reference case (no PCM), while it was around 30 h later for the 10 mm PCM layer. Therefore, the authors tried to verify the feasibility of the proposed solution as an alternative for a traditional semi-trailer diesel-driven refrigeration unit. A 13.2 m x 2.42 m x 2.45 m refrigerated cell was modelled. A 6 mm PCM layer was added to the cell wall. The analysis was run by means of the COMSOL software. To follow the ATP procedure, as done by [70], an external temperature of 30 °C was set. The authors aimed at evaluating the ability of the PCM in maintaining the temperature level lower than -20 °C, to make this solution suitable for transportation of frozen products. The results revealed that the inner temperature didn't exceed the targeted limit for more than 20 h. Moreover, 6 mm PCM layer distributed on the refrigerated cell walls resulted in about 900 kg, which is a value comparable to a big semi-trailer refrigeration unit. The authors also declared a 86% reduction in energy consumption with the novel system cooled down by an external electrical refrigeration unit (COP 1.5) compared with a traditional diesel-driven one (COP 0.2). Nevertheless, Zdun and Uhl [84] considered only the stationary case, the external solar radiation contribution was neglected and no food cargo inside the refrigerated cell was taken into consideration.

A different PCM location was investigated by Copertaro et al. [74]. In [83] and [84] the PCM layer faced the refrigerated space, whilst in [74] it was applied to the external side of a traditional 20' ISO refrigerated container. The authors aimed at analyzing the advantages in terms of energy need reduction due to the application of the new container envelope. To reach this goal, a numerical FEM (finite element method) model in COMSOL Multiphysics environment was developed. In particular, a 6.058 m x 2.438 m x 2.591 m container was modelled having an insulation wall which consisted of 0.001 m external steel sheet, 0.03 m PCM layer, 0.10 m Poly-Urethane foam and 0.001 m internal steel sheet, as shown in Fig. 2.12. Nine different PCMs were analyzed (from 27.5 °C to 46.5 °C), whose detailed characteristics can be retrieved from Tables 1 and 5. Milan, Ancona and Palermo were selected as the reference cities from which retrieving the data of the extreme summer weather conditions in accordance with UNI 10349 [128] to be applied as boundary conditions to the model. Moreover, five different exposures were considered: north, south, east, west, and horizontal. The solar radiation was also considered. Compared with a traditional container, the authors evaluated the heat load peak and daily energy rate reductions to ensure the temperature inside the refrigerated space to be maintained at 0 °C. The internal air temperature was set at 0 °C, consequently, suggesting the adoption of an active refrigeration unit if considering a real

application. Under the applied summer conditions, the RT35HC resulted the best PCM to be employed. In fact, it experimented delay in heat load peak of about 2 or 3 h.

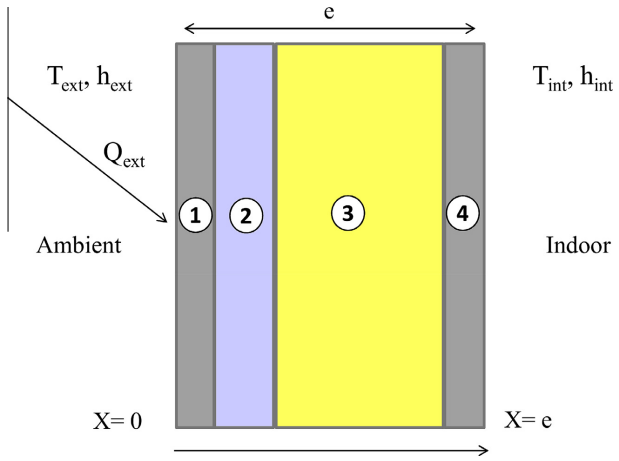

Figure 2.12 Section of the new envelope having the PCM layer. "2" is the PCM layer [74]

Moreover, heat load peak reductions from 20% to 20.9% and total daily energy rate reduction between 4.6% to 4.7% were calculated. The RT35HC was able to delay the complete melting and able to solidify during the night when the external temperatures are lower. Therefore, the heat could be transmitted into the cold space during the night, when high refrigeration unit performance and reduced energy costs occurred. On the contrary, RT42, RT44HC, RT47, and C48 did not perform properly as their phase change temperatures were too high, causing only partial melting. PCMs with melting temperatures lower than 35 °C were not able to address the required energy demand during the critical periods since they were completely melted during the first hours of the day. Based on [74], Fioretti et al. [75] experimentally studied the heat transfer performance of an insulation layer equipped with RT35HC on its external face. In particular, two experimental campaigns were conducted: an indoor and an outdoor one. For the indoor analysis an insulation prototype was developed whose main constituents were a 3 cm PCM layer consisting of RT35HC encapsulated in 81 polyethylene capsules sheet, and 10 cm PU-foam insulation layer. This prototype served as a wall of a small refrigerated test box put inside a climate chamber. The difference between the climate room and box temperatures was maintained at 19 °C. Moreover, a solar simulator (1000 W m^{-2}) was inserted in the climate room. The results of the test revealed a 59% reduction in the total energy for the PCM prototype wall. The external surface temperature remained at 63 °C against 90 °C for the reference case, suggesting the absorption of the solar irradiation due to the phase change process. Moreover, the internal surface temperature always remained 1 or 2 °C lower than that of the reference

case. The outdoor campaign aimed at testing the proposed insulation wall in conditions closer to a real container. Therefore, on the external sides of a cold room (2.2 m x 1.4 m x 1.4 m) 3 cm of PCM layers contained in polyethylene capsules were mounted. The cold room presented a refrigeration unit ensuring the inside temperature is maintained at 0 °C. The external conditions were mimicking those of Ancona during summer in 2014, presenting maximum solar irradiation value at around 800 W m^{-2} and temperature from 13 °C to 28 °C. Even in this large-scale application, as already reported in [74], the PCM layer absorbed significant amount of heat under harsh conditions (intensive solar irradiation and high ambient temperatures). The authors chose two characteristic days to evaluate the performance of the PCM-based new application: 30/Aug/2014 and 09/Sep/2014. By considering only the value of the thermal flux peak, 5.5% (10.38 W m^{-2} and 10.99 W m^{-2}) and 8.57% (10.56 W m^{-2} and 11.55 W m^{-2}) reductions between the reference and the PCM cold room were found for the first and second selected day, respectively. However, the PCM significantly prolonged the time to reach the peak temperature. Delays of 4.5 h and 3.5 h were found for the two days, respectively. In particular, the heat flux peak occurred at 9 PM, when the cooling required by the refrigerator is lower, due to more favorable external temperature conditions. The more efficient operating conditions lead to lower energy/fuel demand, which can be easily translated into lower gas emissions. Similar to [75], Chandran et al. [76] investigated the integration of a PCM layer into the insulation wall of a refrigerated semi-trailer rigid box truck (13.56 m x 2.60 m x 2.75 m). The insulation wall consisted of a 0.03 m PCM layer sandwiched between a 0.035 m thick Stainless Steel 304 layer and a 0.05 m thick expanded polyurethane layer. Moreover, the internal face of the insulation wall was covered with a 0.005 m thick mild steel foil. Nine different PCMs were considered by the authors with different melting temperatures, coming from several suppliers. In particular, RT31, A31, A30, PT29, A29, RT28HC, A28, PT28, PT 27, and A27 were tested. The authors analyzed the best solution in terms of energy savings, economic and environmental benefits. In details, they estimated the energy saving percentage, the payback period and the greenhouse gas emission (GHGE) reduction percentage. As done by [75], Chandran et al. [76] evaluated the refrigeration loads for each external truck surfaces exposed (or not) to the sun. The loads were calculated for two typical months in Kuala Lampur (Malaysia) by choosing a daily operation truck time period of 8 hours from 7 AM to 3 PM. The authors assumed that the refrigerated semi-trailer was mounted on a mover for the transportation of frozen goods maintained at -10 °C. It was found that when 80 kg of A28 organic PCM was used, a maximum reduction of refrigeration load of 28.5 % was reached. Moreover, 105 kg of PCM resulted in an additional energy saving with average load reductions

of about 8.5%. From an economic point of view, the benefit-cost ratio exceeded unity for the top performing PCMs (A28, RT28HC, A29, PT28, PT29). The payback time of these top performing PCMs reduced as the masses increased, reaching a minimum of 2.07 years when 105 kg of PCM is employed. Like the payback time, the emissions savings increased as the PCM mass increased, with a maximum of 3060 kg CO_2/year saved by A28. Moreover, Chandran et al. [76] stated that if considering a longer travel distance, the advantages coming from the adoption of the PCM decreased and GHGE increased since a heavier vehicle consumes more fuel. However, compared with short-haul travel vehicles, a GHGE savings of 138 kgCO_2/year can be performed.

A different approach was followed by Tinti et al. [72], who aimed at developing an innovative insulating material having low thermal conductivity (good insulation properties) and, contemporary, good latent heat storage properties. Instead of adding macro-encapsulated PCM (in tubes, slab, etc.), as reviewed so far, hybrid poly-urethane foams with diverse weight fraction of micro-encapsulated n-tetradecane were developed. By measuring the surface temperature evolutions over time when subject to a radiative heater, the best composite material was selected and proposed for further utilization. To conduct the thermographic analysis, five different foams were prepared with different amount of PCM (0 wt%, 4.5 wt%, 7.5wt%, 12 wt%, 13.5 wt%). By means of a halogen lamp (1000 W) which simulated the external radiation and under room temperature set at 15 °C, the specimens were heated, and the surface temperatures were mapped.

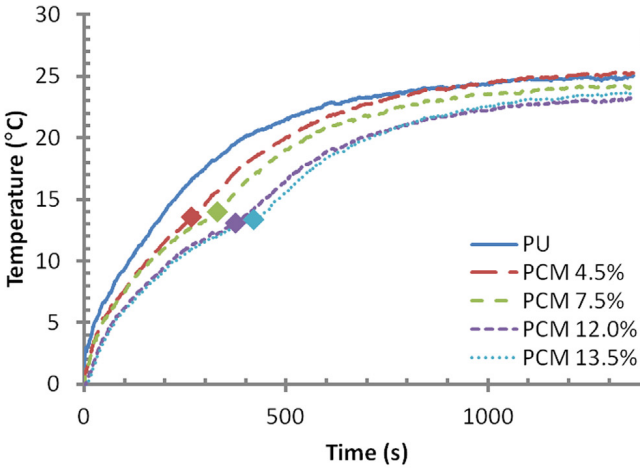

Figure 2.13 Surface temperature over time trends of the different foam specimens [72]

Fig. 2.13 demonstrates the advantages associated with the integration of micro-encapsulated PCM inside the insulation foam material. As the PCM content grows, the temperature increase rate is lowered mainly because the heat us absorbed by the PCM and spent on phase change. Moreover, implementing the thermographic analysis, the maximum temperature difference between the reference foam and the composite one was detected. A maximum temperature difference of 3 K was observed for the lowest PCM content, 7 K for 13.5 wt% PCM. These results suggest that the proposed hybrid foam, if translated into a hybrid insulation panel of a refrigerated vehicle for the transportation of perishable foodstuffs, can have a positive effect on reducing the cool loss when doors are opened and when a sudden refrigeration unit black-out happens or when significant solar irradiation changes along the route.

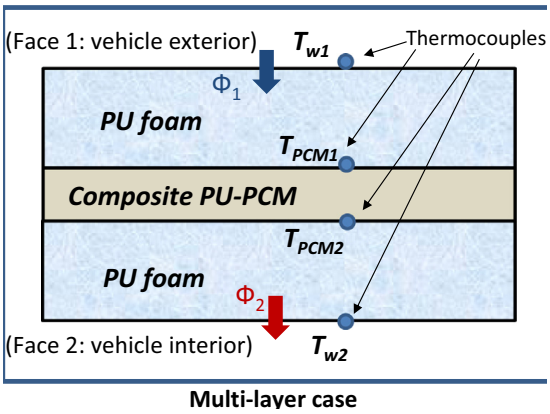

Figure 2.14 Surface temperature over time trends of the different foam specimens [27]

A hybrid insulation wall containing composite layer of poly-urethane foam and PCM (43 wt%, phase change temperature = 14 °C) for a refrigerated transport application was also investigated by Michel et al. [27]. The insulation wall, having a total thickness of 6 cm, consisted of two PU-foam layers sandwiching a composite PU-PCM one, as reported in Fig. 2.14. A reference case, only 6 cm of PU-foam, was also considered. To reproduce the operating refrigerated vehicle conditions, the authors imposed a temperature profile. A period of 8 h denoted as "cooling period", 8 h for "road delivery period" and 8 h for "door opening period". During the first stage, the upper face of the multi-layer, which represents the insulation side facing the external environment, was set at 10 °C. During the "road delivery period" the temperature was constantly increased up to 30 °C for 2 h, then maintained at 30 °C for 4 h, and then constantly decreased down to 10 °C for the other 2 hours. Finally, during the last period, a temperature of 10 °C was set. The lower face, representing the interior insulation wall face, was maintained at 0 °C for the first two stages (16 h) and then set to 10 °C during the "door opening period". The

authors numerically analyzed, in COMSOL environment, different scenarios by varying the thicknesses of the three layers making the insulation multi-layer. They verified that by inserting the PCM layer as closer as possible to the layer representing the vehicle exterior, the maximum reduction of the energy entering the cold space could be achieved (74.9 Wh m^{-2} against 78.2 Wh m^{-2}), since the cooling PCM capacity was exploited, correctly.

2.3.2 Refrigeration system equipped with PCM

In this section, the works regarding the adoption of the PCM as an integral part of the refrigeration system of a refrigerated vehicle are reported.

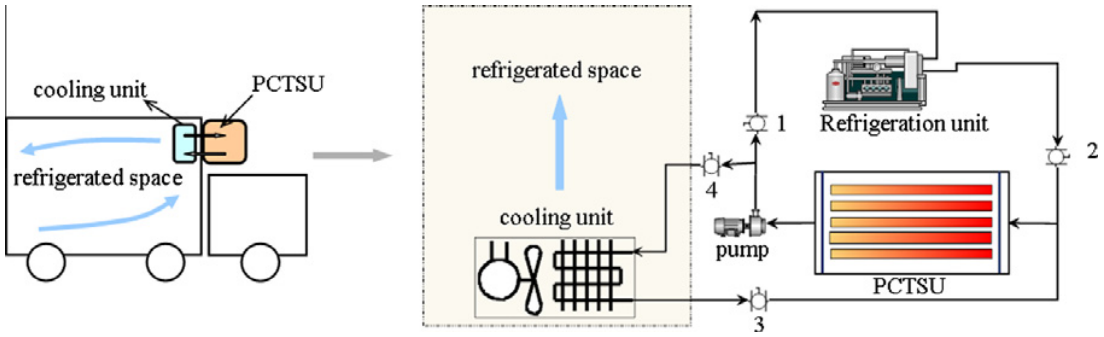

Figure 2.15 PCTSU developed by Liu et al. [26]

A novel refrigeration system concept for refrigerated trucks was proposed by Liu et al. [26]. As shown in Fig. 2.15, the system consists of an insulated Phase Change Thermal Storage Unit (PCTSU) in which the PCM is encapsulated inside flat containers. A new PCM was prepared, that is an inorganic salt aqueous solutions having melting and solidification points of -26.7 °C and -30.6 °C, respectively. The PCTSU is connected to an external electrical refrigeration unit which aims at freezing the PCM when the truck is stationary in the depot by means of a heat transfer fluid (Dynalene HC-40). On the contrary, during operation, the PCTSU is linked to a cooling unit which is located inside the refrigerated space. By adopting a thermostatically on/off controller the temperature inside the refrigerated cell is maintained at -18 °C. The air is cooled down by the HTF circulating between the PCTSU and the cooling unit. The authors aimed at ensuring the appropriate target temperature for frozen food transportation for 10 h of a hot summer day in Adelaide (Australia). By means of the TRNSYS simulation program the authors considered the operating time from 8 AM to 6 PM. If a refrigerated space of 4.2 m x

2.4 m x 2.2 m is supposed, a total of 360 kg of PCM is required, by encapsulating it in 27 PCM container of 0.96 m x 0.52 m x 0.02 m, with a gap of 4 mm between two adjacent containers. The potential of this system is the possibility of reducing energy cost and GHG emissions. Nonetheless, lower noise and maintenance required levels can be accomplished. Being the system employing an electrical stationary refrigeration unit, a more efficient and reliable cooling process is accomplished. The risks deriving from potential refrigeration leakages are also reduced. By using TRNSYS an annual refrigeration load of 4380 kWh was estimated. In this value, among several assumptions, 10 door openings/day and an average annual temperature of 17 °C were supposed. By considering different factors, such as the cost of diesel and energy (off- or on-peak) and the efficiency of the system (COP 1 or 1.5) or diesel engine (0.2) the authors estimated up to 86.4% cost reduction (off-peak fee and COP=1.5). More specifically, when a COP=1 and on-peak electrical fees are considered, 51% of cost savings can be reached. If COP=1.5, the reduction can increase to 67.3%. Finally, when an off-peak fee and lower COP (1) are taken into consideration, almost 80% reduction in cost can be materialized compared with a traditional diesel-based refrigeration unit. Besides, the authors reported that a cooling system for a refrigerated truck usually weighs around 370 kg, comparable with that of the proposed PCM-based system.

The potential of the innovative system developed in [26] was demonstrated and further developed in [71]. By assuming a typical refrigerated van, the daily cooling loads were estimated using TRNSYS. In particular, the transmission loads through roof, floor and walls, the heat load due to cooling unit equipment (fan motor, pump motor, etc.), the product load and the infiltration of the air during the door-opening periods were taken into consideration. A fully charging period of 8 h during the off-peak electricity fee period, that is from 11 PM to 7 AM, was supposed. Based on the climate data for the city of Adelaide (Australia), the maximum and the minimum loads were calculated. When considering the maximum heat load without door openings, it was obtained that from 8 AM to 9 AM of 14th of February, the cooling unit was able to cool down the refrigerated space from 25 to -18 °C by keeping the maximum pump speed. Just by regulating the pump speed, the temperature is maintained at -18 °C for an additional 10 hours, ensuring the suitable conditions for frozen foodstuffs carriage. When the entire PCM in the PCTSU released its latent heat, the refrigerated cell temperature started to grow. If 20 door openings lasting 36 s each with an interval of 30 min between two subsequent openings were assumed, the cooling system would require an amount of PCM equal to 390 kg to ensure the desired safe conditions. In this situation, it was found that the temperature increased up to 8 °C during the door-opening period and, the additional cooling energy

requested to the PCTSU was accomplished by increasing the pump speed to recover the appropriate conditions. By tuning the PCTSU size, and the PCM amount consequently, the innovative system can be adapted for refrigerated van, trailer, or truck. For this latter, the PCM mass can be as high as 1000 kg if 20 door openings are considered. Since the refrigeration unit doesn't work when the refrigerated vehicle is in operation, the developed system can be assumed as a passive solution. In fact, the cold source is represented by the PCM and the only pieces of equipment consuming energy are the fan and pump motors; contributing only to a small fraction of the entire energy consumption of a refrigeration system.

An air heat exchanger containing the PCM, located inside the refrigerated space, and coupled with a traditional refrigeration system was, instead, developed and proposed by Principi et al. [77]. In particular, an air heat exchanger, consisted of six PCM flat aluminum containers encased in a polystyrene channel, was located close to the evaporator, as shown in Fig. 2.16.

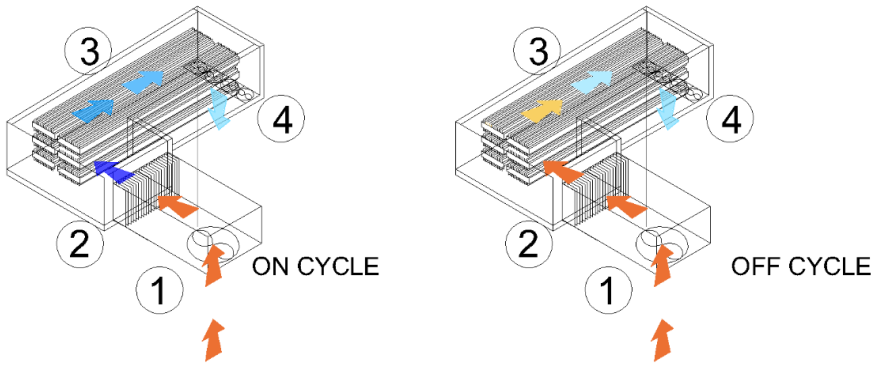

Figure 2.16 PCM based air heat exchanger (3) close to the evaporator of the refrigeration system (2) [77]

Each PCM container has dimensions of 1.00 m x 0.03 m x 0.14 m. Moreover, since the temperature target inside the refrigerated space was set to the carriage of fresh products, the paraffin RT5HC with melting temperature of 5 °C, close to desired operating conditions (refrigeration unit is in operation to ensure the inside temperature level between 0 °C to 8 °C), was selected. A total of 19.15 kg of PCM was contained inside the air heat exchanger. A cold room (2.2 m x 1.4 m x 1.4 m), having 10 cm of polyurethane foam insulation layers equipped with a 1140 W cooling capacity unit was assumed as the refrigerated space of a refrigerated transport application. To investigate extreme conditions, the cold room was located inside a climate room maintained at 32 °C. The aim of the system was to enhance the energy performance of the refrigerated transport application by reducing the temperature fluctuations inside the refrigerated space under high external ambient temperatures. When the compressor was activated, the cold air exiting the evaporator passed through the air heat exchanger freezing

the PCM. In fact, the average air temperature inside the refrigerated space was calculated to be 5 °C when the PCM was employed scenario and 3.68 °C for the reference case. During the OFF-time, the heat gain from the environment was absorbed by the PCM, lowering the temperature increase. Moreover, the ON-time of the compressor was prolonged with PCM, but its ON/OFF-cycles were reduced. The authors stated that, by considering a reference period of 2 h, thirteen ON/OFF compressor cycles were needed for the traditional configuration, against six for the PCM system. The refrigeration unit efficiency increase led to a 16% reduction of the total electric power consumption, suggesting consequent reduction in GHG emissions.
The concept of installing PCM just after the evaporator of the cooling system of a small truck was also taken on by Ben Taher et al. [80], as shown in Fig. 2.17.

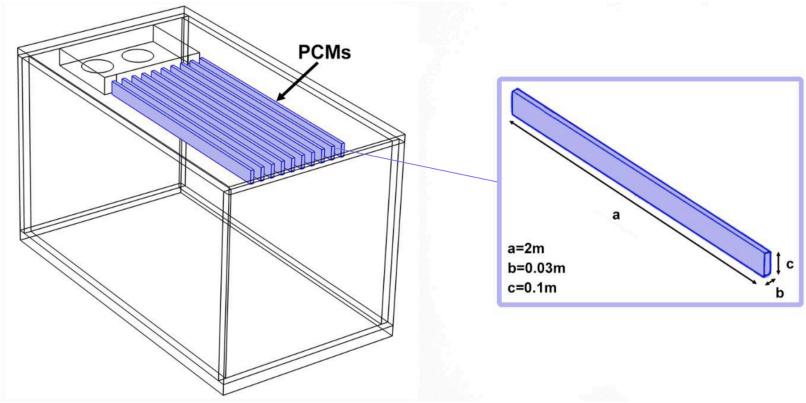

Figure 2.17 Small truck equipped with PCM rods [80]

The authors numerically investigated the cooling performance of ten aluminum rods (2 m x 0.03 m x 0.1 m) encapsulating PCM, mounted on the ceiling of a small truck (1.6 m x 1.7 m x 3 m). The truck presented 10 cm of polyurethane foam insulation on the floor and 7 cm thick insulation layer on the other walls, being designed for the carriage of fresh perishable products (maximum temperature admitted: 12 °C). Moreover, the authors analyzed the effect of 15 min door openings after 60 min of refrigeration unit operation and compared the performances with or without the PCM. Firstly, the adoption of paraffin wax RT8HC was suggested. It was found that the PCM significantly lowered the temperature fluctuations inside the refrigerated space. In fact, as already demonstrated in [77], the cold air exiting from the evaporator is heated due to the effect of freezing the PCM before being released in the cold space. This let the cold space to be cooled down from 20 °C to 1 °C, and from 20 °C to 2 °C for the reference and PCM scenarios, respectively. Besides, when considering the door openings period, the mean cold temperature increased from 1 °C to 17 °C for the reference truck, and from 2 °C to 11 °C for

the truck equipped with PCM rods, with consequent beneficial effects for the carried foodstuffs. The authors also simulated a long route scenario, that is with multiple close/open doors cycles (10 cycles) and, the performances of other two paraffins were investigated (RT3HC and RT5). It was revealed that RT5 is more suitable for middle distance route in which products like industrial milk, butter, and meats are transported. RT5, in fact, after the fourth close/open door cycles stabilized the temperature inside the refrigerated cell at 6 °C. The best performance was, instead, achieved through the employment of RT3HC. With RT3HC, the air temperature was maintained at 4 °C for a longer time, suggesting this PCM for the transportation of highly perishable foodstuffs. In terms of required cooling energy reduction, savings of 35%, 57%, 61% can be addressed when RT8HC, RT5, RT3HC are employed, respectively.

The ability of the PCM of ensuring suitable storage and transport temperature was also investigated by Orò et al. [69]. The authors wanted to analyze the thermal behavior of a "non-refrigerated" chamber, that is a space where the cooling is provided only by the phase change material. In particular, focusing on the refrigerated transport sector, the authors referred to non-refrigerated vans whose main aim is maintaining the temperature of frozen cargos only by the action of the insulation layer. A vertical freezer (370 L), with a 5 cm polyurethane insulation, was selected to replicate a small-scale van or other perishable products transportation units. Two different PCMs were studied to choose the one that ensured the best performance: Climsel C-18 (melting temperature -18 °C) and Cristopia E-21 (melting temperature -21.3 °C). The PCM was encapsulated in seven stainless steel containers ($1.3 \cdot 10^{-3}$ m^3 each) and located on the food trays evaporator. Moreover, to investigate a real transportation scenario, product load was considered during the experiments, by inserting a total of 42 kg of M-packs. The freezer was placed into a climate chamber maintained at 25 °C to approximate the average European summer temperature. To evaluate the cooling performance of the PCM, the freezer was cooled down to -22 °C and then the electrical power was switched off. Significant improvements in lowering the temperature in the cold space to increase were calculated. The time to reach 0 °C was used as parameter to compare the different performances. It was obtained that in the reference scenario (without PCM) the system took 1.5 h to reach 0 °C, whilst 6.5 h and 8 h when C-18 and E-21 were employed, respectively. The reference cold chamber needed 11.5 h, against the one equipped with PCM which took 15.6 h and 21 h for C-18 and E-21, respectively. Moreover, against the two different PCMs, E-21 ensured that the air temperature could be maintained at colder values (between -16 °C and -12 °C) than C-18. The results suggest that the employment of PCMs for cold transportation can effectively enhance the transportation

health conditions for perishable food carriages, by contemporary mitigating the polluting emissions.

A real scale refrigerated transport application was developed and experimentally analyzed by Tong et al. [81]. In particular, the passive cooling performance of an integrated rail-road cold chain container equipped with PCM was investigated. As shown in Fig. 2.18, the container is linked to an external charging facility, which consists of an electrical refrigeration unit, a heat transfer fluid (25 wt% Ethylene glycol acqueos solution) storage tank and a pump. A charging loop connects the PCM contained in ten cold TES plates (126 kg each) and the charging facility, to freeze the PCM.

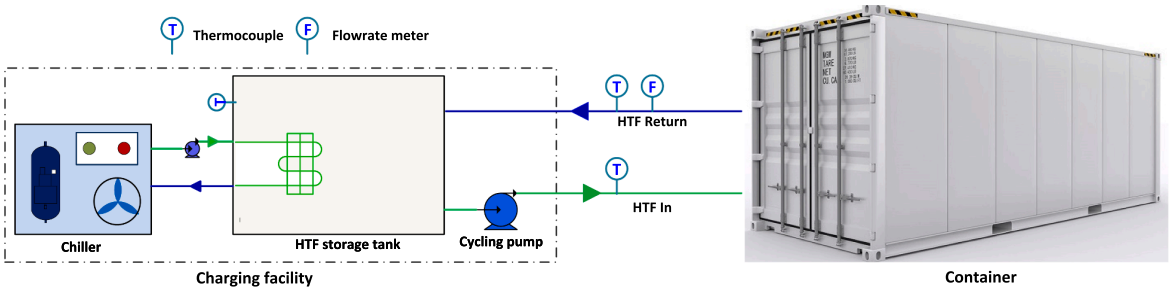

Figure 2.18 PCM-equipped container linked to the charging facility [81]

The cold TES plate (1.8 m x 1 m x 0.1 m) consists of aluminum shell and embedded finned tubes. The container (12.92 m x 2.43 m x 2.896 m) is insulated by 0.1 m of polyurethane foam insulation material. Inside the container, nine TES plates are distributed on the ceiling, and one plate is mounted on the face opposite to the opening doors. Aiming at transporting fresh perishable products, the paraffin wax RT5 was selected as the best candidate, having a melting point of 4.96 °C and latent heat of 180 kJ kg^{-1}. To evaluate the system performance as a whole, different performance indicators were proposed, such as: charging rate, charging efficiency, system COP, energy consumption, cost reduction, emission reduction, and food quality indexes [81]. It was found that with a HTF previously cooled down to -5.5 °C, the charging system needed 6 h to freeze the PCM. As it can be deduced, the charging rate was faster during the initial stages when a great temperature difference between PCM and HTF occurred, then becoming slower. By considering the cold energy stored in the cold plates (PCM and aluminum encapsulation), moist air inside the refrigerated space and the HTF left in the cooling loop, an efficiency of 38.6% was calculated. The authors attributed this value to the long charging time which caused cold energy losses. However, if considering the system COP for the passive discharging process a value of 1.84 was estimated. This value, higher than the COP of

traditional diesel-based refrigeration systems (COP ranging between 0.5 and 1.5), could be due to the constant operation of the large-scale chiller (without on/off cycles which normally occur during the cooling process in a refrigerated vehicle). Additionally, the proposed refrigerator was connected to the grid electricity, which improved the energy efficiency. The passive cooled container could maintain the temperature at an appropriate value (between 4 °C and 12 °C) for the entire 94.6 h route, despite facing very different external conditions (temperatures ranging between 13 and 35 °C). Compared to a diesel-powered refrigerated container, 86.7% reduction in the energy consumption can be achieved. This translates into an emissions reduction up to 78.5%. Four different food cargos, with different quality indexes, were considered: leaf lettuces, lettuces, strawberries, and mangoes. It was reported that the food quality was ensured. A complete analysis regarding the time evolution of relative humidity (RH) was assessed [81]. It was found that the innovative passive solution kept RH always between 80% and 90%, which is an optimal range for the transportation of fruit and vegetable crops. Moreover, the traditional cooling systems generally lead to lower RH values compared to PCM solution. The reason for the optimal RH performance was due to the fact that the passive system reduces the latent air heat transfer.

Liu et al. [96] developed a Phase Change Cold Storage Unit (PCCSU) and installed it inside the insulated compartment of a refrigerated vehicle, as depicted in Fig. 2.19. The PCCSU cools down the refrigerated space at different refrigerated temperatures, by setting different temperature configurations depending on the carried foodstuff. The novel unit is cooled down when the truck is stationary by exploiting the off-peak period, in order to make the cooling process more efficient and cost-effective.

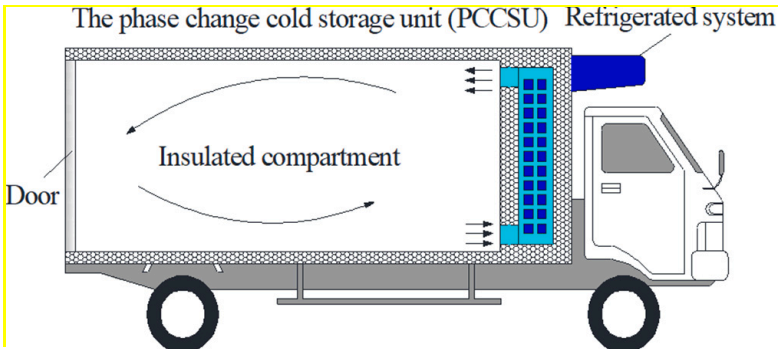

Figure 2.19 The Phase Change Cold Storage Unit proposed by [96]

The PCCSU consists of 24 stainless steel PCM plates, having a thickness of 3 cm and they are cooled down by the on-vehicle refrigeration system. When the truck is in operation, the cooling

process relies on fans which blow the air through the PCCSU being cooled down before entering the cold space. To be as close as possible to the temperature needed for the transportation of frozen products, three different target values of -14 °C, -16 °C, -18 °C were selected. Additionally, a PCM having a melting temperature of -30 °C with a latent heat of 175.3 kJ kg^{-1} was chosen. To assess the feasibility of the idea, the authors installed the proposed PCCSU inside an insulated container (5.00 m x 2.04 m x 2.00 m, internal dimensions) consisting of a 0.12 m thick polyurethane insulation layer and tested it experimentally. The mass of PCM was equal to 275 kg. Varying external temperature conditions were faced during the experiments, resulting, however, in an average external temperature of 29 °C. The set up could maintain the suitable conditions inside the refrigerated space for 16.6 h, 14.7 h, 10 h, presenting an average internal temperature of -12.3 °C, -14.5 °C, - 16.5 °C, when the target temperature of -14 °C, -16 °C, -18 °C were selected, respectively. Moreover, an economic analysis was conducted to verify the financial sustainability of the investment. Assuming that the truck was in operation between 8 AM to 6 PM, for 365 days per year and by considering 10 door-openings per day, the energy cost of the new PCCSU was compared with the traditional diesel engine-driven refrigeration units. It was reported that by adopting different COP values (0.5 – 1 – 1.5) and off-peak, basic, or on-peak energy fees, an energy cost reduction from 15% to 91% could be obtained, making the proposed solution as a promising one.

Ahn et al. [82] proposed an innovative cooling system for refrigerated trucks, consisting of an ice-making unit (IMU) used for the charging phase and a mobile air-cooling unit (MCU) during the discharging phase. In this concept, the phase change material role is played by the ice. In Fig. 2.20 the schematic of the mobile cooling system can be appreciated. The novelty of the proposed solution lies in the direct contact discharging process: in fact, the PCM is not encapsulated, and a direct cooling mechanism between the air to be cooled down and the ice occurs.

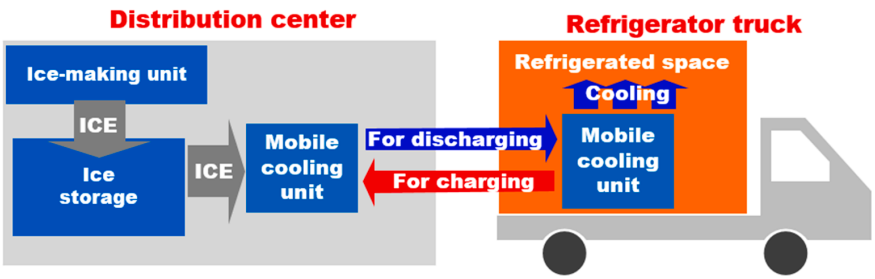

Figure 2.20 Mobile cooling system [82]

As shown in Fig. 2.20, the refrigeration unit, which is located in the distribution center, stores the cooling energy during the day, by generating ice cubes of different sizes. The MCU from the truck moves into the distribution center to be refilled with new ice cubes and then returned to the cooling cell of a refrigerated truck. A small-scale lab test apparatus was built to analyze the performance of the cooling system by varying the mass of the ice cube, the face air velocity, the amount of stored ice, the mass of an ice cube, and the inlet temperature. The COP for the IMU and a global COP which considers the entire cooling process (discharging and charging) were used to evaluate the integrated system performance. By considering only the ice-making unit, the COP of a 6.8 g ice cube was 28.5% higher than that for 10 g ice cube. The main role is played by the face air velocity and the amount of ice, with the highest COPs pertinent to 1.28 m s^{-1} and 6 kg. However, the COP was affected by the variation in the ice cube mass. The system average cooling capacities at 30 °C were 472.4% higher than those at 10 °C. Moreover, by evaluating a modified COP which considers the integrated system IMU and MCU, it was found that the ice mass cube strongly affected the power consumption of IMU and the fan power consumption of MCU.

The last concept to be presented here is the one proposed by Tan et al. [68]. The authors investigated the possibility of coupling PCM (water) and the cold energy recovery coming from Liquefied Natural Gas (LNG) refrigerated vehicles. In particular, a cold storage unit (CSU) was located and mounted at the ceiling of the refrigerated space. The CSU was insulated by 50 mm thick polyurethane foam and presented a cavity of 1.00 m x 0.15 m x 0.20 m hosting the PCM. A 1-m-long copper tube having an outer diameter of 20 mm and a thickness of 1 mm was immersed inside the CSU acting as a cold storage to freeze the PCM. Internally, the tube was cooled down by the cryogenic nitrogen gas which absorbs the heat from the (solidifying) water outside the tube. To improve the heat transfer performance, wave-like fins were added internally the tubes. The schematic of the proposed system can be appreciated in Fig. 2.21.

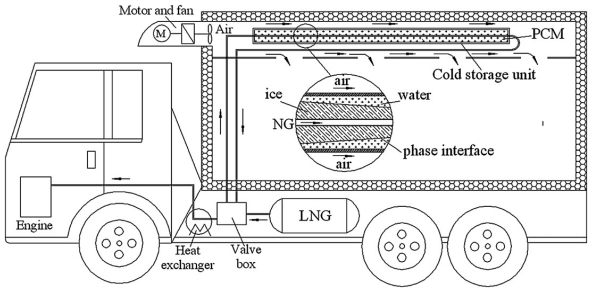

Figure 2.21 LNG refrigerated vehicle coupled with the cold storage unit [68]

By means of a valve box, the LNG fuel circulates into the CSU and then evaporates. The superheated gas returns to the heat exchanger before being directed to the engine for combustion. To cool down the refrigeration space, the air is blown by a fan outside the CSU before being admitted to the refrigerated space. A comparison between this new concept and the standard one was not presented, nevertheless, significant emission reduction can be anticipated.

2.3.3 Eutectic plates

Eutectic plates can be considered as the most mature alternative to the conventional refrigerated unit installed in refrigerated vehicles as they have already found application in the market. It usually involves the use of eutectic mixtures made of sodium chloride and nitrate water solution [73] having very low melting points. The eutectic plates technology is also reported and regulated by the ATP agreement [29]. Therefore, in this section, only a few recent works, covering the use of eutectic plates into refrigerated container [73], refrigerated truck [79], medium refrigerated transport [126], and refrigerated truck trailer [127] are reported aiming at showing the application of this technology in refrigerated vehicles of different sizes.

Sepe et al. [73] applied FEM to study an innovative 20 feet refrigerated container equipped with PCM contained in eutectic plates for the carriage of fresh (between 1 °C and 4 °C) and frozen (from -20 °C to -18 °C) products. Moreover, the authors designed a passive equipment connected to a remote-control system and shaped air channels to ensure the cool air circulation and the stabilization of the internal temperature at the desired level. Different PCMs were evaluated to fill the eutectic plates and E-26 was finally selected due to its high latent heat value (260 kJ kg^{-1}) and relative low cost. Six eutectic plates were mounted on the ceiling of the refrigerated compartment. By means of fans, having 0.2 m diameter, 0.10 m^3 s^{-1} of air pushed through the cold plates and then is released into the cold space. Moreover, the air flow can be regulated to ensure a certain thermal gradient. All the information regarding container position and conservation status of cargo were monitored and registered by an electronic control system during the route. The container was insulated by a composite insulation wall consisting of polyethylene terephthalate (PET) foam sandwiched between thermoplastic matrix and glass fibers. The PET foam was selected aiming at limiting algae or bacteria growth, ensuring contemporary high structural property. It was found that this innovative PCM-based container can maintain the temperature inside the cool space at the desired level for almost a week. Moreover, the employment of fans and air duct ensured a good circulation of cold air,

maintaining the relative humidity at suitable values. Besides, the new panel wall resulted in light and environmentally friendly design composed of recyclable material.

The installation of eutectic plates into a 6-ton refrigerated truck was instead proposed by Mousazade et al. [79]. In particular, the refrigerated box had dimensions of 2.05 m x 2.2 m x 4.8 m and was equipped with 6 cold plates and insulated by sandwich panels whose core consisted of 10 cm traditional polyurethane foam. Each cold plate was made of a parallelepiped macrocapsule (1590 mm x 690 mm x 52) hosting the PCM and the 18 m long coil pipe. During the refrigeration period, that is the time needed to freeze the PCM, an expansion valve lets the refrigerant of the cooling unit (5.5 kW nominal power and COP = 3.5) to pass through the coil pipe inside the cold plate. The condensing unit was not incorporated on board, therefore, after the refrigeration period, the refrigeration system was detached from the vehicle and only the cold plates ensured the cooling enroute. The performance of three different eutectic solutions (E-26, E-29, E-32) was tested at four diverse truck speeds (80 km h^{-1}, 90 km h^{-1}, 100 km h^{-1}, 110 km h^{-1}) and the overall heat transfer coefficients were calculated.

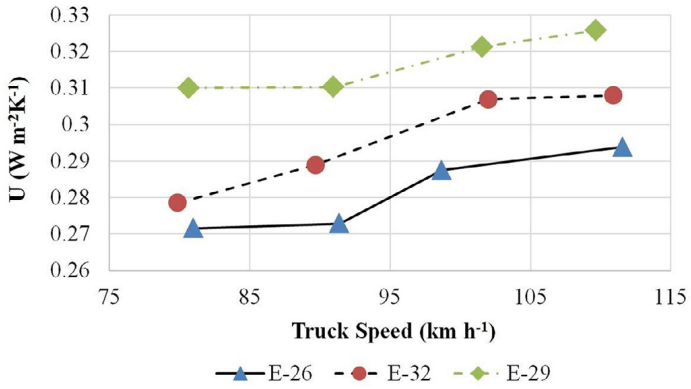

Figure 2.22 Overall heat transfer coefficient varying with the truck speed [79]

As per Fig. 2.22, an increasing trend in the overall heat transfer coefficient versus the truck speed was reported. This phenomenon can be attributed to the external convection that promotes heat transfer. The minimum heat transfer coefficient was obtained for E-26 at about 80 km h^{-1}. By monitoring the air temperature in the refrigerated compartment, the authors found a plateau at the melting temperature followed by a temperature rise increase after the melting was completed. Since among the different investigated PCMs, E-26 presented the lowest U values for all the diverse truck speeds, it ensured the longest keeping of appropriate transport conditions of frozen foods. It had, in fact, the longest melting time for all the investigated scenarios compared with the other eutectic solutions, due the lowest gradient between external

and internal temperatures. Nevertheless, by considering concurrently the melting time at different truck speeds and the truck speeds themselves, the travelling distance (that is, the distance in which the suitable temperature is maintained) can be calculated. It was found that the longest travelling distance (almost 500 kg) was accomplished by E-26 at 110 km h^{-1}, since the higher vehicle velocity compensated the lower melting time.

A eutectic plates-equipped medium refrigerated vehicle was numerically analyzed by Radebe et al. [126]. In particular, the eutectic plates position was investigated aiming at finding the best configuration for the carriage of agricultural products. The best configuration contained two eutectic plates located on the ceiling of the truck insulated compartment keeping the temperature at 0 °C for five hours. For agricultural goods, entering at 15 °C, a refrigerated space temperature of 0 °C can be considered a suitable temperature level for transportation.

Numerical analyses aiming at investigating the heat transfer and fluid flow behavior of air of a refrigerated truck trailer equipped with eutectic plates were performed by Jeong et al. [127]. The authors focused on the door opening period. Different cold plate configurations were evaluated by setting the cold plates in a series mode opposite to the door openings or in series at the ceiling of the refrigerated compartment, as shown in Fig. 2.23.

The numerical analyses were conducted by running 2D simulations in CFX Ansys v19 environment. An external air temperature of 293 K was fixed. Moreover, the effect of the presence of the cargo, and the suction or blowing configurations of the fan were also investigated. Five boxes full of frozen meat were added in the truck trailer. The cold plates' temperature was set at -29 °C, as the typical melting temperature of a eutectic mixture. When the compartment was empty of foodstuffs, it was found that the best configuration dealt with the cold plates set in series at the ceiling. In this configuration, recirculation zones could be detected which prevented the hot air to infiltrate from the outside environment. This recirculation zones were cut off when the cargo was added. Moreover, when the eutectic plates were at the ceiling level, the presence of the cargo caused blockage of air and therefore a pre-existing flow inside the trailer was found. The consequent effect was the possibility of the external hot air to find preferrable paths to enter quicker inside the cold compartment. As a result, the higher maximum temperature for the foodstuff was observed. Nevertheless, by considering that during the route the amount of cargo boxes progressively decreases, the authors stated that the configuration showing the cold plates mounted at the ceiling can improve the performance since, as the number of cargo boxes decreases, it tends to reach the empty cargo scenario.

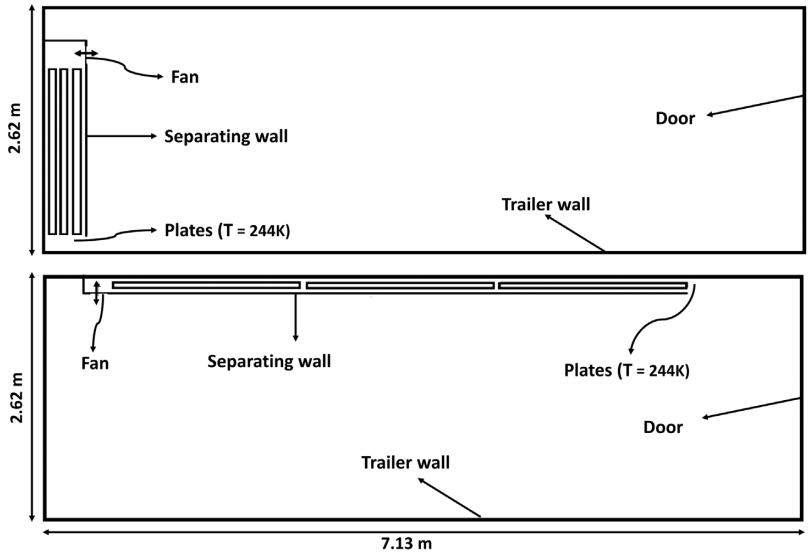

Figure 2.23 Different cold plates positions [127]

2.4 Phase change materials in cold storage boxes for distribution of perishable products

As stated in the introductive section, the distribution of the temperature sensitive products is a crucial activity which usually occurs during the last stages of the cold chain. Appropriate distribution conditions are fundamental to ensure the safety and the quality of the products to the final consumers. The perishable products delivery is normally accomplished by the employment of insulated box or specific packages which preserve the products themselves. As reported in the previous section, some passive system involving the adoption of phase change material for refrigerated transportation have been developed demonstrating promising results. The same concept may be applied for a cold storage box: the integration of PCM to improve the cooling capacity maintaining the suitable product temperature during the distribution.

A cold storage package was experimentally and theoretically investigated by Kozak et al. [85]. In particular, two different packages were tested. The smaller package consisted of a 4 mm thick fitting cardboard box (32 cm x 25 cm x 25 cm), a high-density polystyrene insulation layer which formed a cylindrical cavity in which a double wall plastic container was inserted. The plastic container hosted a green aqueous salt solution PCM (melting temperature of -10 °C) in the double wall cavity, leaving space for the products in the inner cavity. On the contrary, the larger box consisted of a 4 mm thick cubic cardboard box (side of 50 cm), a high-density polystyrene insulation layer with a cylindrical cavity to host 4 arched bottles filled by purple aqueous salt solution PCM (melting temperature of -33 °C) which wrapped a cylindrical plastic

container of the delivered product. The water was selected as the product to be transported by means of the cold boxes. The PCM was cooled down to -70 °C in order to ensure its complete solidification, and the experiments lasted until product temperature was close to the ambient one.

Based on experiments, a one-dimensional analytical model was developed. Moreover, one- and two-dimensional numerical models were developed in Ansys Fluent 13 environment. The theoretical analysis based on the analytical and numerical models aimed at finding the best configuration among the different parameters (as shown in Fig. 2.24) which prolonged the melting time finding the optimal insulation thickness. For additional details, the reader may refer to [85]. From the analysis, it was found that an optimal ratio between insulation thickness and PCM thickness existed which let to maximize the melting time. Moreover, the results revealed that the melting time is strictly affected by the ratio of the PCM thermal conductivity and insulation one. Almost negligeable dependance from Biot number was demonstrated

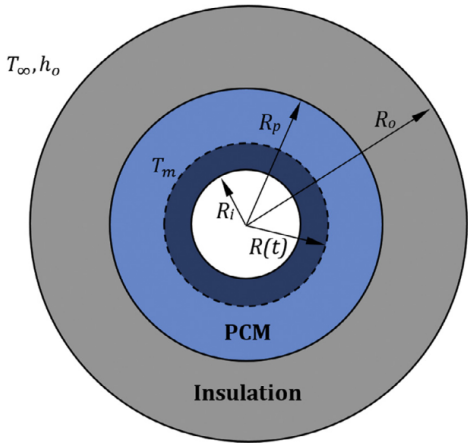

Figure 2.24 Analytical model [85]

All of these results must be carefully taken into consideration when designing an optimal cold box. Besides, the 2D numerical model carefully predicted the experimental results, and the authors stated it can be a useful instrument to support the design stage by investigating different materials, dimensions and operating conditions.

Huang and Piontek [86] developed a cold chain insulated box for the transportation of perishable products at a temperature level ranging from 2 °C to 8 °C. The authors improved the box performance by the insertion of PCM.

As shown in Fig. 2.25, the insulated box (540 mm x 420 mm x 480 mm) had insulation walls which consisted of a triple layer of 10 mm poly-urethane foam, 10 mm vacuum insulation

panel, and 10 mm poly-urethane foam. Two different PCMs (water and OP5E, melting point 0 °C and 5 °C, respectively) were encapsulated into two different high-density polyethylene slabs having dimensions of 350 mm x 290 mm x 15 mm. Since the PCM equipped insulation box aimed at keeping the desired temperature (2 °C to 8 °C) under diverse external conditions, three scenarios were investigated: *extremely high temperature condition*, during which the water and OP5E started at 0 °C and 5 °C, respectively, with chamber temperature of 35 °C; *extremely low temperature condition*, during which only OP5E panels were adopted and the controlled climate room temperature was set at -20 °C; *alternating temperatures condition*, during which the external temperature was set at 35 °C for the first half and -20 °C for the last half.

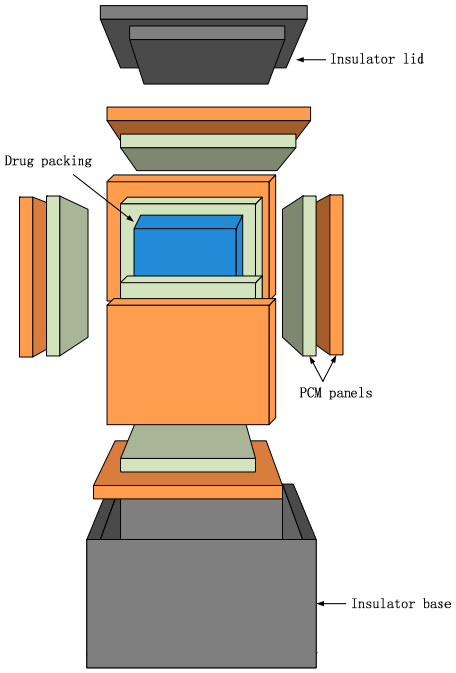

Figure 2.25 PCM based cold chain insulated container [86]

When adopting only water as PCM, it was found that under extremely high temperature condition, the air temperature inside the cold box can be maintained at the appropriate level for more than 78 h, whilst only 54 min with the box empty of PCM. Moreover, the addition of OP5E layer assured the air in the cold space to be maintained under 8 °C for 81 h. Under extremely low temperature the box ensured the suitable transport temperature for only 62 min. The addition of the water slabs let the temperature to be lower than 2 °C after 10 h, whilst the combined effect of OP5E and water assured 102 h of appropriate air temperature level. Under alternating external temperatures, it was found that OP5E and water ensured the temperature

between 2 °C and 8 °C for 100 h. In [86] it was shown that the right PCM selection is crucial to contribute to the extension of the shelf-life of perishable products during the transportation. The importance of the appropriate PCM coupled with the optimal PCM arrangement for the cooling performance of a cold energy storage portable box was deeply analyzed by Du et al. [87]. The box had external sizes of 430 mm x 285 mm x 345 (length x width x height). Five different configurations were studied by varying the PCM location maintain the same PCM amount (1371.75 cm^3): case 1 presented the PCM entirely located at the box ceiling, case 2 20% of PCM on the four sides and 20 % on the top, case 3 25 % of PCM distributed on the four sides, case 4 20% of PCM on the four sides and 20% on the bottom, and, finally, case 5 having the PCM entirely located at the bottom of the box. Different performance indexes were proposed such as the cooling time, that is the time in which the central box temperature remains under than 8 °C (temperature limit for the transportation of fresh perishable products), the discharging efficiency, i. e. the amount of provided cooling energy against how much of it could have been provided, and, the discharging depth, that lets to quantify the amount of cold energy remained in the cold plates.

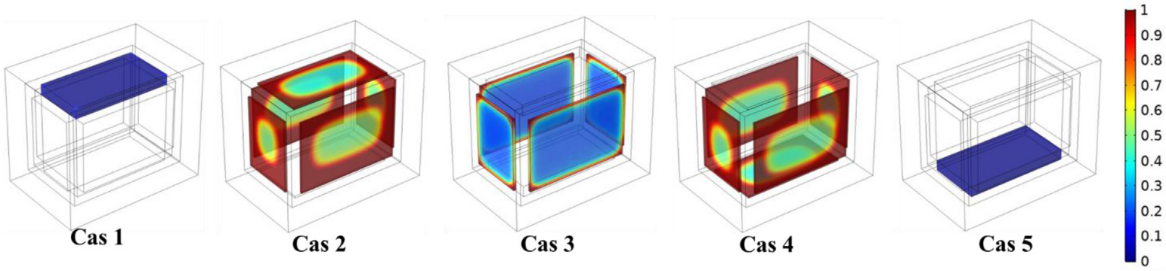

Figure 2.26 Liquid fraction for the five different investigated cases in [87]

By employing the wax paraffin RT5HC as PCM, it was found that, under an external temperature of 25 °C, the longest cooling time (9.5 h) could be reached by considering the PCM equally distributed on the top and sides of the cold box (case 2). Case two also showed the highest discharging depth value (74.1%). In fact, by observing Fig. 2.26, in the case 2 configuration, almost melted PCM can be found in the cold plates, suggesting the appropriate exploitation of the cooling energy which can be supplied by the phase change material. By fixing configuration 2, the effect of other wax paraffins were tested (RT0, RT2HC, RT3HC, RT4, RT8HC, with 0 °C, 2 °C, 3 °C, 4 °C, 8 °C melting points, respectively). It was found that the lower melting point led to a higher discharging depth and longer cooling time consequently. Moreover, a lower melting time ensured a higher thermal difference between external and internal temperature which caused higher heat transfer rate. Therefore, the best trade-off was

obtained by employing RT2HC. Finally, by modifying the insulation material, changing from traditional poly-urethane foam to vacuum insulation panel (VIP), a longer cooling time was reached (46.5 h against 9.6 h).

Similarly to Du et al. [87], Burgess et al. [97] aimed at optimizing a portable phase-change material storage system for cold chain delivery fresh foodstuffs applications. In particular, the authors evaluated three different layouts, by locating the PCM containers on the top and bottom of the box (layout 1), only along the sides (layout 2) or uniformly on top, bottom and sides (layout 3). To assess the best solution, the ability of the system to maintain the majority of the contents under 5 °C was chosen as an important performance indicator for the comparison. The authors firstly run experiments by adopting the "layout 1", i. e., by using PCM bricks (total amount 2 kg) on top and bottom of the box (internal dimensions: 500 x 300 x 180 mm^3). The cold space was filled with M-Packs and filler packs to replicate the fresh cargo. The temperatures at different locations were monitored over time and a numerical model in Ansys Fluent was developed and validated based on the experimental results. Therefore, the different layouts were investigated, and it was found that the uniformly distributed PCM let to reach the longest time under the temperature threshold of 5 °C (15.8 h). This value is significantly higher if compared with the reference case (without PCM) which ensured the suitable conditions for 5.3 h only. Nevertheless, "the layout 3" presented a significant temperature deviation (± 5.64 °C). The best performance in terms of temperature uniformity among the contents was obtained by adopting the "layout 2" configuration. This result shows that when designing the best cold storage box, the content typology must be considered: for example, for high-value perishable products (such as medicines, etc.) the local temperature uniformity inside the cold space (without hot spots possibly) is more important than the average value of the cold space temperature under a specific threshold. Moreover, the authors analyzed the effect of four different PCMs, water, potassium sorbate (PS), tetradecane + ducosane (TD) and tetradecane, having different melting points and latent heat values. It was found that the highest latent heat let to prolong the time the system was under the temperature threshold, while a lower PCM melting points permitted to obtain a higher discharging efficiency but temperature inhomogeneity contemporary.

The thermal performance enhancement of a portable box equipped with phase change material (PCM) was also studied by Nie et al. [88]. A composite PCM was developed, consisting of RT5, fumed silica (SiO_2) and graphene. The cold box presented external dimensions of 460 mm x 300 mm x 340 mm (length, width, height, respectively) having 30 mm of poly-urethane

foam insulation material on the walls. A total of 8 high-density polyethylene PCM containers (28 mm x 120 mm x 190 mm) were inserted inside the cold box: four at the top, and the rest in proximity of the internal walls. The amount of the adopted PCM was 2.64 kg. Bottles filled with water (2 L) were used as the transported temperature-sensitive product. The PCM were frozen by means of a freezer having -19 °C as set point temperature. To evaluate the cooling performance of the PCM, the box was set in a climate chamber maintained at the temperature of 30 °C. As done by Du et al. [87], the discharging phase ended when the transported goods reached the temperature of 8 °C. As Du et al. [87], the cooling duration index was adopted to evaluate the cooling performance. Moreover, the charging and overall energy efficiencies were calculated. The former was formulated as the ratio between the sum of the sensible and latent heats exchanged by the PCM and the energy requested to cool down the PCM itself. The overall efficiency, instead, was defined as the ratio between the energy absorbed by the products (water) and energy consumed to freeze the PCM. As stated in section 3.4, the leakage occurrence is a great drawback when employing PCM, especially when dealing with food transportation. Therefore, by adding 4 wt% to the RT5 PCM, the authors found that the leakage issue might be overcome. Moreover, the composite PCM presented good cyclability, having thermophysical properties almost constant even after 200 cycles, with melting point close to 6.5 °C. By considering the cooling performance of the box, it was found that the pure PCM ensured 11.8 h of cooling time, whilst 11.35 h the developed composite material, since this latter had a slightly lower latent heat value (131.86 kJ kg^{-1}, against 143.74 kJ kg^{-1}). However, if focusing only on the charging time, the composite PCM presented a solidification time which was 11.5% shorter than the pure one, which increased the charging efficiency by 6.09%. Additionally, the composite PCM enhanced the overall energy efficiency by 12.58%.

With the aim of developing a phase change material with transition temperature between 2 °C and 8 °C to be employed in vaccine cold storage equipment, Zhao et al. [89] added expanded graphite (EG) into a mixed tetradecane (TD) and lauryl alcohol (LA) solution to obtain a new composite PCM. The insulation box had vacuum insulation panel as insulation material. The box possessed a shell with hollow plate structure, with the space inside the shell hosting the cold storage agent. The cold storage box (shown in Fig. 2.27) had dimensions of 200 mm x 95 mm x 55 mm. It presented a storage hole in which the vaccine reagent tube could be inserted.

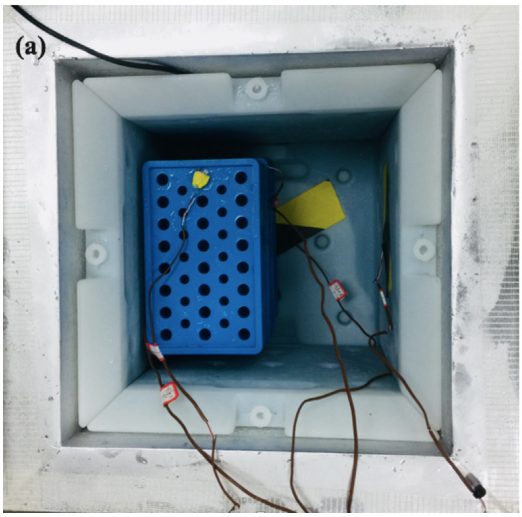

Figure 2.27 Cold storage box inside cold insulation box [89]

It was found that a so developed vaccine box could exchange the cold energy in a more proper way, keeping the temperature of each vaccine tubes at a suitable level and reducing the temperature fluctuations during the transportation. To evaluate the cooling performance, no-load and load scenarios were investigated. During the first scenario, three cold storage boxes were inserted in the cold insulation box with 6 cold plates arranged around. A varying external ambient temperature from 28.2 °C to 40.6 °C was detected. It was obtained a cooling time (time in which the temperature inside the box was maintained between 2 °C and 8 °C) of 47.73 h for the vaccine box. The top plate inside had a cooling time of 40.78 h. For the load scenario, yoghurt was inserted inside the box, due to its intrinsic temperature sensitive nature, being viscous and acid. The temperature between 2 °C and 8 °C was maintained for 52.36 h if considering the cold storage vaccine box, whilst only 44.05 h for the top plate, with an average cooling time of 46.04 h. The so developed new cold chain equipment ensured the required vaccine transportation temperature for a long-time, preserving its quality.

PCM to be employed in vaccine cold boxes was also analyzed by Ray et al. [90]. They numerically investigated the cooling performance when a temperature interval from -55 °C to -40 °C is required. The SP-50 PCM was selected as the best solution to accomplish the temperature constraint. By means of CFD analyses, two different portable cold storage boxes were studied by maintaining the same constituting materials and amount of PCM. Cuboid and cylindrical configurations were modelled. The cubic box presented polyurethane insulated walls distributed on the inner sides, having 394 mm x 290 mm x 350 mm as external and 324 mm x 220 mm x 270 as internal dimensions, respectively. By assuming the same insulation

material, the cylindrical container consisted of an outer diameter of 371.1 mm and internal one of 285.8 mm, with the gap filled by PCM. The numerical started with an internal temperature of -55 °C to ensure the PCM was completely solid, and the time in which the temperature was under -40 °C was monitored. Two different external summer conditions were considered and applied: a temperature of 45 °C or 30 °C. For both the scenario, the cylindrical configuration showed better cooling performance, due to low surface area to volume ratio of the cylinder. Under 30 °C, the cuboid box resulted in a cooling efficiency of 55.14% and cooling time of 15.4 h. On the contrary, the cylindrical box led to a cooling time of almost 19 h with a cooling efficiency of 60%. The authors reported that this type of passive regulation temperature can be adopted for the storage and transportation of highly temperature sensitive products, such as Covid-19 vaccines.

Liu et al. [98]developed a highly efficient cold box for smart cold chain logistics. They adopted an eutectic brine in Super Absorbent Polymer (SAP). The PCM brine consisted of potassium and ammonium chlorides dissolved in water. The homemade PCM had a melting point close to -21 °C with a latent heat of 230.62 kJ kg^{-1}. This novel PCM also presented relatively high thermal conductivity (0.589 W m^{-1} K^{-1}), high-cost effectiveness (0.00000763 \$ J^{-1}), negligeable supercooling and good cyclability. The PCM was located along the sides of the box and the cold storage times when transporting aquatic or biological samples were monitored. In the first scenario a cold storage time of 21.44 h was obtained whilst 16.37 h for the second case. Moreover, the authors provided temperature sensors and GPS position system in order to monitor the real-time thermal performance by an external device (as a smartphone, etc.)

A cold storage box for the transport of fruits, vegetables and other agricultural products was experimentally tested by Xu et al. [91]. Different PCMs were employed in order to verify which one ensured the desired conditions (temperature of cold space maintained between -5 °C to 8 °C). In particular, water (PCM1), water + 1 wt% sodium polyacrylate (PCM2), and water + 1 wt% sodium polyacrylate + 0.1 wt% multiwalled carbon nanotubes (MWCNTs) (PCM3) were adopted. All the PCMs had phase change temperature of about 0 °C. The PCM was contained in 4 polyethylene cold plates, inserted around the internal walls of a vacuum insulation box having external and internal size of 320 mm x 275 mm x 280 mm and 200 mm x 200 mm x 200 mm, respectively. The experiments were run with an external temperature of 15 °C ± 3 °C. The cooling capacity of the cold plates was investigated, and the experiments were stopped when an average internal temperature of 10 °C was reached. The effect of the presence of transported products was also analyzed by the insertion of four caps of yoghurt in the available

space between the composite layers made of VIP panel and cold plate. When only water was used, the yoghurt was maintained at the desired for about 56 h, with a cold space temperature of 6 °C. When employing PCM2, an extension of the constant temperature phase inside the cooling box was extended of about 9 h, with a temperature lower than 6 °C for 4.5 h more than what done by PCM1. Moreover, when using PCM3, the time in which the temperature was maintained under 6 °C was 87 h. The combined effect of good insulation material and PCM with good heat transfer properties (especially, enhanced thermal conductivity) can create suitable conditions for the transportation of temperature-sensitive products.

By means of numerical analyses, Xiaofeng and Xuelai [92] designed and studied a multi-temperature insulation box presenting two different phase change materials. PCM1, n-octanoic acid-myristic acid composite (7.1 °C phase change temperature, 146.1 kJ kg^{-1} latent heat), and PCM2, potassium sorbate-water composite (-2.5 °C melting temperature, 256.2 kJ kg^{-1} latent heat), were combined with vacuum insulation panels to create three zones at different targeted temperature inside the cold compartment. In particular, zone1 (Z1) was destined to dry products that do not require specific temperature to be transported, zone2 (Z2) with a range between 7 °C and 10 °C for the transportation of melon, pumpkin or some other fruit and vegetable, and a colder zone (Z3) for hosting more temperature-sensitive products, which require a cold space to be maintained between -3 °C and -1 °C. The insulation box consisted of 30 mm polyurethane and vacuum insulation bord sandwiched between two 2.5 mm thick iron plates. Moreover, since the authors wanted to design a box which could ensure the appropriate transport condition with an external environment temperature of 298 K, 13.8 kg of PCM1 and 12.1 kg of PCM2 were inserted in the multitemperature cold box. A roller was arranged, aiming at tuning the size of the different compartment based on the different transported loads need. When the box was experimentally tested, it was found that the temperature inside Z2 was maintained at 7 °C for 13 h. In the coldest zone, the desired temperature of -2 °C was ensured for 13 h, while the temperature for the carriage of dry products remained at 19 °C. More recently, Guo et al. [93] developed a novel cold storage box aiming at investigating the effects of three parameters, such as, the amount of PCM (eutectic salt, melting temperature: -80 °C), adjustment plate opening rate and storage plate heat transfer area on the temperature increasing rate and temperature distribution in the cold space. The box had dimensions of 1000 mm x 500 mm x 500 mm with insulation layers consisting of 2 mm of nested glass, 30 mm of poly-urethane and 20 mm of vacuum insulation board. The system was cooled down by liquid nitrogen injection. The statistical techniques of the variance analysis and response surface methodology were adopted to investigate the relation between the above-mentioned parameters. It was found that the

temperature increase rate and the temperature standard deviation were affected by the coupling of the storage plate heat exchange area (varied from 0.09 to 0.11 m^2) and the amount of PCM (varied from 1.3 kg to 2.6 kg). Moreover, the adjustment plate opening rate was varied from 20% to 40%. It was obtained that the temperature standard deviation decreased as one of the parameters increased, while an increase in one of the parameters generated a temperature elevating rate increase.

The idea of adding PCM slabs to the walls of an insulated cold box, was used by Orò et al. [94] to develop an active phase change material package for an ice cream container. The authors, in fact, aimed at enhancing the quality of the ice cream when maintained outside the freezer, by modifying its thermal protection. In particular, the dead zones of a common 5 L ice cream container were filled by PCM (E-21 with 2 %wt of oxethylmethylcellulose as thickening agent to prevent PCM leakage), as shown in Fig. 2.28. Moreover, 2 cm of additional PCM layer was added to the bottom of the container. In order to ensure the complete solidification of the ice cream and PCM before the beginning of the experiments, the container was maintained at -28 °C. Then it was located in a climatic chamber set at 25 °C. By monitoring the temperature evolution over time, it was found that the use of PCM let the ice cream to be subjected to less temperature differences along its volume.

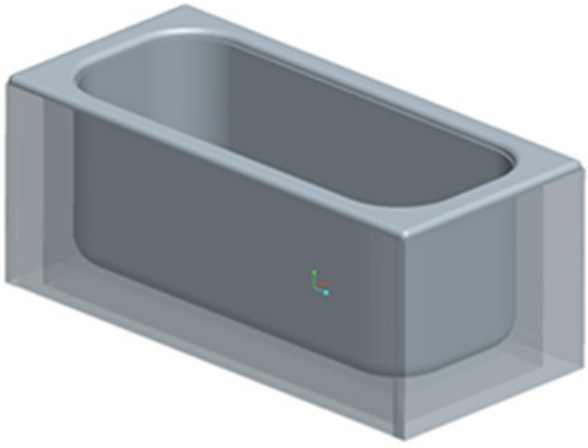

Figure 2.28 PCM-based ice-cream container [94]

In particular, the central part of the ice-cream remained 3 °C lower if PCM was adopted (-15 °C, against -12 °C). Greater temperature gap was, instead, calculated at the corner (-15 °C for the PCM solution compared with -5 °C for the reference container). Smaller temperature zone differences in the ice cream are beneficial for the ice cream quality itself. By the development and appropriate validation of a numerical model, by modifying the PCM thickness, the authors

investigated different scenarios. The obtained results were compared by using the period factor, that is the ratio between the time needed to reach a determined temperature when the PCM was or was not considered. High thermal protection was obtained by adding 20 mm of PCM at the container sides whilst 10 mm at the bottom. This new configuration ensured the optimal protection by occupying a volume which is only 7% larger than the reference container.

Leducq et al. [95] also analyzing the contribution of the PCM to the thermal protection enhancement of ice cream during storage and transportation. The authors conducted experiments by inserting three rectangular cardboard boxes, each of them containing eight 1 L ice containers (100 mm x 100 mm x 70 mm) in a freezer. To the cardboard, PCM (Cristopia E-21) rectangular bricks (220 mm x 150 mm x 25 mm) were added to the walls. Even the solution concerning the thermal insulation improvement by the addition of 25 mm thick expanded polystyrene to the cardboard box was investigated. The reference and the two modified cardboards were subjected to same storage conditions, that is 140 days at a mean temperature of -22 °C, to analyze the long-term storage. The crystal size (which reflects the product quality) was used as the parameter to compare the different thermal performances of the three cardboards. Significant smaller crystal sizes were identified for the cardboards with PCM. The PCM also let to enhance the thermal protection by using a smaller thickness compared with the polystyrene added box, assumed a similar damping effect. To analyze the thermal protection under thermal abuse condition, the boxes were exposed for 40 min at the ambient temperature (20 °C). Only 1 °C temperature rise was detected when PCM was used, demonstrating its great contribution in increasing the maintaining of the safe condition during the transportation of perishable products.

To briefly resume, the main positive and negative aspects regarding the adoption of PCM-based LTES system for the product transportation and distribution sectors along the cold chain are reported as follows.

Compared to a traditional system, a more uniform temperature distribution inside the cold compartment is achievable, which is beneficial for the food quality, especially for foodstuffs carried at positive temperatures, limiting food wastages and losses. Sensible greenhouse gas emissions reduction (up to 90%) can be obtained. The possibility of employing a more efficient stationary cooling unit other than the traditional on-board refrigeration system (low COP) lets to remarkably reduce the operational costs. The LTES can be cooled down by exploiting a renewable energy source, reducing the dependency from fossil fuels. A significant extension of the cooling time of the portable boxes can be reached, which preserves the high-sensible product quality.

On the contrary, the rapid abatement of the heat infiltrations due to door-openings cannot be always easily addressed by a passive PCM-based system only. Besides, the occurrence of a PCM leakage can be detrimental for the carried foodstuffs. Finally, a LTES system seems more appropriate for a short- or daily- operation route.
Finally, on the basis of the present work, the following gaps can be identified:

- Charging and discharging phases of the LTES systems should be studied and optimized contemporary.
- The effect of the relative humidity on the cold compartment should be considered.
- The effects of the foodstuff precooling should be analyzed.
- Economic analyses to verify the convenience of the LTES system.
- A clear and uniform way for the selection of the PCM to be employed should be defined.
- Studies closer to real-life conditions, in terms of external conditions and system sizes should be run.
- Multi-temperature PCM for refrigerated vehicles can be an option to maximize the advantages of the passive systems.
- Life Cycle Analyses to demonstrate the advantages of the technology for the environment should be considered.

3. Development and study of an innovative LTES for refrigerated truck: the empty case

3.1 Introduction

From the introductive section of this thesis, it can be easily noticed that a great space for the spread of the LTES in the cold chain transportation field is available. In particular, the literature lacks studies involving the development of an almost passive technology for the transportation of fresh foodstuffs. Therefore, to fill the aforementioned gap, we decided to investigate the thermal behaviour of an innovative LTES system involving PCMs as schematically described in Fig. 3.1. More specifically, a numerical model representing the novel insulation wall consisting of the traditional Poly-Urethane (PU) foam insulation layer and an additional layer filled with a PCM was proposed and studied. The PCM is uniformly distributed on the ceiling and both sides of the refrigerated cell.

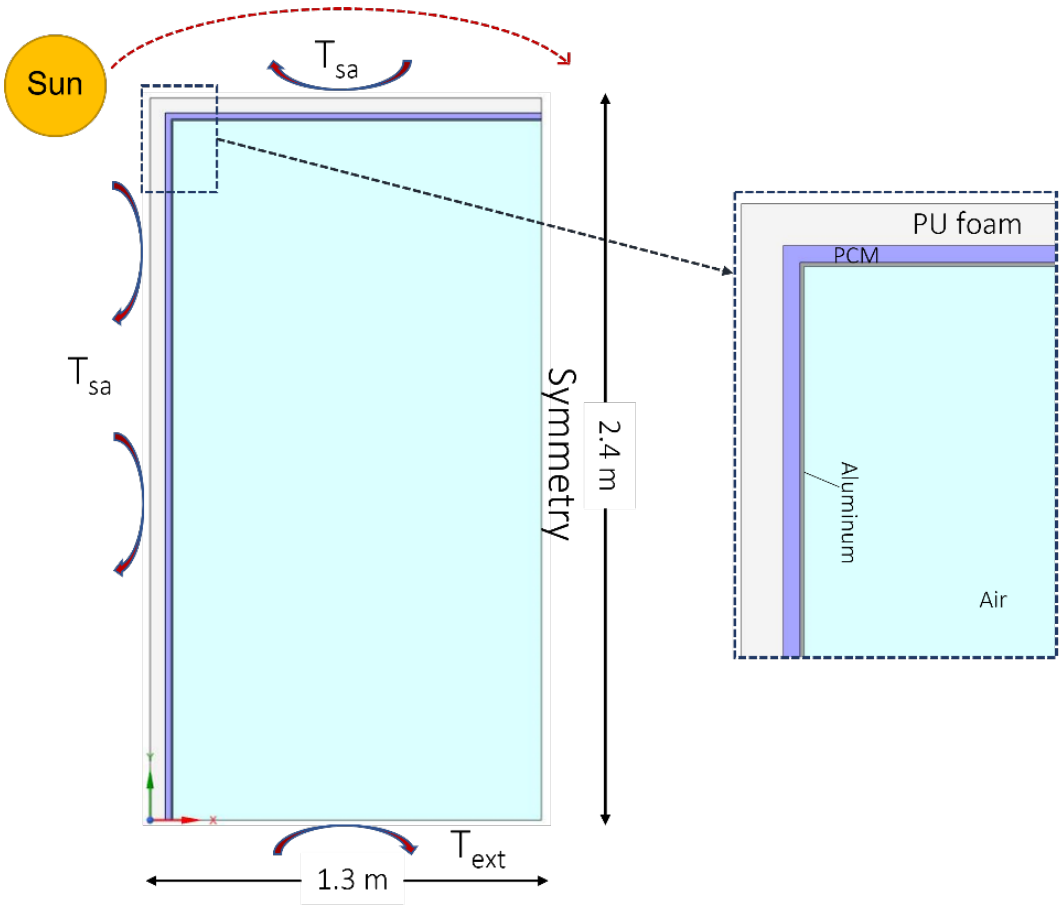

Figure 3.1 Model description and boundary conditions

In order to simplify the simulations, a 2D section (2.4 m x 2.6 m) of a semi-trailer insulated rigid box was taken as our computational domain. This type of refrigerated vehicle is the most popular one in

Europe and its external width and length are fixed: 2.6 m and 13.56 m, respectively, (Tassou et al.[30]). The trade-off between the maximum admissible vehicle width (2.6 m) and the Europallet's dimensions (1 m deep x 1.2 m width) limits the maximum possible thickness of the insulation layer considered in this study. If 2 Europallets are located side by side in the refrigerated cell the insulation layer thickness can hardly exceed 5 cm.

Hence, for the numerical simulations, a 5 cm thick PU-layer was chosen. To evaluate the ability of PCM in counteracting the heat loads transmission into the refrigerated cell, different PCM layer thicknesses were selected, ranging between 0.5 cm and 2 cm. An aluminum encapsulation layer of 0.5 cm was located between the PCM and the air, as demonstrated in Fig. 3.1. The thermo-physical properties of the materials and PCMs are reported in Table 3.1 and 3.2, respectively.

Table 3.1 Material main properties

Material	k [W m^{-1} K^{-1}]	ρ [kg m^{-3}]	c_p [J kg^{-1} K^{-1}]
Poly-Urethane foam	0.03	35	1380
Aluminum	202.4	2719	871

Table 3.2 Phase Change Materials main properties

PCM	k [W m^{-1} K^{-1}]	ρ_{sol}/ρ_{liq} [kg m^{-3}]	c_p [J kg^{-1} K^{-1}]	L [kJ kg^{-1}]	$T_{solidus}/T_{liquidus}$ [°C]
RT2HC	0.2	880/770	2000	200	1/3
RT4	0.2	880/770	2000	170	3/5
RT5HC	0.2	880/760	2000	250	5/6

To take into account the effect of the solar irradiance on the top and on the side of the truck, the sol-air model was applied as proposed and validated by Calati et al. [129] and Villi et al. [130]. The sol-air model allows for a great simplification of the boundary conditions to be assigned to the numerical model; in fact, the proposed model permits to evaluate a fictious temperature T_{sa} that includes both the radiation and convection contributions. As given by Eq. (3.1), this temperature is always greater than the free stream air temperature because is obtained as the sum of dry bulb air temperature and a term which is the ratio between as the radiative contribution divided by the convective heat transfer coefficient. Hence, for a given solar irradiance, the sol-air temperature tends to the free stream one as the convective heat transfer coefficient increases.

$$T_{sa} = T_{ext} + \frac{G_{\beta t} * a}{\alpha} \qquad \text{Eq. (3.1)}$$

The absorptance a was fixed at 0.5, while a global heat transfer coefficient α of 10 W m^{-2} K^{-1} was selected to investigate the stationary vehicle scenario. Glouannec et al. [70] chose 7 W m^{-2} K^{-1} for the external heat transfer coefficient, whereas Cengel and Gajar [131] suggested a value of 10 W m^{-2} K^{-1}. Therefore, we opted for the coefficient of 10 W m^{-2} K^{-1}. Besides, to take into consideration the different truck speeds, the heat transfer coefficient α was estimated by assuming a forced convection flow along flat plates (Incropera et al. [132]). For each truck surface, the global solar irradiance $G_{\beta t}$ was obtained following the procedure described in section 3.1.1.

To simplify the numerical analysis, only half of the entire section was simulated making use of the symmetry condition depicted in Fig. 3.1. The truck presented the side walls oriented at East or West facing North. Hence, the sol-air temperatures for each oriented surfaces were estimated, and their trends can be appreciated in the top-left side of Fig. 3.2. However, in order to study the worst-case scenario, the maximum hourly calculated T_{sa} between those for the eastern face and the western one was set for the truck side, assuming the route to occur along an ideal straightaway from South to North. From 6:00 to 12:00, the temperature values for the eastern surface were chosen, since they were always greater than the western ones. On the contrary, from the noon to the end of the simulated route (16:00), the temperature values of the West-oriented truck surface were applied as free stream temperature for the side of the developed numerical model. In Fig. 3.2 the curve “max” represents the hourly values of temperature sol-air used for the numerical analyses. The sol-air temperature for the top of the truck was also calculated and its trend is depicted in Fig. 3.2 (bottom-right).

At the bottom of the cell an overall heat transfer coefficient of 0.7 W m^{-2} K^{-1} was applied which took into account the conductive heat transferred through a standard 5 cm PU insulation layer and the convective coefficient of 7 W m^{-2} K^{-1} [70] considering a free stream temperature equal to the ambient temperature T_{ext} (no effect of solar radiation).

The initial air temperature inside the refrigerated cell was set to 2 °C for the all simulated conditions. The PCM initial temperature was assumed to be 0.5 K lower than the $T_{solidus}$ of each PCM, in order to ensure that the PCM was totally solid at the beginning of the simulation. The volume averaged air and PCM temperature were monitored and analysed to describe the behaviour of the LTES. Besides, the temperature distribution inside the refrigerated cell was investigated.

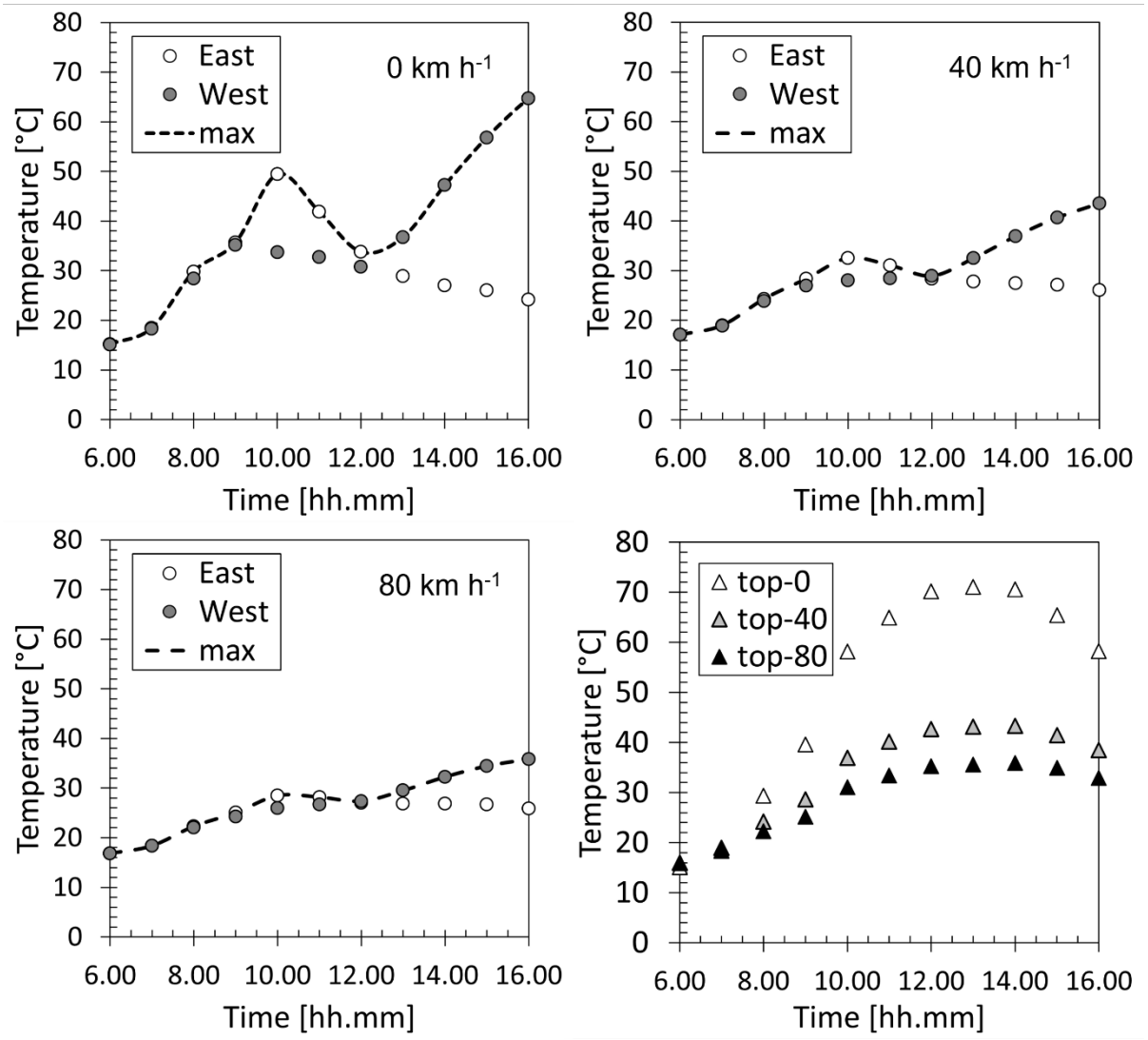

Figure 3.2 Temperature sol-air trends for western and eastern surfaces for stationary vehicle scenario (0 km h^{-1}), urban route (40 km h^{-1}), interurban route (80 km h^{-1}), and Temperature sol-air trend for top surface at 0, 40, 80 km h^{-1}, from 6.00 to 16.00.

3.2 The Equations

3.2.1 Incident Solar Irradiance Estimation

For the entire simulated truck journey (from 6:00 am to 4:00 pm) the hourly solar heat load on each truck surface was estimated. To simulate the worst case scenario, data for a typical North-Italian (Vicenza) summer day was considered. A representative average day of July (n = 196) was chosen because from historical data-series it was observed that July is the warmest month in Italy. The climate data available here www.try.cti2000.it (Italian Thermo-Technical Committee site) was used for our simulation. For each day of the year, the temperature, the hourly beam and diffusive radiation contributions on a horizontal surface are downloaded and used as input for our simulation.

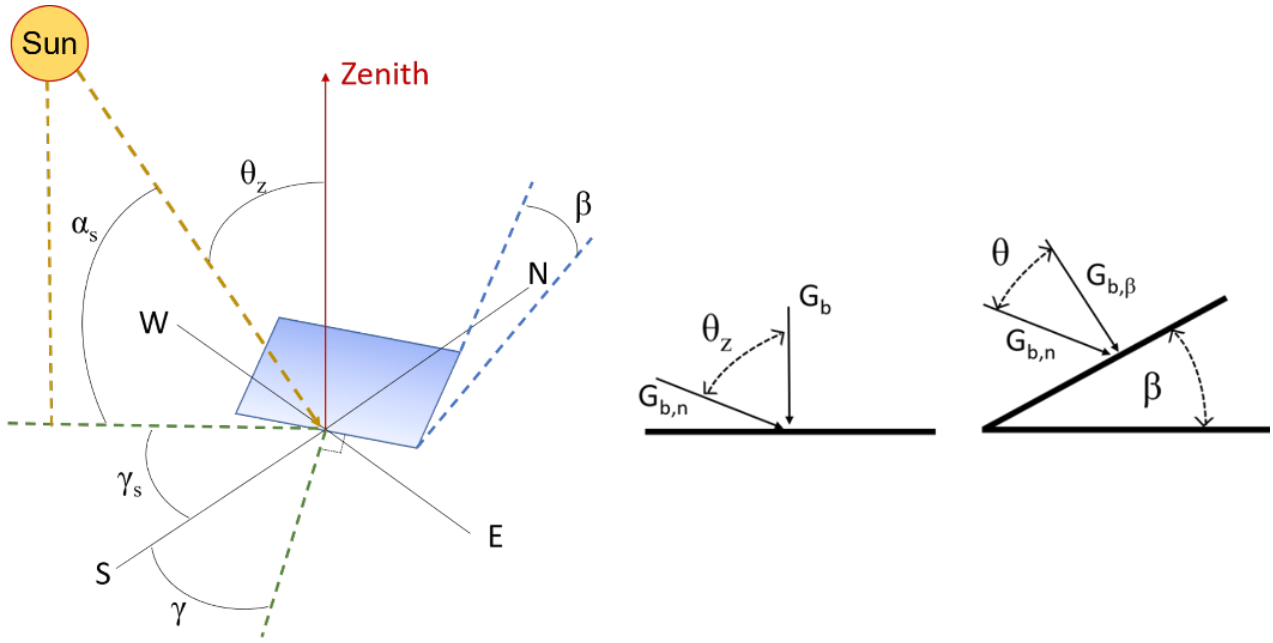

Figure 3.3 The most significant solar variables for a tilted surface (left) and beam radiation on a tilted surface (right).

The following equations were adapted from Duffie and Beckman [133] in order to estimate the hourly global radiation on a tilted surface.

The first step was the calculation of the solar time as reported in Eqns. (3.2-4), for obtaining the solar angle (5):

$$SolarTime - StandardTime = 4(M_{st} - M_{loc}) + E \quad \text{Eq. (3.2)}$$

$$E = 229.2(0.000075 + 0.001868\cos(B) - 0.032077\sin(B) - 0.014615\cos(2B) - 0.04089\sin(2B)) \quad \text{Eq. (3.3)}$$

$$B = (n-1)\frac{360}{365} \quad \text{Eq. (3.4)}$$

$$\omega = 15(SolarTime - 12) \quad \text{Eq. (3.5)}$$

The second step involved the estimation of the Zenith (Eq. 3.7) and solar Azimuth (Eq. 3.8) angles after having calculated the solar rays' declination (Eq. 3.6):

$$\delta = 23.45sen(360\frac{284+n}{365}) \quad \text{Eq. (3.6)}$$

$$\theta_z = cos^{-1}(cos\phi cos\delta cos\omega + sin\phi sin\delta) \quad \text{Eq. (3.7)}$$

$$\gamma_s = sign(\omega)\left|cos^{-1}(\frac{cos\theta_z sin\phi - sin\delta}{sin\theta_z cos\phi})\right| \quad \text{Eq. (3.8)}$$

Knowing the Zenith and solar Azimuth angles, surface tilt and Azimuth angles, the angle of incidence of the beam radiation could be predicted as follows:

$$\theta = cos^{-1}[cos\theta_z cos\beta + sin\theta_z sin\beta \cos(\gamma_s - \gamma)] \quad \text{Eq. (3.9)}$$

Finally, for each truck surfaces the global radiation could be calculated as:

$$G_{\beta t} = G_{b,\beta} + G_d = G_b \frac{cos\theta}{cos\theta_z} + G_d \quad \text{Eq. (3.10)}$$

3.2.2 Governing equations

The commercial CFD software "Ansys Fluent 18.2" was used to run the numerical simulations. The "Solidification and Melting Model" was adopted to investigate the transient behaviour of the LTES system. The model takes advantage of an enthalpy-porosity approximation of the zone involved in the phase change process, denoted as mushy zone (Voller and Prakash [134]). In fact, the liquid-solid mushy zone is considered as a porous one and the porosity is set as the liquid fraction. This latter is a quantity indicating the fraction of the cell volume in liquid state, calculated for all cells in the domain. In the mushy region, the liquid fraction ranges between 0 (PCM solid) and 1 (PCM liquid). Hence, the energy equation Eq. (3.15) is written in terms of enthalpy Eq. (3.11), considered as the sum of sensible enthalpy Eq. (3.12) and latent heat of fusion Eq. (3.13), as reported in the following equations:

$$H = h + \Delta H \quad \text{Eq. (3.11)}$$

$$h = h_{ref} + \int_{T_{ref}}^{T} c_p dT \quad \text{Eq. (3.12)}$$

$$\Delta H = \varphi L \quad \text{Eq. (3.13)}$$

$$\varphi = \begin{cases} 0, if\ T < T_{solidus} \\ \dfrac{T - T_{solidus}}{T_{liquidus} - T_{solidus}},\ if\ T_{solidus} < T < T_{liquidus} \\ 1, if\ T > T_{liquidus} \end{cases} \quad \text{Eq. (3.14)}$$

$$\frac{\partial}{\partial t}(\rho H) + \nabla \cdot (\rho \boldsymbol{v} H) = \nabla \cdot (k \nabla T) \quad \text{Eq. (3.15)}$$

To develop the momentum conservation equation (Eq. (3.16)) for the mushy region, a momentum sink $\boldsymbol{S}$ (Eq. (3.17)) is inserted in the Navier-Stokes equation as:

$$\frac{\partial}{\partial t}(\rho \boldsymbol{v}) + \nabla(\rho \boldsymbol{v}\boldsymbol{v}) = -\nabla p + \mu \nabla^2 \boldsymbol{v} + \rho g \epsilon (T - T_{ref}) + \boldsymbol{S} \quad \text{Eq. (3.16)}$$

$$\boldsymbol{S} = \frac{(1-\varphi)^2}{\varepsilon + \varphi^3} A_{mush} \boldsymbol{v} \quad \text{Eq. (3.17)}$$

In the right-hand side of Eq. (3.16), the last two terms stand for the buoyancy force with Boussinesq approximation and the above-mentioned momentum sink, respectively. In Eq. (3.17) ε is a constant equal to 10^{-3}, which lets to prevent the division by zero when liquid fraction φ is zero (PCM completely solid).

Additionally, to analyse the thermal fluid dynamics the conservation of mass is solved:

$$\nabla \cdot (\rho \boldsymbol{v}) = 0 \quad \text{Eq. (3.18)}$$

The second order upwind scheme was adopted to linearize the convective terms with first order derivatives, while the diffusive terms with second order derivatives were linearized by a second order differencing scheme. The SIMPLE scheme was used to solve the pressure-velocity coupling while the PRESTO! one was chosen for pressure correction, as proposed by Zhao et al. [135]. All of the other equations were linearized using the algebraic multigrid (AMG) iterative strategy.

3.3 Sensitivity Analyses

3.3.1 Time Step and Mesh Sensitivity Analyses

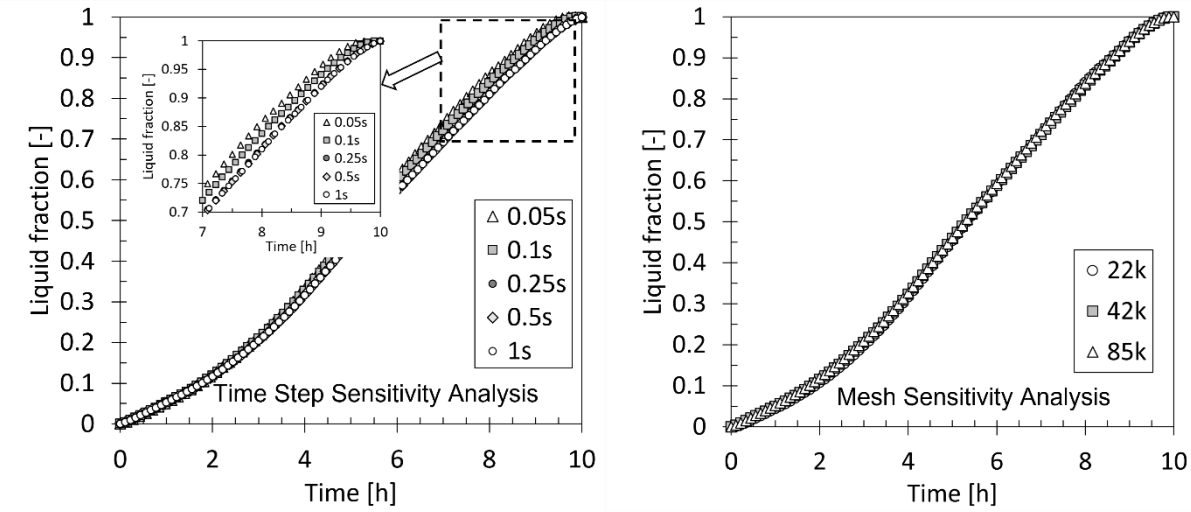

Figure 3.4 Time Step and Mesh Sensitivity Analyses for RT2HC, 0.5 cm PCM layer, for the stationary vehicle scenario.

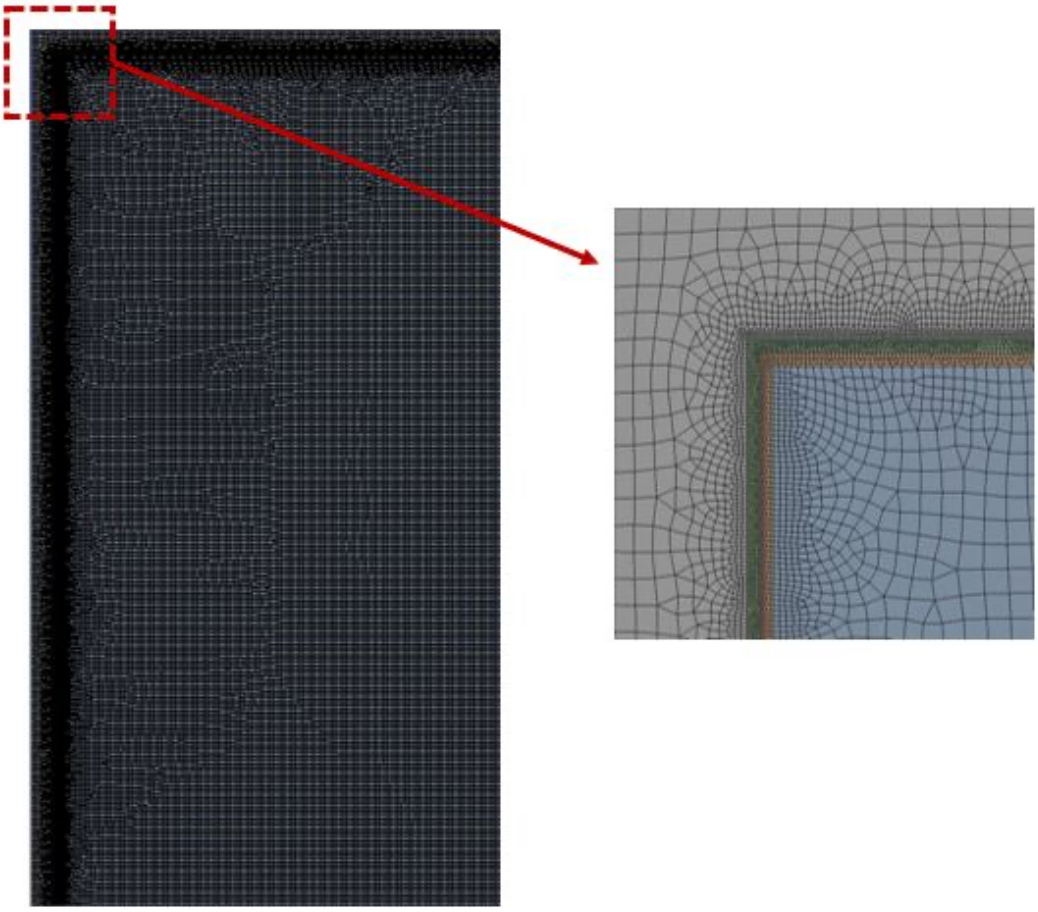

Figure 3.5 Mesh of 42k elements. Details.

The liquid fraction at the end of the simulation (10 h) was chosen as parameter aiming at comparing different results. Among all the investigated configurations, RT2HC and 0.5 cm PCM thick layer were used for the sensitivity analyses, since it was considered the most stringent case, having the smallest size and the minimum amount of PCM. On the left-hand side of Fig. 3.4, when the time step changes from 0.05 s to 1 s some differences between the curves can be appreciated. While the curve for 0.1 s time step size is very close to the lowest time step size curve, the other cases mostly overlap, deviating from 0.05 s curve trend. Therefore, to limit as much as possible the possible source of numerical deviation considering the contemporary need of a reasonable computational time, a time step size of 0.1 s was selected for all the numerical analyses. In Fig 3.4 (right-hand side), the grid independence analysis is shown. To find the optimal trade-off between computational efforts and solution robustness, three different meshes were studied (22k, 42k, 85k elements). From 85k to 22k number of elements, no differences can be noted, confirming the grid independence of the solution, even if the computational time dropped from 2.5 h to 1.2 h, respectively. The 42k (Fig. 3.5) was used for all the other analyses.

3.4 Model Validation

Aiming at validating the numerical we proposed, two different model validation were run. Firstly, the model was validated on preliminary experimental results collected in the Nano Heat Transfer Lab (UniPD) involving the melting process of two paraffins (RT2HC and RT5HC) inside periodically structured aluminum samples. The aluminum samples were set into a small insulated box representing the truck cell environment while the box was located into a climate chamber set at constant temperature. Based on experimental data, a 3D model was developed, and it was validated on data representing the time evolution of the temperature inside the box and the temperature of PCM inside the aluminum sample, as it will be shown in the section 3.4.1. A second step involved the validation of the Enthalpy-Porosity model and the Sol-Air Temperature model contemporary based on experimental results collected by Glouannec et al. [70]. As shown in section 3.4.2, this second validation demonstrated the possibility of studying the thermal performance of the 2D LTES system we proposed without modelling the external air domain which would require remarkable computational efforts.

3.4.1 Model Validation based on preliminary experimental results on a small-scale apparatus

The experimental results referred to the cold energy release performance (discharging) investigation of two commercial paraffin waxes (RT2HC, RT5HC). A small-scale experimental setup was built which consists of a climatic room, an airtight and insulated box and a PCM sample. The box was located inside a hotter climatic room. It was made of 6 cm thick expanded polystyrene (XPS) insulation material presenting a 15 cm^3 internal volume. An aluminum sample (42 x 42 x 40 mm), open at the top, filled with PCM, was located inside the air volume. The ratio between PCM and air volumes is around 2%, i. e., when a PCM layer thickness of 2 cm was considered in the model proposed in section 3.1. Experimental measurements of temperatures as function of time were compared with results coming from numerical simulations to validate the model.

In Figure 3.6 the experimental setup scheme is presented. It consists of a box having $3.38 \cdot 10^{-3}$ m^3 inner volume filled with cold air located in a hotter climatic room able to maintain the temperature with a stability of ±0.2 K. The box walls are made of 6 cm Expanded Polystyrene (XPS) foam (thermophysical properties reported in Table 3.3). For the sake of clarity, the wall thickness is not shown in Figure 3.6.

Table 3.3 XPS thermophysical properties

Density, ρ	**Heat Capacity, c_p**	**Thermal Conductivity, k**

(kg m^{-3})	(J kg^{-1} K^{-1})	(W m^{-1} K^{-1})
35	1380	0.032

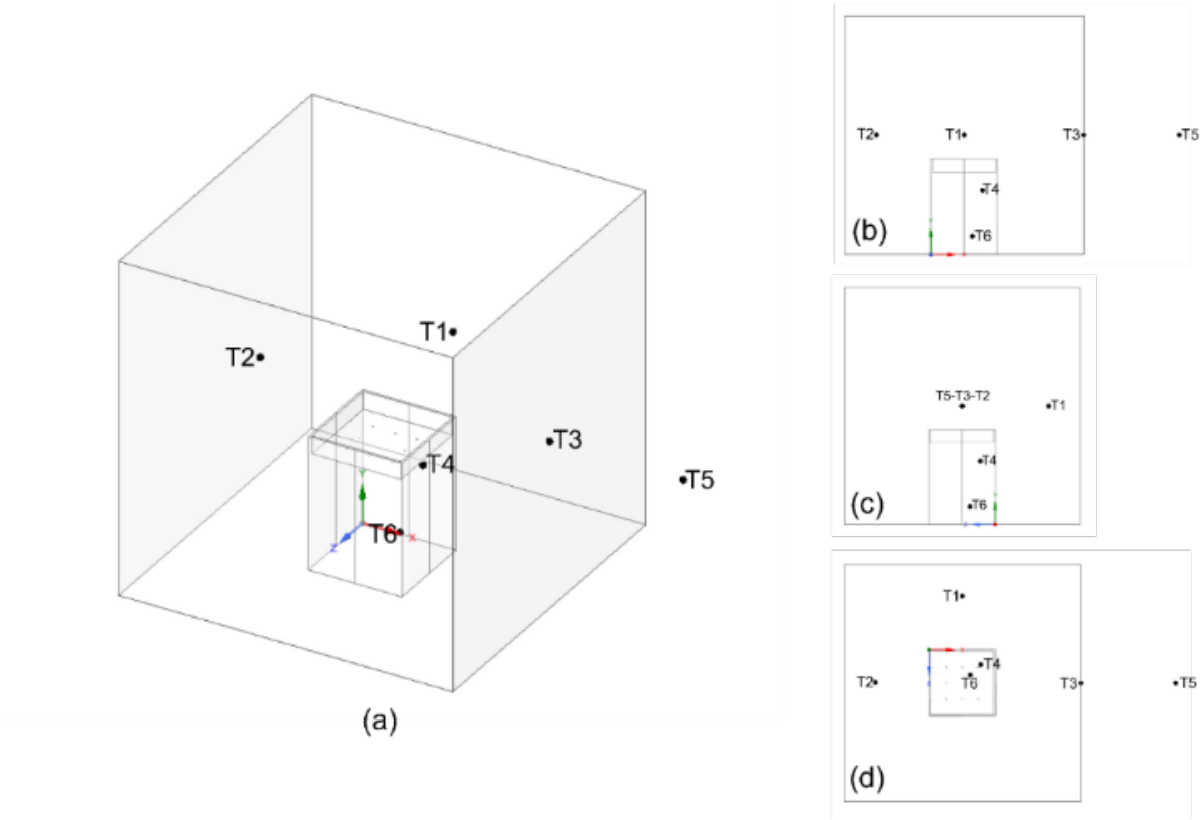

Figure 3.6 3D sketch of the experimental setup (a), 2D frontal view (b), 2D lateral view (c), 2D top view (d).

In the middle of the box, two different samples were inserted, alternately. The two AlSi10Mg-0403 aluminum alloy samples were manufactured via additive manufacturing [12]. The first sample (denoted as reference, "Ref" in the subsequent sections) is completely empty inside, whilst the second one (denoted as "10") presents a periodic structure with a pore size of 10 mm. The "10" sample has a void volume/aluminum alloy volume ratio of 95%, meaning that its porosity is 0.95. These samples are filled with $6.4 \cdot 10^{-5}$ m^3 of PCM (thermophysical properties listed in Table 3.4).

Table 3.4 Phase Change Material thermophysical properties declared by the manufacturer

PCM*	k (W m^{-1} K^{-1})	ρ_{sol}/ρ_{liq} (kg m^{-3})	c_p (J kg^{-1} K^{-1})	L (kJ kg^{-1})	$T_{solidus}/T_{liquidus}$ (°C)
RT2HC	0.2	880/770	2000	200	1/3
RT5HC	0.2	880/760	2000	250	5/6
*as declared by manufacturer [136]					

As depicted in Figure 3.6, six T-type calibrated thermocouples (TCs) (k=2 uncertainty ±0.1 K) connected to a Kaye K-170 ice point reference with stability of ±0.005 K and accuracy of ±0.005 K are inserted in the test apparatus. In particular, two TCs (T1 and T2) are used to monitor the air temperature inside the insulated box, two TCs (T3 and T5) measure the temperature of the internal and external XPS surfaces, respectively, and the last two (T4 and T6) monitor the PCM temperature inside the sample.

The aluminum samples filled with the PCM were previously cooled down to -3 °C to ensure the PCM complete solidification. Then one sample at a time was inserted inside the insulated box that was maintained at 10±0.5 °C by using an external refrigerator and sealed. At the beginning of the test, the airtight box at 10 °C containing the PCM sample was placed inside the climatic room set at 30±0.2°C. By means of a Keysight 34970A data acquisition system, all the data are recorded at a 1 Hz frequency and processed by LabView software.

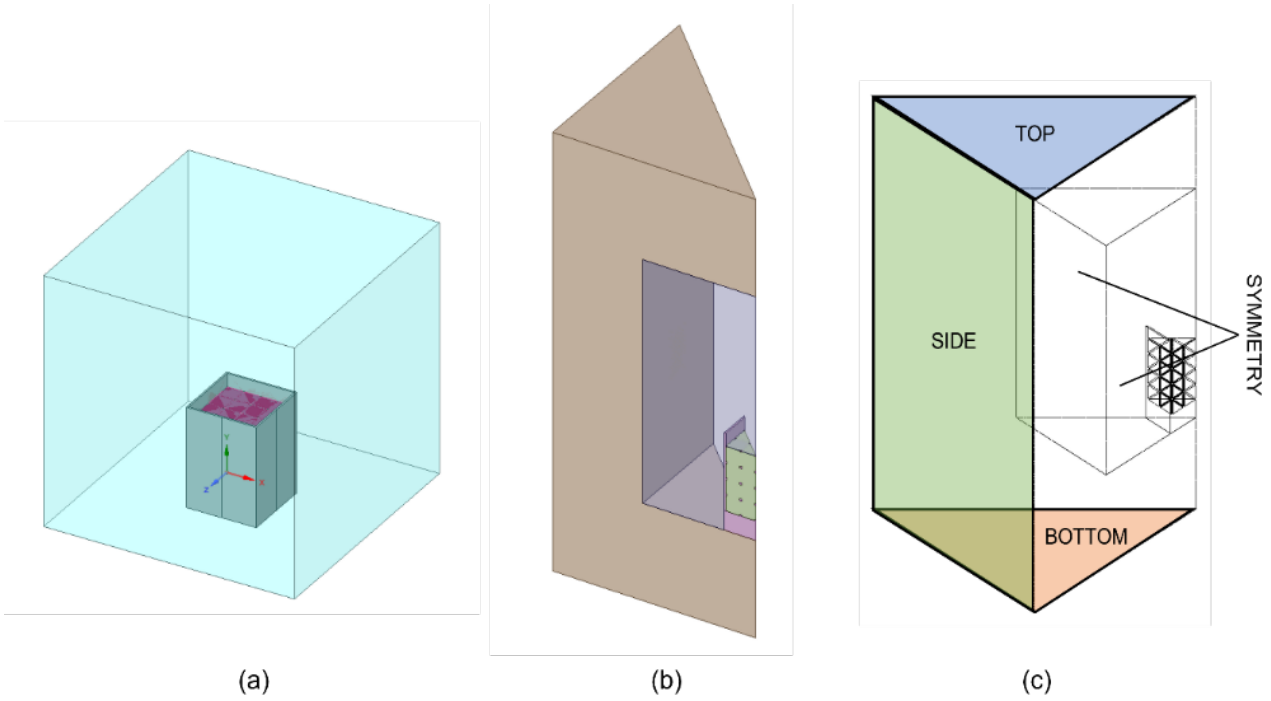

Figure 3.7 3D numerical model (a), one-eighth of 3D model (b), face name selections (c).

A 3D numerical model was developed to study the phase change process by means of the CFD program ANSYS Fluent 18.2. As depicted in Figure 3.7(b) only one-eighth of the entire domain was simulated, by exploiting the symmetry of the system. In this context, as it can be noticed from Figure 3.7(c), the faces of the model assumed as symmetric planes, were denoted as “symmetry”. The external lateral face of the XPS insulation material was named “side” and it was treated as a “wall”: an external heat transfer coefficient of 10 W m^{-2} K^{-1}, since only buoyancy driven airflow occurs, with

a free stream temperature of 303.16 K (the climate chamber is set at 30 ± 0.2 °C) was set. Similar boundary conditions were applied to the "top" wall, whilst for the "bottom" face a global heat transfer coefficient of 5 W m^{-2} K^{-1} was chosen, since the box was placed on a 15 cm wooden shelf inside the climatic room.

Aiming at verifying the solution independence from the grid, a mesh sensitivity analysis was conducted by running several configurations.

Table 3.5 Mesh sensitivity analysis.

Mesh name	#elements ($\cdot 10^6$)	Time-To-Complete-Iteration (s)	ΔTime (%)
A	0.582	diverge	-
B	1.093	≈ 27	-
C	2.474	≈ 29	+7.5
D	4.529	≈ 33	+22.2

As reported in Table 5.3, four different meshes were studied by varying the number of elements constituting the grid. The numerical analyses are run by means of a 128-parallel-core cluster equipped with Intel E5-2640v3 3.6 GHz processors. The time required to complete a single time step (denoted "Time-To-Complete-Iteration" in Table 5.3) and the liquid fraction evolution as function of time (for the sake of brevity, not here reported) are chosen as the variables to identify the best mesh. No appreciable differences between the three different liquid fraction curves (for grids "B", "C", "D") were detected. In this regard, the grid "C" having about $2.5 \cdot 10^6$ elements is preferred as the best trade-off between computational time and solution accuracy, contemporary reducing, as much as possible, the source of numerical errors.

A time step sensitivity analysis was also run. It investigated 4 different time step sizes: 0.05, 0.1, 0.5, 1 s. The optimal selection results in a time step size of 0.1 s, as similarly found in Chapter 3.

3.4.1.1 Results

Figure 3.8(a) reports the comparison between the 10 mm ("10") and reference ("Ref") samples in terms of experimental average air temperature (T1 and T2) and experimental average PCM temperature (T4 and T6). The paraffin considered is RT2HC. Besides, the air temperature when the PCM is not inserted in the air domain ("empty" scenario) can be appreciated.

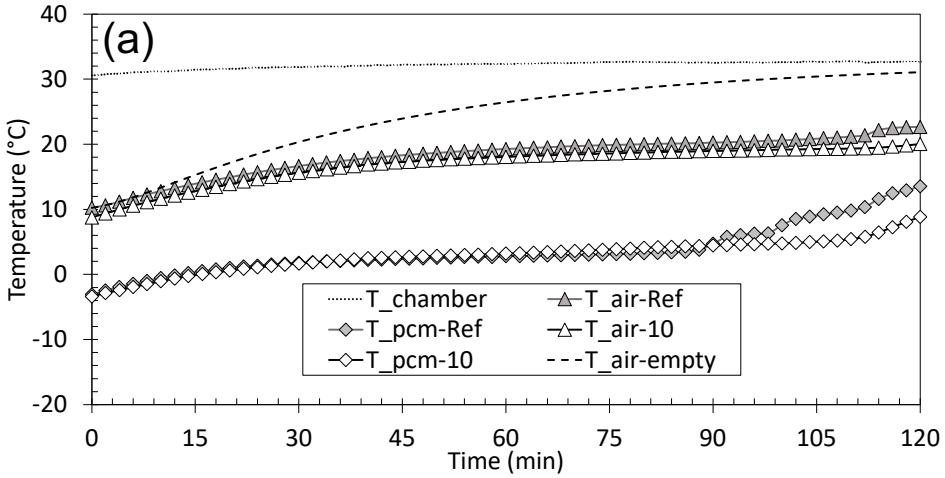

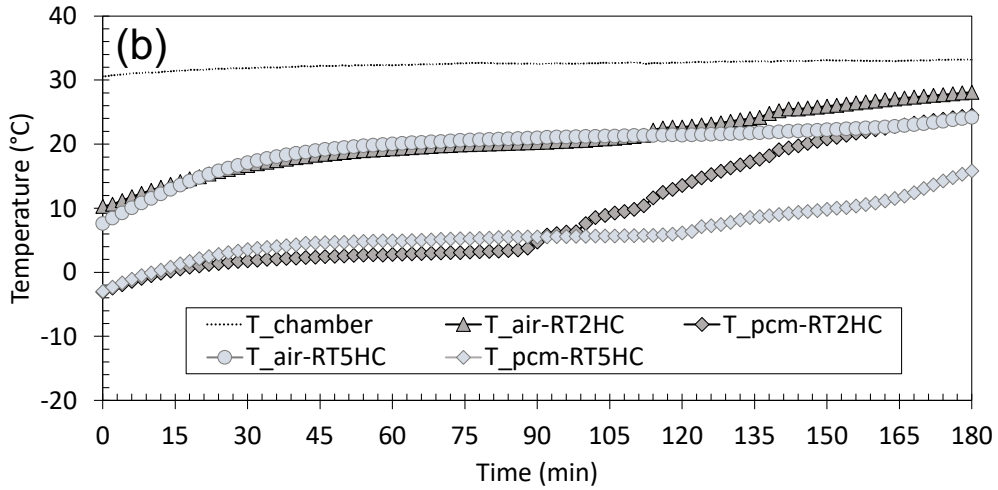

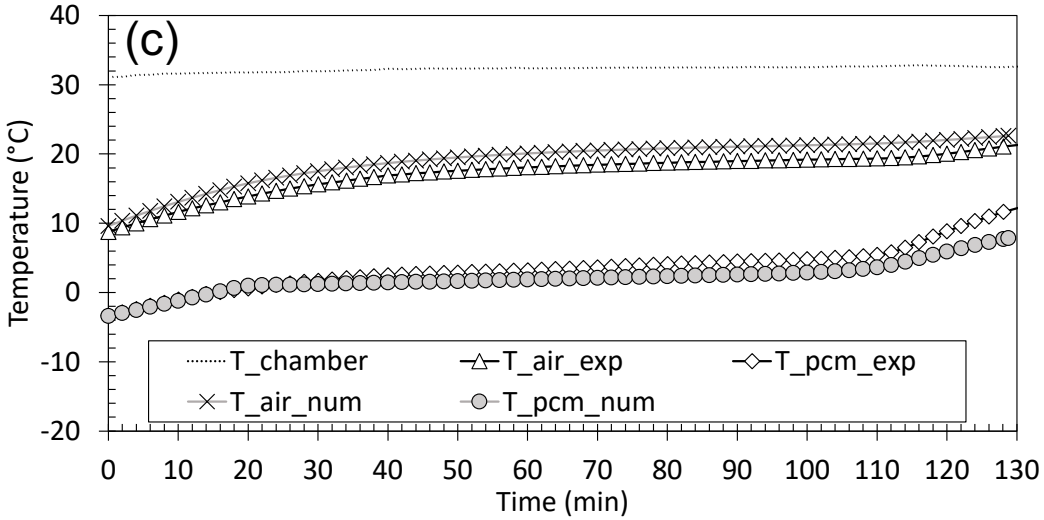

Figure 3.8 Comparison between "10" and "Ref" samples, RT2HC (a), between RT2HC and RT5HC, reference sample (b), between experiment and simulation, RT2HC "10" sample (c).

It can be noticed that, compared with the empty scenario, the temperature rise is weakened when the PCM is added inside the insulated box. In fact, the air temperature curve for the empty scenario (black dotted line) increases faster approaching the temperature of the chamber, asymptotically. For instance, after 60 min from the beginning of the test, the average box temperature air is at 18 °C when the PCM is used, while it is at about 25 °C in the empty scenario. The PCM, acting as a cold storage, counteracts the temperature growth. More specifically, if focusing on the air temperatures (triangles), it is clear that a temperature increase occurs in the very first minutes, but then, when the phase change process starts, no more significant air temperature increasing can be observed for about 90 min, the period of time in which phase change lasts, absorbing heat coming from the environment. Similar results can be found for both the PCM samples (Ref and 10) and both the materials (RT2HC and RT5HC).

Specular trends between air and PCM temperature curves can be appreciated over time. From -3 °C to 1 °C, it means for about 20 min, the PCM temperature increases, when sensible heat was exchanged. When reached 1 °C (i.e., the *solidus* threshold), the PCM started melting, stabilizing its temperature. After a lead time of about 10 min from the beginning of the PCM phase change, the air temperature changed its growth rate. Indeed, after about 30 min its slope became almost zero, suggesting the temperature increase is very low.

If focusing on the reference PCM temperature curve (grey rhombi), at about 88 min a sharp change of slope can be observed: this suggests that the PCM inside the aluminum reference sample has weakened its ability in absorbing the heat. Consequently, with a delay of about 20 min, even the air temperature started growing with a greater rate. Adversely, when looking at the PCM temperature in the 10 mm sample (white rhombi), it can be observed that the curve remains almost horizontally up to 116 min, that is around 30 min longer than the reference case. Since the amount of PCM is the same, it can be speculated that the reference sample is not capable to take advantage completely of the phase change process. More specifically, the absorbed heat is not able to spread through the paraffin due to its intrinsic low thermal conductivity. As a consequence, the latent heat is not exchanged efficiently, resulting in an increase of the mean wax temperature. On the contrary, the periodic structures inside the 10 mm sample let the heat to be conveyed more homogeneously, thus a better exploitation of the melting process occurs. This behavior is reflected into a delay of the air temperature increase (white triangles) compared with the reference case. By considering a refrigerated transport application, the delay in the air cell temperature growth has positive implications for prolonging the healthy conditions of transportation of perishable temperature-sensitive products.

In Figure 3.8(b) the comparison between RT2HC and RT5HC inside the reference aluminum sample can be appreciated. It can be seen that the RT5HC average temperature is higher than the RT2HC one since its melting point is higher (5 °C against 2 °C) but it flattens asymptotically for a longer period compared with RT2HC. This behaviour can be explained due to a higher latent heat value (250 against 200 kJ kg^{-1}). In accordance with what explained in Figure 3.8(a), a beneficial effect on the air temperature trend is obtained. Hence, as already found in [12], for a cold chain application the PCM having the high as possible latent heat value must be preferred.

The enthalpy-porosity model was validated based on the experimental results described above. It is found that, when considering the declared melting enthalpy for the RT2HC (i.e., 200 kJ kg^{-1}), the simulated average volume PCM temperature was able to predict only the onset of the melting process but phase change time was then largely overestimated.

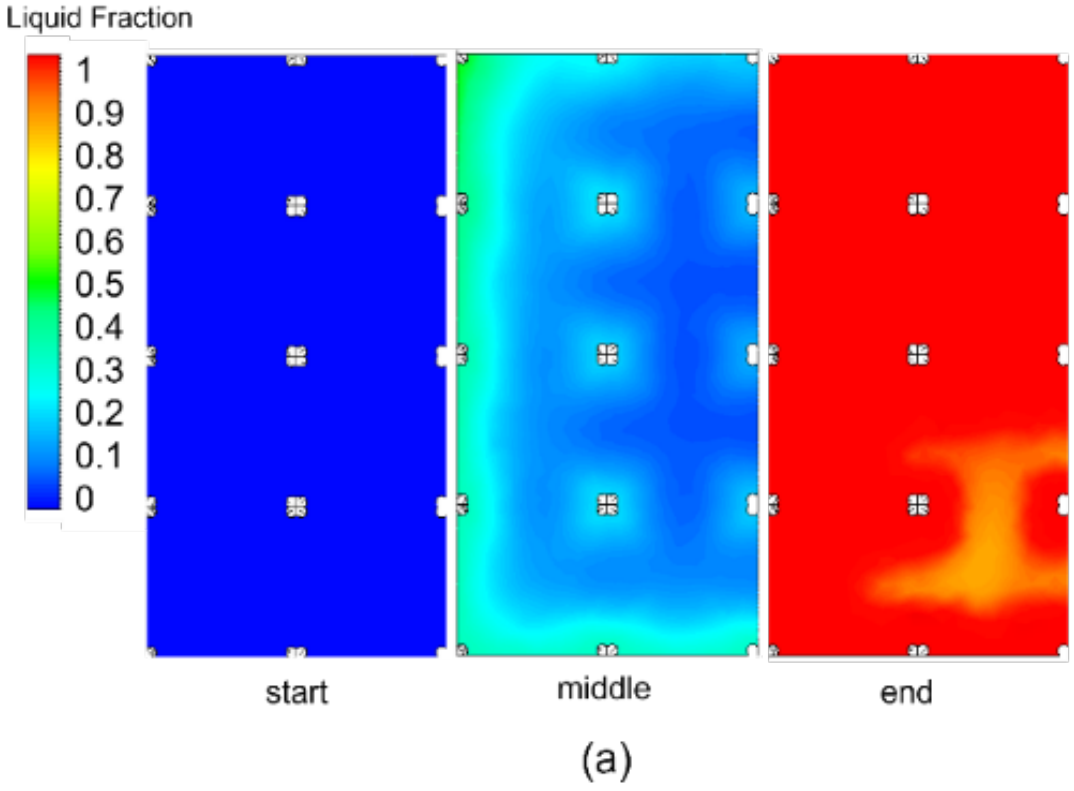

(a)

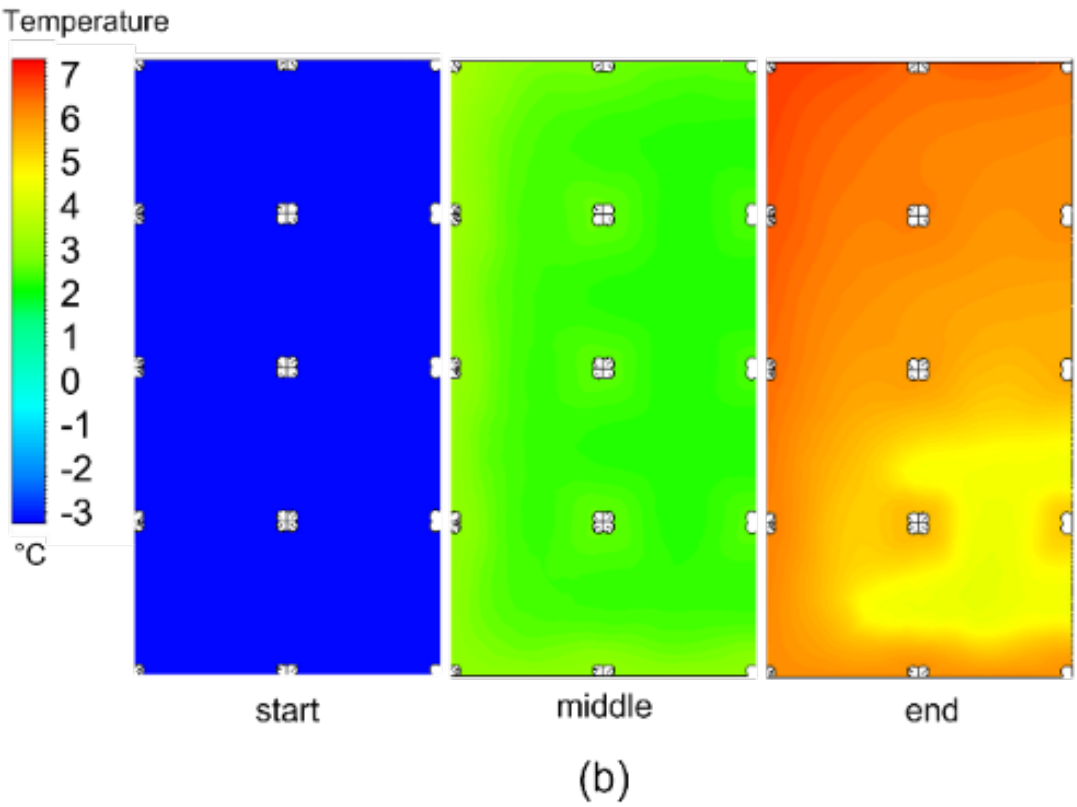

Figure 3.9 Liquid fraction evolution (a), temperature distribution (b).

As said before, the phase change time experimentally lasted about 116 min when the 10 mm sample is adopted. The simulation, instead, returned a value of 190 min. Consequently, another value for the latent heat is proposed to match the experimental results: 72 kJ kg^{-1}. This number is suggested by the technical datasheet of RT2HC [15]. In fact, it is stated that the phase change process occurs between 1 °C and 3 °C. In particular, between 1 °C and 2 °C the enthalpy difference is 32 kJ kg^{-1} and between 2 °C and 3 °C is 40 kJ kg^{-1}. The sum of these two values gives 72 kJ kg^{-1}. By assuming the value of 72 kJ kg^{-1} the numerical PCM temperature curve mostly overlaps the experimental one and the end of the melting process is caught too (112 against 116 min), as shown in Figure 3.8(c). So, it can be inferred that, the most realistic latent heat value to be considered is that measured among the peak phase change temperature, rather than declared by the datasheet. Finally, in Figure 3.9 the liquid fraction evolution (a) and temperature distribution (b) inside the aluminum specimen at three different times can be appreciated. It can be noticed that the liquid fraction was generated from the sides and in proximity to the aluminum fibers of the periodic structure. It evolved almost homogeneously, as the temperature did (Figure 3.9(b)). At end of the simulation the liquid fraction was 1 and the average PCM temperature was 5.5 °C, suggesting the melting process was finished and that the entire amount of latent heat was exchanged.

It can be concluded that the adopted numerical model can be considered a valid model, since it was able to predict the temperature of the phase change material over time and the temperature of the environment (the air in the box) in which the aluminum sample is set.

3.4.2 Model Validation based on experimental results collected by Glouannec et al. [70]

It is clear that, the experimental apparatus presented in section 3.4.1 referred to a small scale one. The 3D numerical model which involved the modelling of the entire system was reasonable for a small scale system but it can be difficult to be applied for the simulation of a real-scale applications. Therefore, we propose to develop a 2D model representing the section of a traditional European truck as already described in section 3.1. In order to validate the proposed numerical model involving the enthalpy porosity model combined with the sol-air temperature one, the experiments carried out by Glouannec et al. [70] were taken as reference. They studied an insulation wall made of 0.1 cm of metal sheet (denoted as "Body"), an air gap of 10 cm, 0.1 cm of fiberglass, 5.8 cm of polyurethane and 0.2 cm of polyester and fiberglass. The insulation wall was 86 cm tall. They applied a constant free stream external temperature of 10 °C for the first 4 hours and 30 °C for the last four (here also called "case 1").

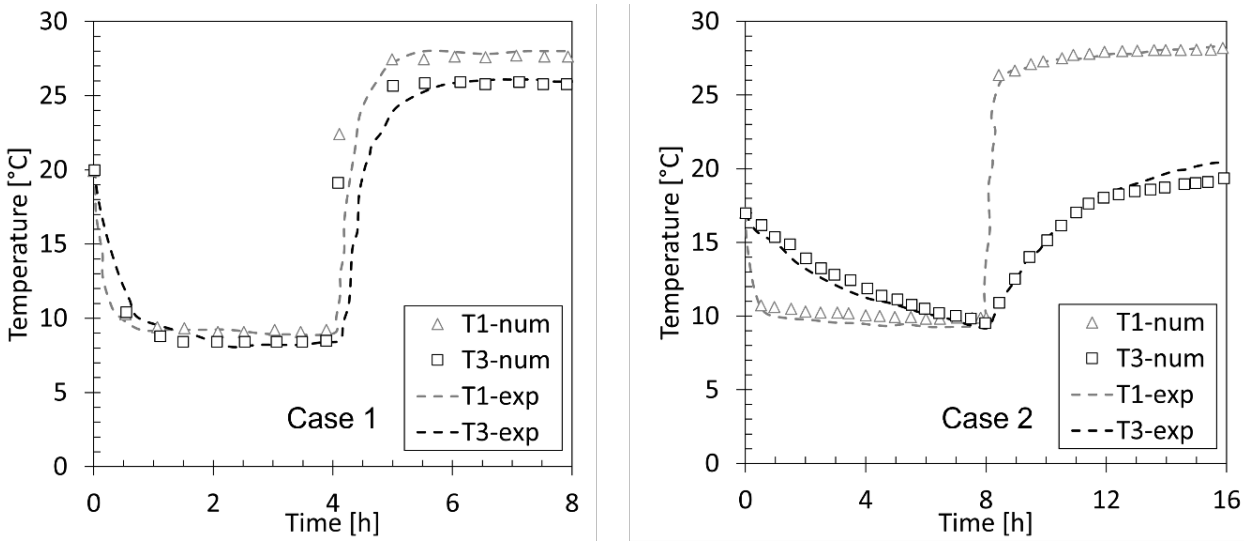

Figure 3.10 Comparison between present results and what obtained by Glouannec et al. [70] for case 1 and case 2.

The insulation wall was installed in a climatic adiabatic room maintained at 0 °C. They validated their numerical model against experimental results. Moreover, in the so-called "case 2", they inserted a panel filled with a phase change material (Energain®) just before the fiberglass layer and evaluated its effect on the heat transmission through the insulation wall measuring the temperature at different

locations. The experiment with the PCM layer (case 2) lasted 16 h. As for the other case 1 (*i.e.* without PCM), the first half journey presented an external free stream temperature of 10 °C while 30 °C for the last 8 hours was assumed. Therefore, the present authors reproduced both the scenarios and obtained results comparable to those reported by Glouannec et al. [70], as shown in Fig. 3.10.
T1 and T3 were the temperatures at mid-height of the inner side of the bodywork and of the outer side of the fiberglass layer (case 1) or PCM layer (case 2), respectively. The term "exp" refers to the experimental results collected by Glouannec et al. [70], whereas "num" refers to results coming from the developed numerical model. As seen, the present numerical model is able to reproduce the experimental data from Glouannec et al. [70] for both cases (with and without phase change). This let to study the thermal performance of the LTES adopting a simplified 2D model which does not require the modelling of the external air domain.

3.5 Results

As preliminary analysis, the effect of different truck speeds on the LTES performance was investigated. Three possible scenarios were investigated: a stationary vehicle (0 km h^{-1}), an ideal urban route (40 km h^{-1}) and an interurban route (80 km h^{-1}). The PCM and air temperature evolutions during the 10 h were evaluated. The LTES system based on the 0.5 cm RT2HC paraffin layer was selected for the analysis.

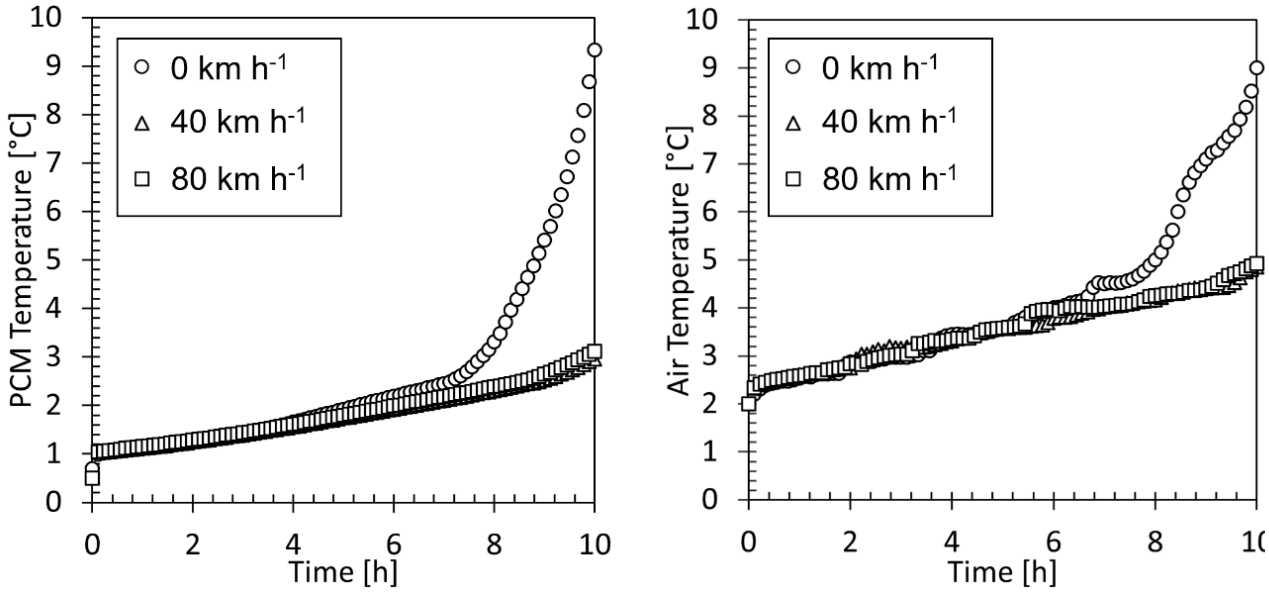

Figure 3.11 PCM and Air temperature curves for the RT2HC 0.5 cm layer at 0, 40, 80 km h^{-1}.

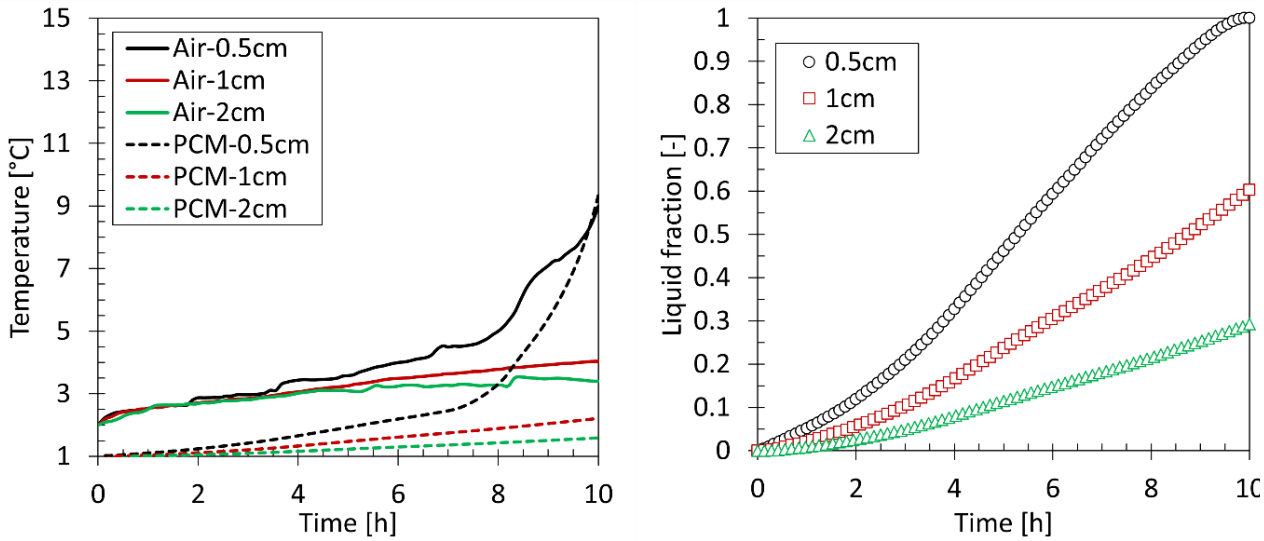

Figure 3.12 Volume-averaged PCM and air Temperature (left) and Liquid Fraction (right) for RT2HC at three different PCM layer thicknesses.

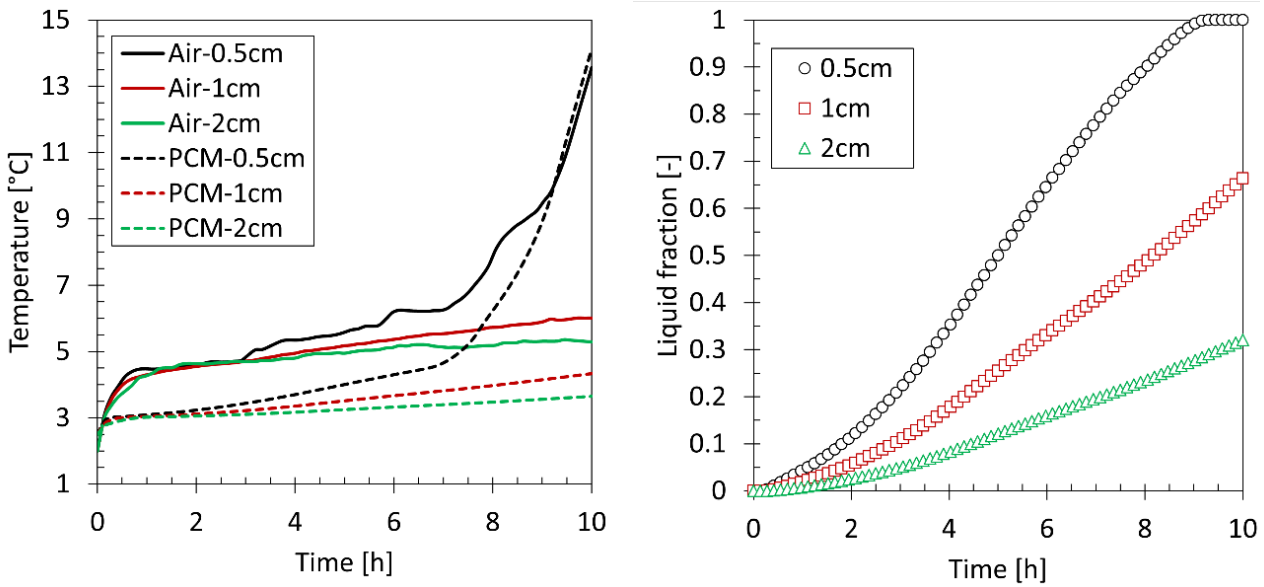

Figure 3.13 Volume-averaged PCM and air Temperature (left) and Liquid Fraction (right) for RT4 at three different PCM layer thicknesses.

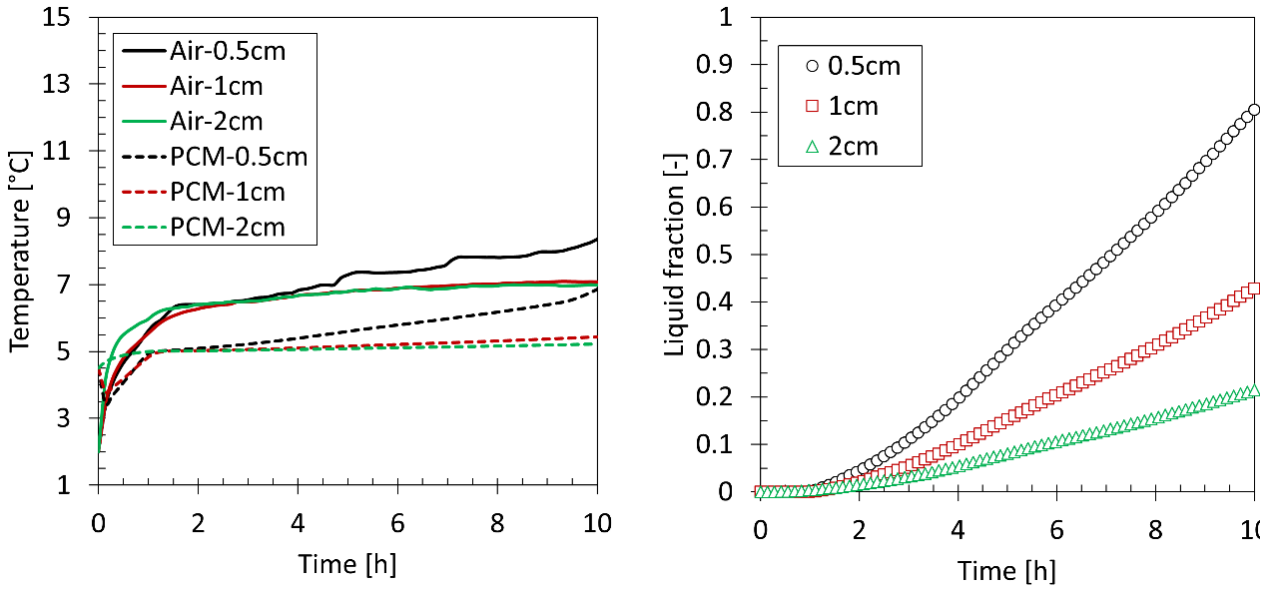

Figure 3.14 Volume-averaged PCM and air Temperature (left) and Liquid Fraction (right) for RT5HC at three different PCM layer thicknesses

As shown on the left-hand side of Fig. 3.11, the PCM temperature was noticeably lower for the urban and interurban scenarios (40 and 80 km h^{-1}, respectively) if compared with the stationary vehicle (0 km h^{-1}). In fact, under stationary truck condition, the PCM temperature reached about 9 °C at the end of the simulation whilst around 3 °C in case of moving truck. Similar conclusions may be taken for the air temperatures (Fig. 3.11, right side). This means that, in the investigated range of operating conditions, the convection helps in limiting the amount of heat entering in the truck cell by reducing part of the incident solar radiation. On the basis of these results, only the stationary vehicle condition was adopted for the subsequent numerical analyses being the worst-case scenario.

In Fig. 3.12-13-14 (left sides), the volume-averaged PCM temperature and air temperature for the three paraffin-based PCMs investigated with three different PCM layer thicknesses (0.5, 1, 2 cm) are plotted. The ability of the LTES system in maintaining the air temperature inside the cell as close as possible to the ideal melting PCM temperature without the use of refrigerated system is demonstrated. Considering the results for RT2HC, as shown in Fig. 3.12, the 0.5 cm layer permitted to maintain the air temperature inside the refrigerated cell below 3 °C for the first 4 h. This threshold (3 °C) is the *liquidus* temperature of RT2HC: it means that when the temperature exceeds 3 °C the PCM is locally melted. For the next 4 h, the air temperature ranges between 3 and 4 °C, while, at the ninth simulated hour a sharp temperature increase is noted. In fact, from the end of the eighth hour till the end of the simulated truck journey, an evident change of slope for the air temperature curve can be appreciated. This can be attributed to the advance of the PCM melting process which weakens the ability of PCM

in counteracting the external heat load entrance, resulting in an air temperature increase. Between the seventh and the eighth hour, a sudden PCM mean temperature rise can be observed, as shown by the black dotted line plotted in Fig. 3.12. Comparing the PCM temperature curve with the liquid fraction one (Fig. 3.12 (right side), black line), it can be noted that for the most part of the melting process (about 8 h, *i.e.* 85% liquid) the PCM temperature was maintained between the *solidus* and *liquidus* temperatures. Therefore, the ability of the PCM layer in limiting the heat load to be transmitted inside the refrigerated cell is weakened as the PCM is almost completely melted. The sharp rise in the PCM temperature reflected in the increase in air temperature, up to 9.5 °C; this is mainly due to the sensible heat transfer to liquid PCM. This can potentially be detrimental for fresh foods which must be transported and delivered at temperatures around 2-3 °C. Hence, a design with a thicker layer was investigated. Focusing on the left side of Fig. 3.12, a similar trend in the air temperature curve for the 1 cm and 0.5 cm cases can be noted during the first 4 h of the simulation. Nevertheless, from the 4th till the 10th hour the curve slope is steeper for the 1 cm PCM layer scenario compared with 0.5 cm one, and no air temperature rise. In fact, studying the mean PCM temperature curve trend (red dotted line, Fig. 3.12), it is evident that RT2HC temperature was in the melting range for the entire simulated truck journey. On the right side of Fig. 3.12, it is shown that only some 59% of PCM melted at the end of the simulation. However, the air temperature stabilized at about 1°C above the *liquidus* temperature, *i.e.* at 4 °C, during the last 2 hours. If the temperature requirements are not so strict for the carried foodstuff, the 1 cm configuration can be considered as the best one. On the contrary, for more temperature sensitive products, a thicker layer can be used. The PCM layer was therefore increased to 2 cm. In this scenario, the air temperature curve assumed a different trend, as plotted in Fig. 3.12 (green line). It flattened asymptotically along the *liquidus* temperature threshold. After ten simulated hours, only a quarter of RT2HC melted, as shown in Fig. 3.12 (right side), and an air temperature of only 3.3 °C was reached. The air temperature curve trend and the amount of liquid fraction suggest the LTES with 2 cm layer design to be suitable for a prolonged truck route. However, this suggestion will be investigated in future works. What discussed for RT2HC, can be extended to RT4 and RT5HC. Nonetheless, for 0.5 cm RT5HC layer the air temperature did not show any sudden temperature rise; in fact, the air temperature for all the investigated thicknesses increased with an almost constant slope. Moreover, it is interesting to notice that, despite of having an higher melting point, RT5HC let the air temperature to be at a lower value if compared with the other two paraffins at the end of the tenth simulated hour. In fact, when considering RT5HC, the air cell temperature reached a value around 8 °C, which is very close to the value in the case of RT2HC (9 °C) but remarkably lower compared with RT4 (14 °C). This is due to the high latent heat value of RT5HC compared with the others (250 kJ kg^{-1} against 170-200 kJ kg^{-1} of the other paraffin waxes) which

improved the paraffin ability in acting as a thermal barrier for the external heat load transmission. Thus, it can be stated that the optimum PCM must be selected considering the best trade-off between the melting temperature that controls the air temperature and the values of the latent heat and thickness that control the energy capacity and thus the available operating time.

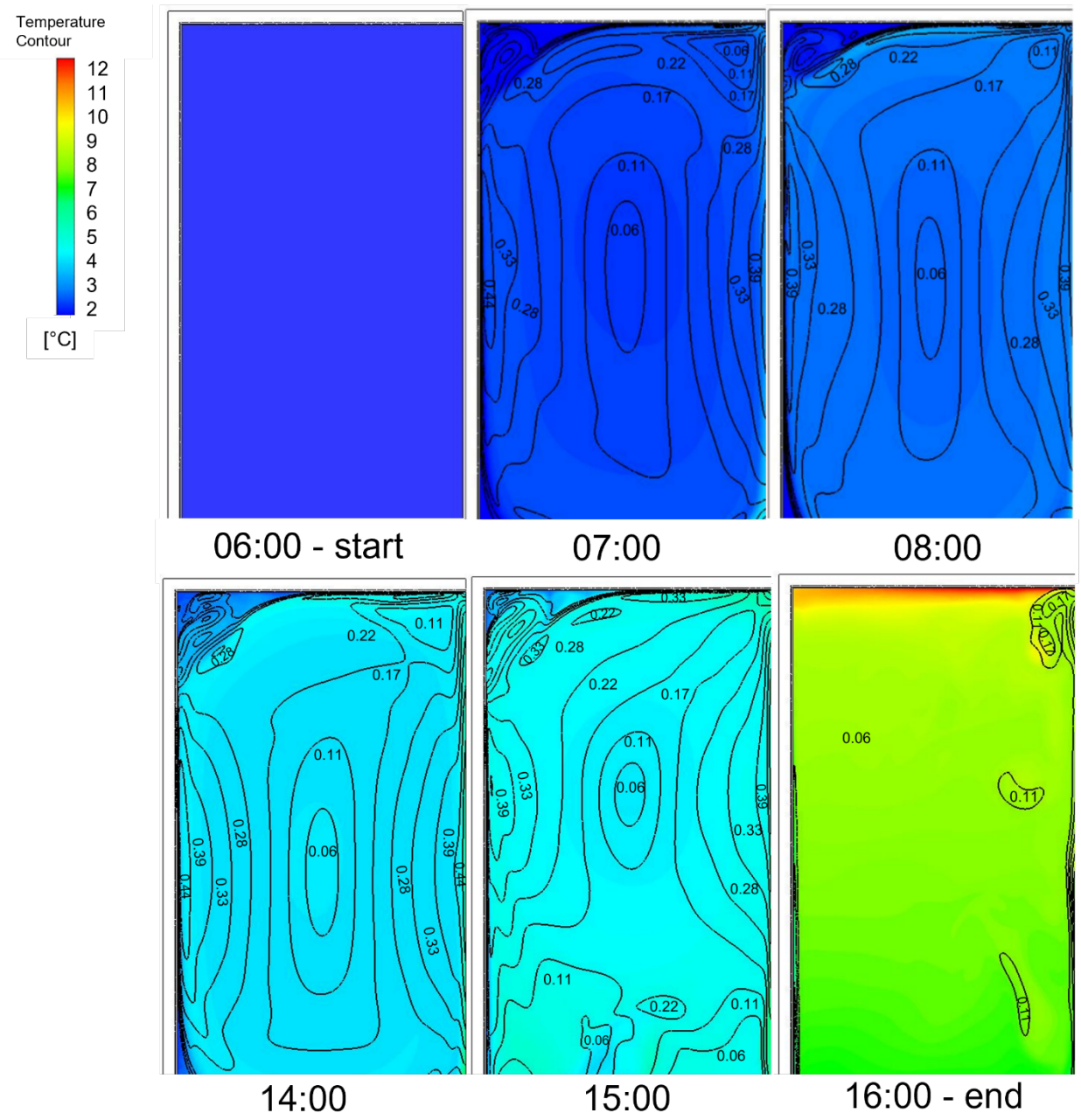

Figure 3.15 Air temperature contours and velocity isolines inside the refrigerated cell at the early (from the start to 8.00) and final stages (from 14.00 to the end) for 0.5 cm RT2HC layer

For the LTES system with 0.5 cm RT2HC layer, the temperature and velocity distribution inside the refrigerated cell are demonstrated in Fig. 3.15. In particular, in Fig. 3.15 (top line) the temperature distribution during the first three hours of the simulated route is visualized. As seen, a main convective

cell is formed in the middle of the cabin. In fact, the air, being heated up from the bottom of the cell, moved upwards. When the cell ceiling was reached, the air was cooled down by the PCM which was at a lower temperature (see Fig. 3.12 (left side)) and moved downwards.
These convective movements continued until an appreciable temperature gradient between the air and PCM existed. In Fig. 3.15 (bottom line) the air temperature behaviour during the last three simulated hours is shown. As shown in Fig. 3.12, after the 9th hour, the PCM temperature approached that of air thus weakening the convective air movement. In particular, as shown in Fig. 3.15 (bottom-right), during the last hour, a horizontal temperature stratification occurred. The air in the upper part was warmer (about 12 °C) compared with the air close to the side of the cell. Comparing the all frames in Fig. 3.15, it can be stated that the air velocity never exceeded 0.5 m s^{-1}, demonstrating that the air motion inside the cell is almost laminar.

The PCM at the uppermost part of the cell (denoted as "top" in Fig. 3.16) reached the complete melting earlier than the side of the cell (denoted as "side" in Fig. 3.16) justifying a greater PCM temperature (and of the closest air, consequently). The RT2HC on top was completely melted at the eighth simulated hour, while the PCM along the side of the cell was not melted at all during the tenth hour. In fact, a liquid fraction of some 80% can be found, as shown in Fig. 3.16. The PCM contained in the side enclosure of the cell reached the end of melting process only close to the tenth hour.

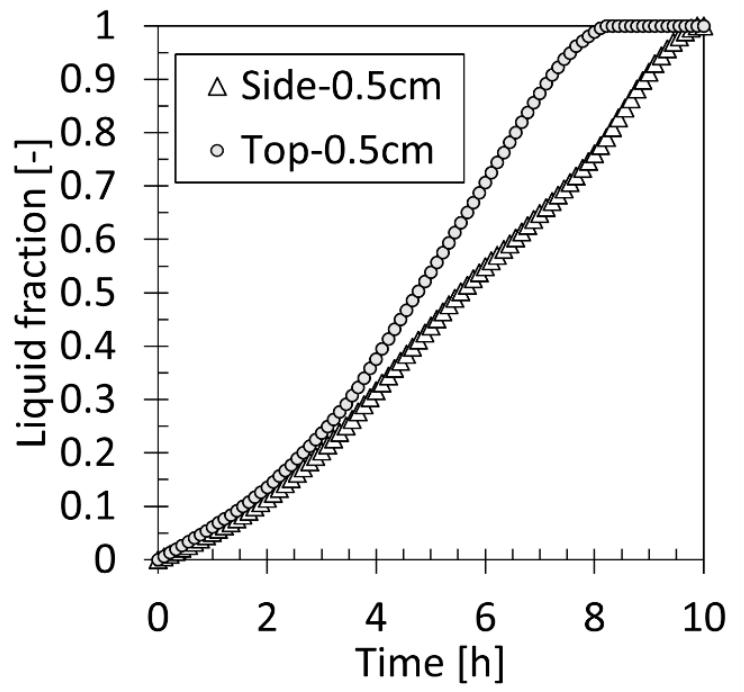

Figure 3.16 Liquid fraction trend, for the side and top of the refrigerated cell.

The different behaviors between the PCM on top and side of the refrigerated cell call for investigating a different scenario. In particular, a non-uniform wall was considered: a PCM layer of 0.7 cm on the top wall and 0.4 cm thick layer on the side. The amount of PCM was kept constant in order to fairly compare the two case studies. Observing the left part of Fig. 3.17, it is clear that not appreciable differences can be detected between the PCM equally distributed on the truck refrigerated cell scenario and the non-uniform one. The two curves representing the liquid fraction for the investigated innovative insulation walls in these two situations mostly overlap. Anyway, if liquid fraction trends on side and top are separately analysed, it is noticeable that in the case of insulation layer wrapping a non-uniform PCM layer (Fig. 3.17 (upper part)) the side and top trends are closer than in the case with uniform PCM layer (Fig. 3.16). There's only a gap of 1 hour between side and top in reaching the end of the melting, compared with 2 hours for the 0.5 cm RT2HC uniform layer. It is possible to find an optimal configuration resulting in a temperature distribution as uniform as possible along the cell's top and sides. Therefore, in the nextcoming work the performance of an optimized non-uniform layer will be investigated aiming at discovering its effects on the ability in maintaining the proper temperature inside the refrigerated cell.

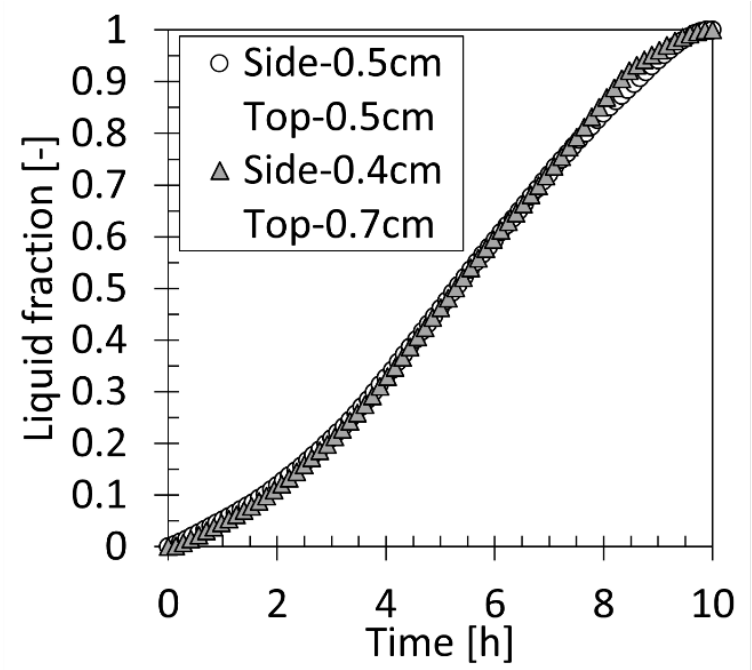

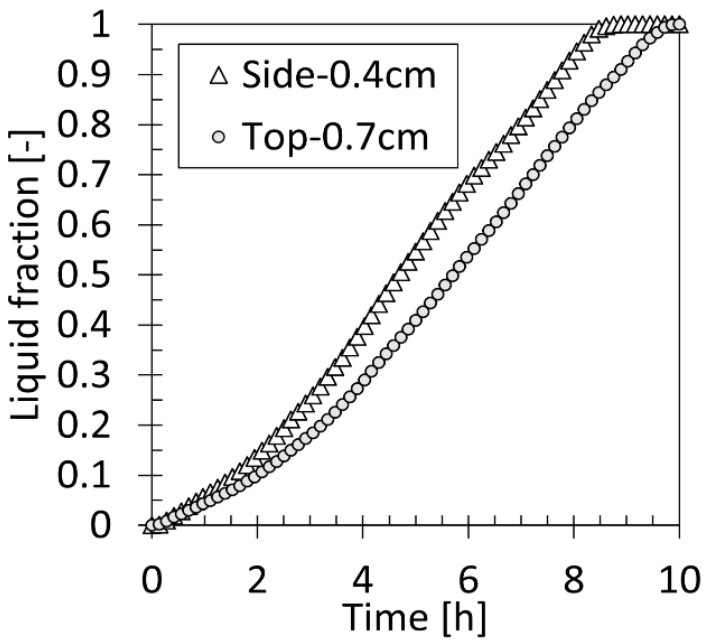

Figure 3.17 Comparison in terms of liquid fraction trend between uniform and not-uniform RT2HC layer (up), between side and top RT2HC layer for the not-uniform layer (down).

Finally, it is significant to stress that the solutions proposed in this work can potentially have a further development in order to be employed in real applications. Actually, considering a 6 m long truck and assuming 1 cm PCM layer, approximately only 200 kg (440 lb) of PCM are required making the novel ideal insulation wall suitable for a concrete application.

4. The effects of the food cargo on the performance of the proposed solution

As reported in Chapter 3, a 2D section of a typical European refrigerated vehicle was modelled. Its external width ("top" and "bottom" in Fig. 4.1(a)) was set equal to 1.3 m (half of 2.6 m) aiming at exploiting the symmetry of the system, while its height was supposed to be 2.4 m ("side" in Fig. 4.1(a)). The problem is, in fact, axisymmetric with respect to an axis dividing the section in two identical zones (denoted as "symmetry", as shown in Fig. 4.1(a)). Aiming at counteracting the heat load entering from the external environment, an innovative insulation layer was developed, having a 5 cm thick poly-urethane layer which wraps a second one of 0.5 cm filled of the commercial paraffin-based PCM RT2HC supplied by Rubitherm [136], whose main properties are resumed in Table 4.1.

Table 4.1 Phase Change Material thermo-physical properties

PCM	k (W m^{-1} K^{-1})	ρ_{sol}/ρ_{liq} (kg m^{-3})	c_p (J kg^{-1} K^{-1})	L (kJ kg^{-1})	T_{sol}/T_{liq} (°C)
RT2HC	0.2	880/770	2000	200	1/3

The authors also added a thin layer of 0.5 cm consisting of aluminum which acts as the PCM encapsulation, separating the PCM and the air domains. For the sake of avoiding redundancy, the entire description of the geometrical model will not be reported in the followings; the reader may refer to the previous chapter for additional details.

In Fig. 4.1(b) the presence of the cold cargo that was considered in the present work can be appreciated. Different food loads were investigated, 25%-50%-75%. The smallest food load percentage represents the volume occupied by the foodstuffs during the final daily operation, 50% stands for an average value of the transported cargo, while 75% represents the almost full-loaded scenario, i.e., at the start of the truck daily operation. These different scenarios were compared among each other and with the empty scenario. The food cargo was modelled as a solid domain and consisted of, alternatively, three different materials (apple, broccoli and tunafish) in order to investigate the effect of different food characteristics (see Table 4.2) on the thermal performance. Moreover, it is known that fresh foodstuffs (fruits and vegetables) are temperature-sensitive goods, and, having metabolic activity [75], they usually release the heat of respiration to the environment in which they are located [83]. The food was set at a margin of 50 mm from the aluminum encapsulation and 20 mm from the axis of symmetry; two consecutive boxes are 40 mm spaced, consequently. Each box was supposed to have the x-dimension of 1170 mm and located on a 140 mm high europallet.

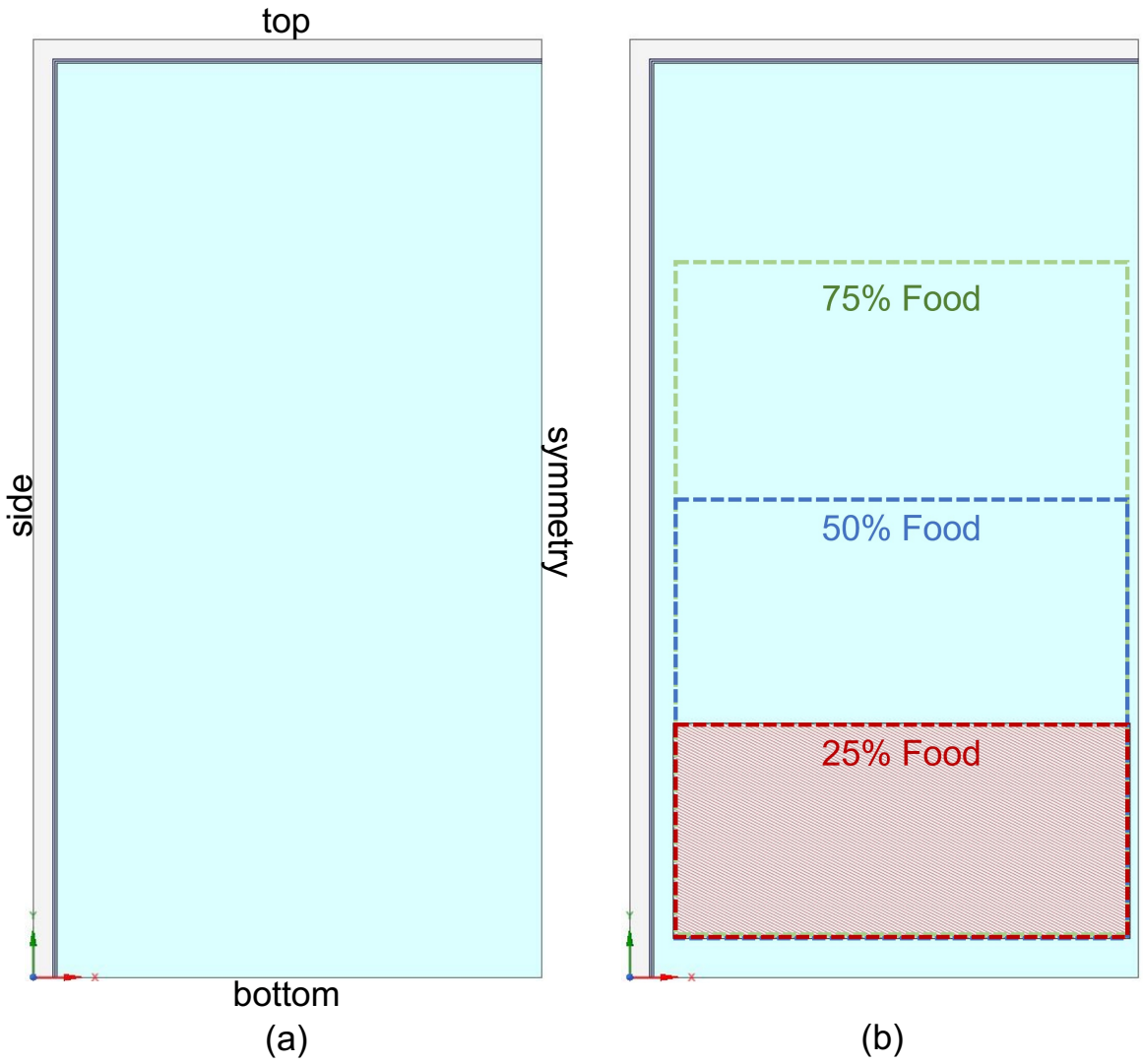

Figure 4.1 2D section of the refrigerated truck cell: empty (a), with food loads (b).

The boxes were supposed to be located in this way so the generated buoyancy-driven airflow could flow under the pallets, in the space between the encapsulation and the cargo, and between the two cargoes. All the thermo-physical properties of the solid domains are shown in Table 4.2.

Table 4.2 Solid materials thermo-physical properties.

Material	k (W m^{-1} K^{-1})	ρ (kg m^{-3})	c_p (J kg^{-1} K^{-1})
Poly-Urethane foam	0.03	35	1380
Aluminium	202.4	2719	871
Apple	0.418	450	3840
Broccoli	0.385	560	4010
Tunafish	0.531	1070	3430

The presence of the external hourly solar irradiance was used to calculate the heat load entrance. By adopting the sol-air model [129] the fictitious free stream temperature T_{sa} was obtained as the sum of the external temperature and the ratio between the product of the solar irradiance for a tilted surface and the surface absorptance divided by the heat transfer coefficient *HTC*, as already shown in the previous chapter. The *HTC* was set equal to 10 W m^{-2} K^{-1} for the side and top of the cell, whilst 0.7 W m^{-2} K^{-1} at the bottom which takes into consideration the non-modelled 5 cm poly-urethane foam layer. The appropriate T_{sa} was set for the side and top, which exchanged the heat by means of convection and radiation, whilst the external temperature was set as free stream temperature for the bottom, which, being in shadow, was not affected by solar radiation. The truck was supposed to be stationary aiming at investigating the worst-case scenario. Three different scenarios had been previously analyzed: stationary-scenario (0 km h^{-1} truck speed), urban-route-scenario (40 km h^{-1}) and interurban-route-scenario (80 km h^{-1}). Among them, for the stationary-scenario, the highest sol-air temperatures for each truck surfaces were obtained. Therefore, this scenario was considered for the subsequent analyses. The boundary condition of the side of the truck involved the setting of the maximum hourly value of T_{sa} among the western and eastern ones for each simulated hour from 6 AM to 4 PM. The climate data refer to the city of Vicenza, Northern Italy. For all the scenarios (with or without food load) the temperature of the air in the refrigerated cell was initialized at 2 °C. The PCM, instead, was initialized at 0.5 °C in order to ensure its complete solid state before running the simulations. The food load was initialized at 2 °C, but, when investigating the pre-cooling temperature effect, it was initialized at 5 °C or 10 °C.

4.1 The Equations

To estimate the global solar radiation for each truck surfaces, the same equations reported in the previous chapter were adopted.

To study the thermal performance of the innovative proposed LTES system, the “Solidification and Melting Model” was adopted to run the CFD numerical simulation in the “Ansys Fluent 18.2” environment [137] (see Chapter 3).

In order to analyse the food heat respiration effect on the thermal fluid dynamics, an energy source in the energy equation was added by treating the food domain as a heat source. A user-define-function (UDF) was developed to calculate the heat respiration as a function of the food temperature and implemented accordingly. The equation (Eq. (4.1)) of the heat of respiration of the food, *HR* (W m^{-3}), adapted from [123], considered in the present analyses is:

$$HR = \rho \frac{10.7f}{3600} \left(\frac{9}{5}t + 32\right)^g \quad \text{Eq. (4.1)}$$

Where, t (°C) is the food temperature, ρ (kg m^{-3}) is the food density, f and g constant respiration coefficients which are specific for each fresh foodstuff (apples or broccoli) [123].
Additionally, the conservation of mass is solved:

$$\nabla \cdot (\rho \boldsymbol{v}) = 0 \quad \text{Eq. (4.2)}$$

The convective terms with first order derivatives were linearized by adopting a second order upwind scheme, while a second order differencing scheme was preferred to linearize the diffusive terms with second order derivatives. The SIMPLE scheme was used to solve the pressure-velocity coupling while the PRESTO! one was chosen for pressure correction, as proposed by Zhao et al. [138]. All of the other equations were linearized using the algebraic multigrid (AMG) iterative strategy.

4.2 Sensitivity Analyses

The proposed model of the novel LTES system had been already validated using the data collected in the lab and the experiments reported in [70]. In fact, as already shown in Chapter 3, the numerical results coming from the here presented model are very close to the experimental results, with average percentage errors less than 5% for the sensible and latent cases, suggesting the validity of the model.

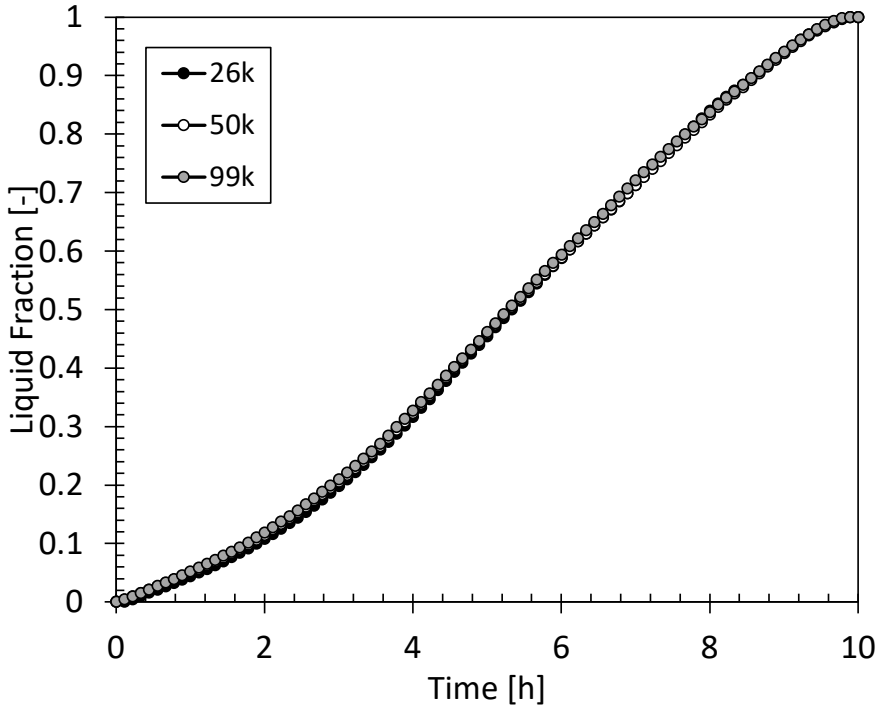

Figure 4.2 Mesh sensitivity analysis for the 25% food loaded scenario

As shown in Fig. 4.2, an additional mesh sensitivity analysis was run. The 25% food loaded refrigerated cell was selected as reference case, on which tuning the best grid constructive parameters. To compare the different results, the liquid fraction evolution curves over the 10 simulated hours were chosen. From Fig. 4.2 the independence of the solution from the grid can be appreciated. It is clear that the three different investigated meshes (26k, 50k, 99k elements) didn't take to different solutions, even if having different computational times to complete the simulation. Therefore, aiming at limiting as much as possible the computational errors, the 50k elements mesh was considered the best compromise and, the parameters chosen to generate the 50k elements mesh were fixed and adopted for the simulations of the other scenarios.
For what concerns the time step size, the value of 0.1 s was considered the best trade off between solution accuracy and computational efforts, thus selected and adopted even for the subsequent analyses. For additional details, the reader may refer to Chapter 3.

4.3 Results

In Fig. 4.3, the volume-averaged air temperature (Fig. 4.3(a)), PCM temperature (Fig. 4.3(b)), liquid fraction (Fig. 4.3(c)) and apple temperature (Fig. 4.3(d)) as function of the simulated hours for the empty and apple cargo loaded scenarios are shown. The potentiality of the LTES system in ensuring the air temperature inside the cell as closely as possible to the reference phase change PCM temperature without involving the adoption of the refrigerated system is investigated. By focusing on the empty scenario (white triangles) it can be noticed that the air temperature of the refrigerated cell is maintained below 3 °C for the first 4 h. This threshold (3 °C) is the *liquidus* temperature of the PCM: therefore, when the temperature exceeds 3 °C the PCM is locally melted. For the subsequent 4 h, the air temperature is kept between 3 °C and 4 °C while, just after the eighth investigated hour, a sharp temperature increase is detected. Indeed, from the ninth hour till the end of the simulated vehicle route, a noticeable change of slope for the air temperature can be observed. This behavior can be ascribable to the progress of the PCM melting process causing the ability of the paraffin in counteracting the external heat load penetration to be weakened, resulting in an air temperature increase. Additionally, in the period from the seventh and the eighth hour, a sudden average PCM temperature rise can be appreciated (Fig. 4.3(b)). The comparison between the PCM temperature curve with the liquid fraction one lets to point out that for the most part of the melting process (about 8 h, i. e. 85% liquid, Fig. 4.3(c)) the PCM temperature is maintained between the *solidus* and *liquidus* temperatures.

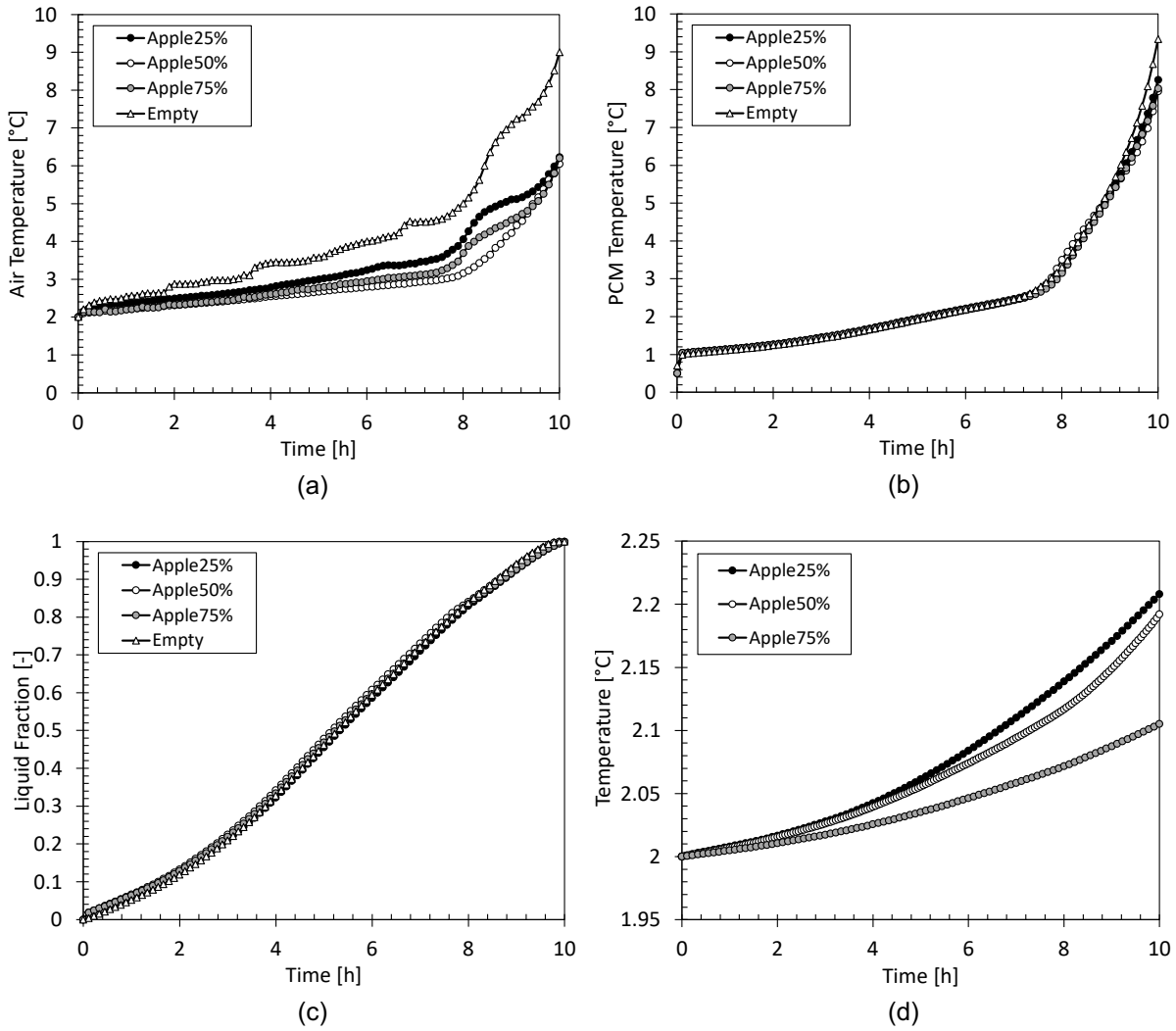

Figure 4.3 Air temperature (a), PCM temperature (b), liquid fraction (c), apple temperature (d) curve evolutions, with different food loads

As a result, the capacity of the paraffin-based PCM layer in slowing down the external heat to be transmitted inside the refrigerated cell is lessened since the PCM is almost completely fused. The sharp rise in the PCM temperature causes the air temperature to be increased, up to 9.5 °C; this is essentially imputed to the sensible heat transfer due to the almost complete liquid PCM. It is well known that this value can potentially be detrimental for perishable goods which must be transported at temperatures around 2-3 °C.

Nevertheless, different air temperature evolutions can be detected when the cold freight is inserted inside the refrigerated cell. Focusing on Fig. 4.3(a) it can be immediately observed, that, despite the similar trends, significantly different final air temperature values are reached. As already stated, in the empty scenario the final air temperature reaches 9.5 °C. When the cold cargo is inside the refrigerated truck cell a final temperature of about 6 °C is calculated, which lets to maintain the

perishable transported goods in an appropriate environment for the preservation of their quality and safety. By comparing the four air temperature curves in Fig. 4.3(a), it can be affirmed that all of them present a sharp temperature increase at the eighth hour, since the air temperature is strictly related to the PCM temperature evolution. Despite the diverse food loads, the PCM temperature curves (Fig. 4.3(b)) and liquid fraction curves (Fig. 4.3(c)) mostly overlap. This is due to the fact that the PCM temperature and the melting process, consequently, depend mostly on the external applied environmental conditions which are exactly the same for all the investigated scenarios. The presence of the different cold freight has a more evident impact on the air temperature inside the refrigerated cell (Fig. 4.3(a)) and, obviously, on the food temperature (Fig. 4.3(d)). By focusing on Fig. 4.3(a), the effect of the three apple load percentages on the air temperature evolutions can be detected. It is interested to notice that the lowermost temperature curve for every simulated instant is ensured by the 50% food loaded case, the 75% is set at an intermediate level while 25% leads to the highest temperatures. It is clear that all the food loaded investigated cases lead to an air temperature lower than the empty scenario at every instant. This phenomenon can be explained by comparing the air temperature distributions among the three food load scenarios and with the temperature distribution inside the refrigerated cell for the empty case, as shown in Fig. 4.4.

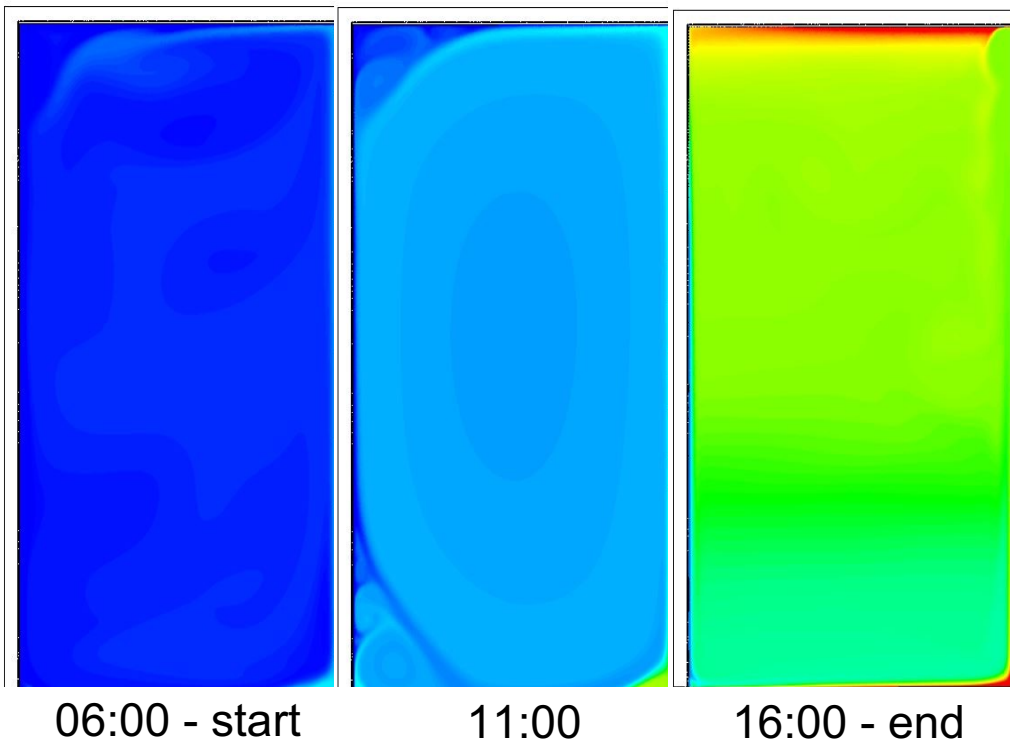

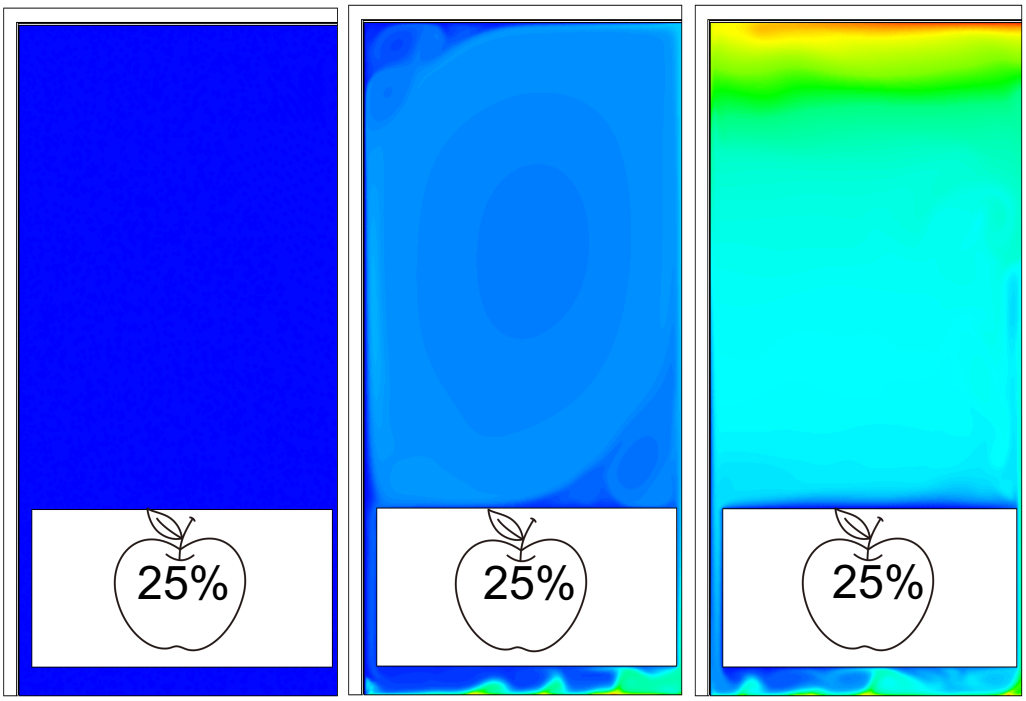
25%
25%
25%
06:00 - start
11:00
16:00 - end

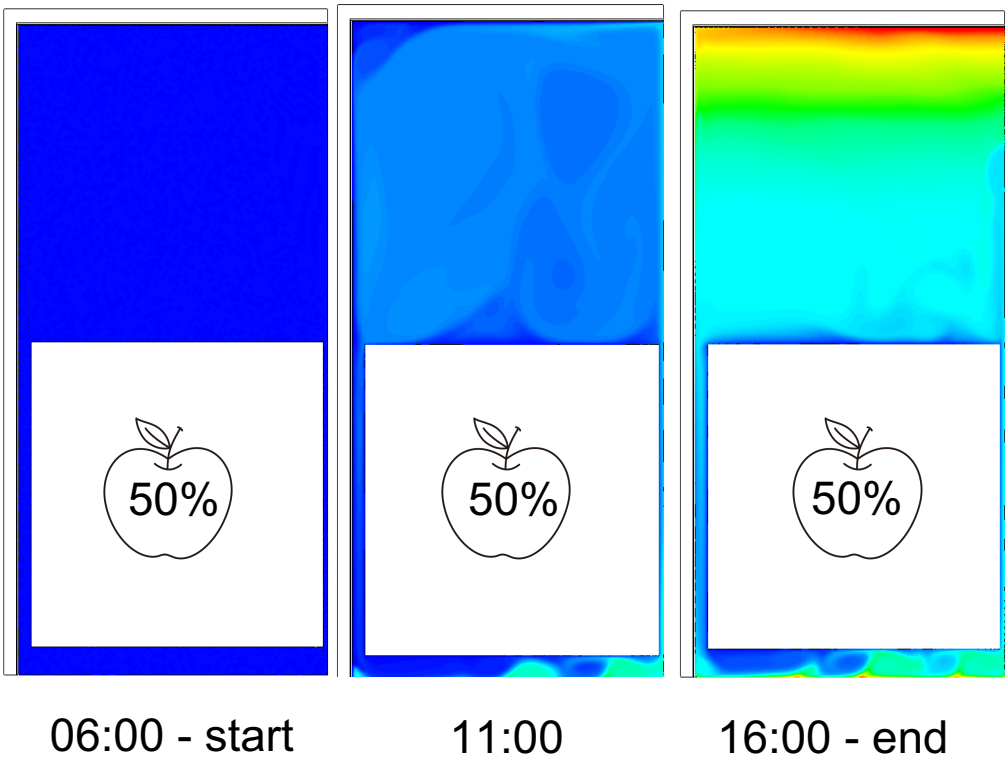
50%
50%
50%
06:00 - start
11:00
16:00 - end

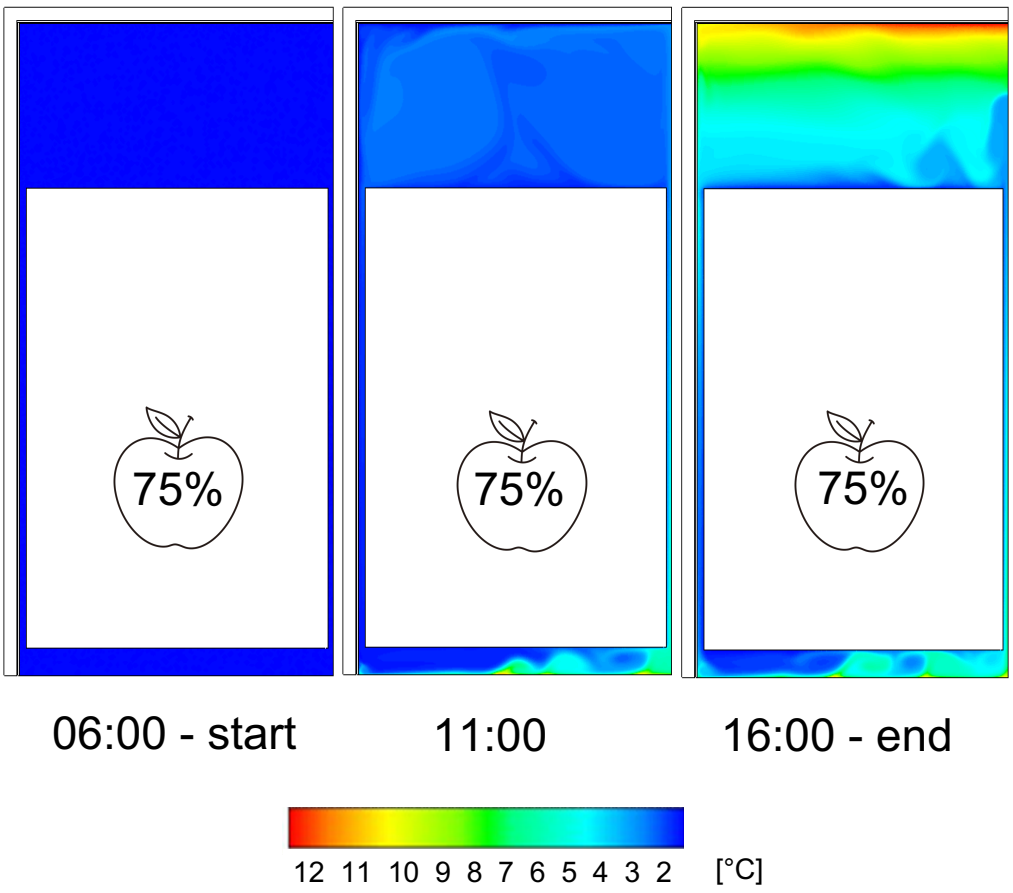

Figure 4.4 Air temperature distribution inside the refrigerated cell, for the empty scenario and 25% -50% - 75% food load scenarios, at three different instants.

Three instants are chosen to compare the different scenarios: the start of the route (6:00), the middle of the route (11:00) and the end of the route (16:00). By focusing on the empty cabin firstly, it can be observed that a main convective cell is formed in the middle of the refrigerated compartment. The convective movement is due to the air heated from the bottom which causes the air to be moved upwards. When reaching the top of the cabin, the air is cooled down by the PCM which is a at a lower temperature value, as it can be noticed by comparing Fig. 4.3(a) and Fig. 4.3(b). The air circulation exists until a temperature gradient between the air and PCM can be appreciated. As a result, during the end of the simulation, when the temperature differences become negligeable, the air tends to stratify horizontally, reaching an average value around 9.5 °C. A similar behaviour can be detected when a 25% apple load is put inside the cold cabin. A main convective cell is, in fact, generated during the journey while a horizontal temperature distribution is visualized during the final stage of the daily operation. Unlike the empty scenario, the final average air temperature is significantly lower, since the addition of the food load acts as a cold thermal mass which weakens the air temperature increase, even if the PCM is completely melted. Therefore, a final average temperature of 6 °C can be appreciated. A different temperature distribution can be identified for the 50% food loaded

scenario. When considering the temperature contours at 11:00 (Fig. 4.4) a main convective cell cannot be observed anymore. There are only some local generated vortices since the presence of half of the volume occupied by the food cargo does not let the air to easily recirculate. When 75% of foodstuff is analyzed, local vortices cannot be clearly identified, since the low space available for the air movement. However, from what just stated and from what shown in Fig. 4.3(a), the 50% food loaded cabin always presents the lowest temperature since it can take advantage of the double concurrent effects of the air heat exchanged by convection and the presence of a significant additional thermal cold mass during the simulated route. The scenario involving the insertion of 50% food cargo can be therefore considered the best trade off. It can also be concluded that the placement of the cold food cargo inside the proposed LTES system has a positive contribution in preserving and maintaining the optimal temperature distribution condition.

The same conclusions can be also stated for the other two investigated food cargo materials: broccoli and tunafish.

As, in fact, reported in Fig. 4.5, broccoli (Fig. 4.5(a)) and tunafish (Fig. 4.5(b)) present an air temperature curve evolution over time which is strictly comparable with what obtained by adopting apples (Fig. 4.3). This suggests that our LTES system is a valid solution, independently from the transported cargo typology.

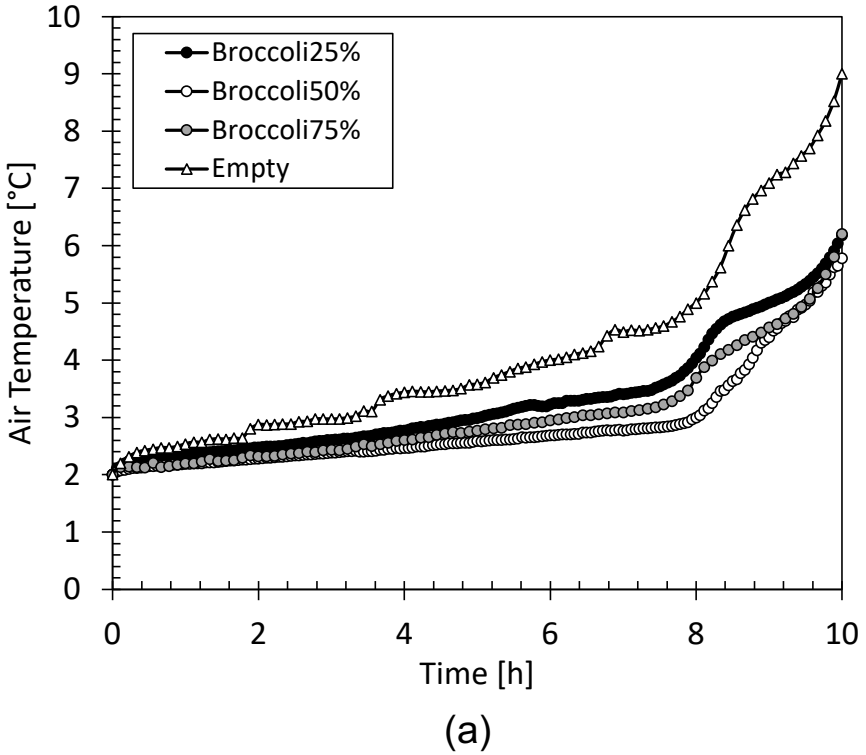

(a)

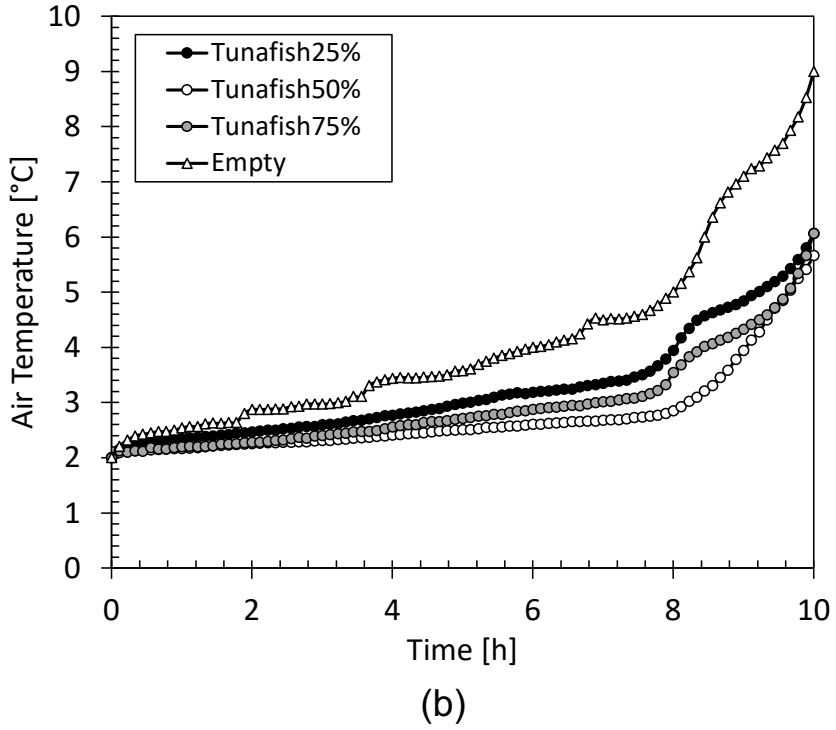

(b)

Figure 4.5 Air temperature curve evolutions for different food loaded scenarios and materials: (a) broccoli, (b) tunafish.

When dealing with temperature sensitive perishable foodstuffs, it is necessary to take into consideration the effect of their intrinsic metabolic activities since they can potentially negatively affect the maintenance of the suitable temperature condition. In the worst case, uncontrolled metabolic activities can take to food losses and wastages.

Therefore, the present authors investigated the effect of the heat of respiration, as reported in Eq. (4.1), by monitoring the air cabin temperature and the food temperature during the daily simulated route.

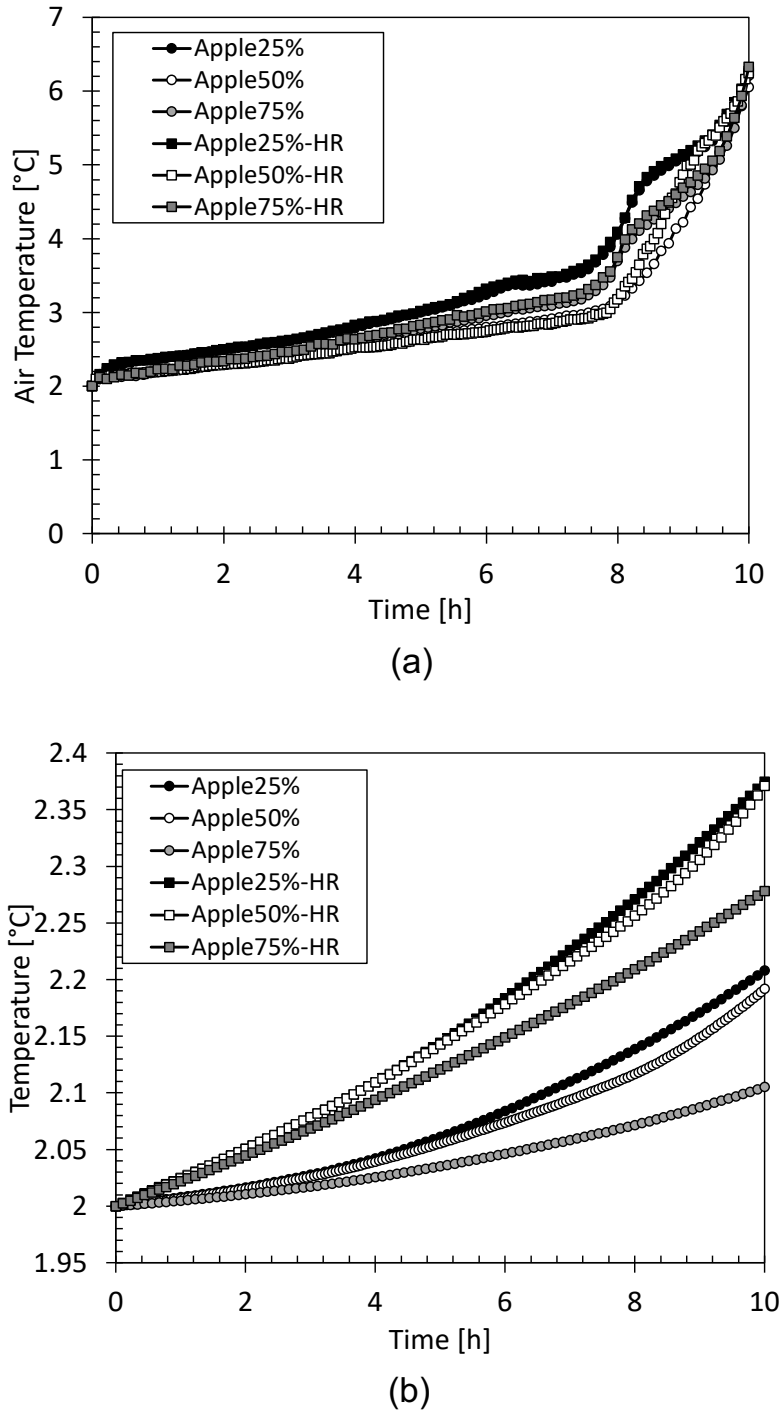

Figure 4.6 Air (a) and food (b) temperature curve evolutions for different food loaded scenarios, with and without considering the effect of the heat of respiration.

As shown in Fig. 4.6, the effect of the heat of respiration (denoted as "HR" in the legends) can be appreciated. By following the air temperature curves for the three food loaded studied scenarios, it can be observed that the heat of respiration does not have an evident impact on the air temperature. Consequently, for each food loads the air temperature curves with or without the considered relative heat of respiration tend almost to overlap. In fact, under the simplified conditions set for the proposed

LTES system (no heat infiltrations due to door openings and only 10 h daily route supposed) the heat of respiration seems to be negligeable since the temperature increase occurs at the final stages only. However, by focusing on Fig. 4.6(b) and by choosing, for example, the 50% food load case, it is evident the effect of the heat of respiration on the food temperature. At the tenth simulated hour, when the heat of respiration is not added to the numerical model, the temperature of the food reaches 2.17 °C, while it reaches about 2.38 °C under the effect of the heat of respiration. Moreover, the growing rate of the curve incorporating the effect of the heat of respiration is sensibly higher than the one without it. Thus, it can be speculated, that, since the role of the PCM in counteracting the external heat load entrance is extinguished at the end of simulation, having reached the complete melting, the role of the heat of respiration would be more important if an extension of the truck route is simulated.

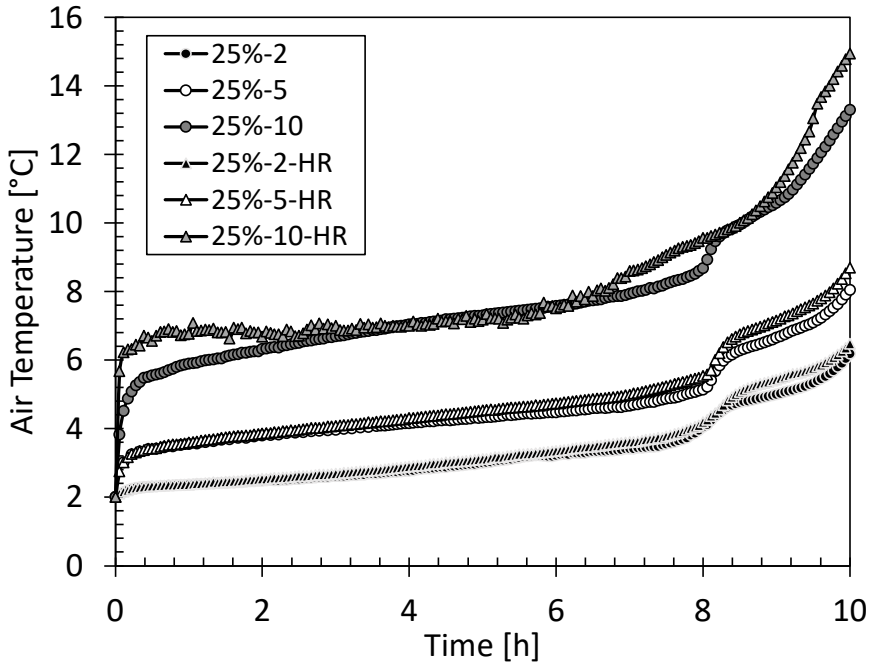

Figure 4.7 Air temperature evolution for the 25% food load and different pre-cooling temperature (2 °C, 5 °C, 10 °C) with or without heat of respiration

Moreover, the fresh foodstuffs usually receive a pre-cooling process before entering the refrigerated truck [123]. It is not always necessary for the cargo to be cooled down to the temperature of the cold air (2 °C in the proposed solution). Therefore, by fixing a food load of 25%, the authors investigate the effect of the food precooling temperature. Three different values are chosen: 2 °C, 5 °C, and 10 °C. Additionally, for each pre-cooling level, the effect of the heat of respiration is also studied.

From what demonstrated in Fig. 4.7, it can be noticed that the pre-cooling food temperature has an impact on the thermal performance of the system. When the food enters at a temperature of 5 °C, the air, starting at 2 °C, needs about 8 h to reach that temperature, since the ability of the LTES in reducing the temperature increase. However, when the food is pre-cooled at 10 °C, the air jumps in few times

to 5.5 °C and then grows up to 8 °C in 7 h. 8 °C can be considered the critical threshold at which the fresh product can be maintained in order to not lose the quality. Thus, the suitable conditions are ensured for 7 h only. Moreover, the higher the pre-cooling temperature, the higher the heat of respiration effect. In fact, the heat of respiration let the final temperature to be 0.3 °C, 0.65 °C, 1.08 °C higher than the one without the heat of respiration, for 2 °C, 5 °C, and 10 °C, respectively. Besides, from the simulations, when the heat of respiration is not considered, it is found that the food temperature remains almost constant during the route, facing a very low temperature decrease: when the food is inserted at 10 °C it reaches 9.59 °C at the end of simulation, while when entering at 5 °C, it reaches 4.93 °C. This suggests that for a such proposed LTES system, the determination of the appropriate pre-cooling temperature is essential. In fact, the system seems not able to cool down the food, but, only able to not cause its temperature sudden rise. Moreover, it is interesting to compare the food and air temperature increase at different food loads and different pre-cooling levels.

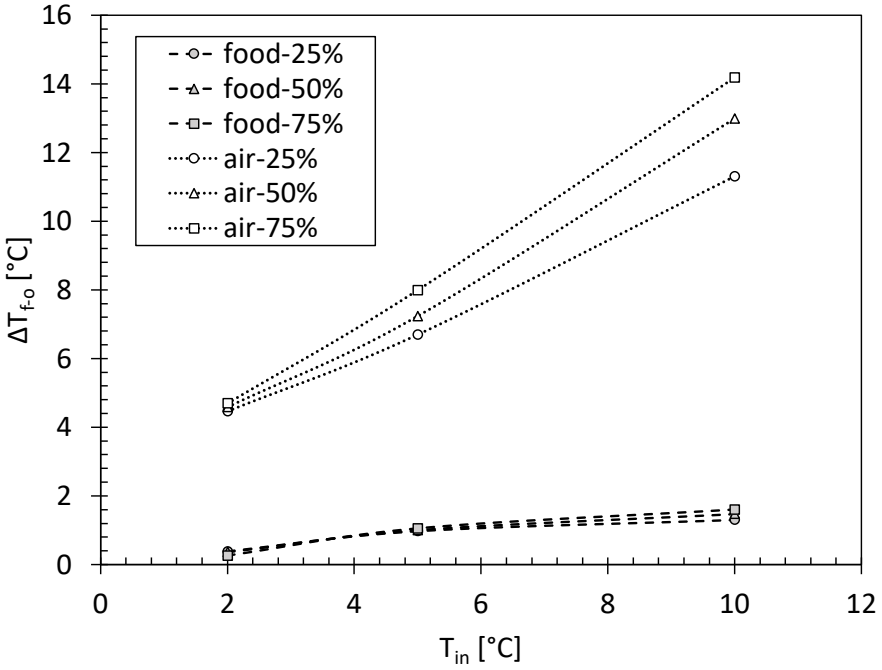

Figure 4.8 Air and food temperature increase for different food loads (25%- 50%- 75%) and different pre-cooling levels (2 °C, 5 °C and 10 °C).

In Fig. 4.8 the temperature increases $\Delta T_{f\text{-}o}$, defined as the difference between the final temperature T_f and the initial temperature T_o, for the air and food cargo, against the pre-cooling temperature T_{in} is plotted. It is clear that, when the cargo is put inside the truck at a temperature level equal to the air cell (2 °C) the food experiments a very low temperature increase (almost 0.3 °C) for each food load values, even if the effect of the heat of respiration is taken into consideration. In fact, the cold mass lets to mitigate the temperature growth. Even the air temperature increases for the three food loads

are very similar, being limited at about 4.2 °C. A different behavior happens when T_{in} is equal to 5 °C. In this scenario, the food temperature grows of some of 1 °C for the 25%, 50% and 75% food load cases. Being the heat of respiration function of the food temperature, as stated above, higher the food temperature, higher the HR effect. It is evident that higher the food load, higher the air temperature increase. The 75% food load scenario presents a ΔT of about 8 °C, meaning that the final temperature has approached 10 °C, which can be a dangerous level for fresh foodstuffs. A more remarkable temperature increase rate can be observed when the cargo is pre-cooled at 10 °C. In this case, in fact, even if relative low temperature increases are reported for the food (an average increase of 1.5 °C), the final food temperature is over 11 °C. Besides, it can be noticed the air temperatures suffer considerable temperature growths (with a maximum of 14 °C for the 75% food load scenario) since the higher contribution of the heat of respiration due to the food at higher temperatures. This suggests that our proposed system is not able to cool down the cargo. As a consequence, the food, remains at a dangerous level for the entire route, risking losing its quality.

Therefore, for a further development of the LTES system for refrigerated truck, it may be necessary to consider the insertion of a small active refrigeration unit needed for the immediate cooling of the foodstuff only. Then, after having reached the desired temperature, the active system may be switched off and the temperature of the system would be maintained at an appropriate level due to the action of the LTES.

5. Experimental and numerical analyses of propane leakage into a closed environment along the cold chain

To cool down the PCM contained in the innovative system we proposed in the previous chapters (3 and 4), we want to insert a roll-bond evaporator between the poly-urethane foam and PCM layer, in which an innovative refrigerant (propane, R290) evaporates.

Refrigeration and air conditioning industry have faced significant development and modernization in the last thirty years as a consequence of the international environmental policies which aimed at reducing refrigerants causing ozone layer depletion and global warming. The phase-out of ozone depleting substances, under the Montreal Protocol [140], triggered significant changes in the industry moving towards alternative refrigerants and technologies.

In the recent years, in fact, researchers have been focusing their attention on finding and studying innovative environmental-friendly substitutes to hydrofluorocarbon (HFC) refrigerants. With this aim, the European Parliament, by means of the European F-gas Regulation [141], boosted the European Countries to make efforts to replace HFCs by low-GWP refrigerants. More specifically, HFCs have to be phased-out by 80% no later than 2030. In October 2016, the Kigali Amendment to the Montreal Protocol bought another dimension to the mandate of the Montreal Protocol by adding the control of production and consumption of HFCs to add the climate benefits already achieved by the Montreal Protocol. As stated by Dalkiklic and Wongwises [142], hydrocarbons (HCs) are suitable candidates to replace HFCs in the traditional vapor compression systems. Being natural refrigerants, HCs have zero ODP (Ozone Depletion Potential) and very low GWP (about 4 to 6), making them a valid alternative to counteract the present and future global warming. However, it must be contemporary considered that hydrocarbons are flammable gases, so it is mandatory to take into account the risks of a possible leakage.

In Fig. 5.1, an overview of the current and alternative refrigerants for the refrigerated transport sector along the cold chain can be noticed.

In literature, different works involving the effect of HCs substitution can be retrieved, as reviewed by Harby [143]. From the above-mentioned review [143], it can be deduced that HCs assure high system performance requiring about half the refrigerant charge required by HFCs. Undoubtedly, reducing the fluid amount is a valid way to limit the hazardous effects of a leakage.

Transport Refrigeration		
Types of transport	Current higher GWP refrigerants (GWP kg•CO_2)	Alternative lower GWP refrigerants (GWP kg•CO_2)
Refrigerated containers, road transport, trains	HFC-134a (1360); HFC-404A (3920), HCFC-22 (1810)	R-744 (1), HFC-452A (1950); HFC-513A (573); HC-290 (5)

Figure 5.1 Summary of current and alternative refrigerants [2]

Nevertheless, to study what happens in case of a HC leakage in a closed environment is fundamental. This potentially risk scenario was already experimentally and/or numerically investigated by some researchers. Among the different works, Jia et al. [144] experimentally studied the effect of R32 leakage from a wall-mounted air conditioner. Okamoto et al. [145] conducted some experimental tests to investigate the leakage of mildly flammable refrigerants (R32, R1234yf, R1234ze(E)) into a room. The authors numerically tested several inlet positions. Maojuan et al. [146] numerically analyzed the propane leakage from a split-type air conditioner indoor unit. Li [147] experimentally investigated the propane diffusion in a closed room leaked from an air condition unit under several working conditions (compressor and fan on/off, different leaking rates and points). Zhang et al. [148] evaluated the distribution of propane following a leak in room at several propane amounts.

Therefore, this works aims at analyzing the effect of a propane leakage from an indoor air conditioning unit into a closed room which can be approximated as a cold warehouse, having a large volume in the middle to simulate foodstuff, or a generic item.

The analysis of the propane leakage into a warehouse can be easily extended to a refrigerated space of a refrigerated vehicle. As stated above, we propose to cool down the PCM by means of a roll-bond evaporator located between the poly-urethane foam and the phase change material layer itself. During the cooling period, however, a potential gas leakage may occur: therefore, by investigating the propane leakage into a cold warehouse, it can be studied how the system behaves when the propane leakage occurs during the charging phase of the innovative LTES system.

A small-scale experimental set up was built. It consists of a parallelepiped box (60 x 60 x 35 cm^3) that simulated a small-scale environment in which a propane leakage occurs. A propane detector was set in the middle of the ceiling to record the propane concentration during and for some minutes after the leakage. Additionally, a numerical model implemented in Ansys Fluent 18.2 was developed to estimate the propane diffusion field. It was validated on the experimental results and then adopted for further analyses of different leakage position scenarios. The results were compared and discussed.

5.1 Experimental Setup

Figure 5.2 presents a scheme of the experimental setup. It consists of a parallelepiped box, having all the walls insulated by means of polyurethane covered by a 1 mm aluminum layer to avoid propane diffusion. Its dimensions are 60 x 60 x 35 cm^3 for width, length, and height, respectively. These dimensions were chosen to represent an average closed room, such as a bedroom or a dining room, at a scale of 1:8. Exactly in the middle of the box, a smaller volume made of polyurethane covered by a 1 mm aluminum layer, having dimension 31 x 18 x 18 cm^3 was located in order to take into consideration the presence of obstacles. This could simulate the presence of a table, a bed, or another piece of furniture.

Four grams of propane (assay 99.5%) have been released by a 1.6 mm diameter tube located at 3 cm from the ground and 9 cm from the lateral side. They are the equivalent of almost 2 kg of propane spilled in a real-size room, so this case study should never be reached in real working conditions. On the other hand, this propane amount was selected to reduce the measurement errors and to clearly highlight the gas diffusive movements. The propane mass was weighted by a scale (uncertainty ±0.01 g) and stored in a small buffer tank connected to the sealed box by a valve. At the beginning of the test, the valve was opened and the propane leaked into the box. At the end of the test, after closing the valve, the propane tank was weighted again to correctly evaluate the amount of propane dispersed during the experiment.

The box was located inside a larger climatic room set at 20 °C (stability ±0.2 °C). It was supposed that 20 °C represent the initial temperature at which the charging period of the LTES starts. The temperature was maintained constant during all the test to ensure to not affect the propane diffusive movements due to thermal gradients. The temperature was measured in two locations inside the box (depicted in Figure 5.2) and in two locations in the climatic room by means of calibrated T-type thermocouples (uncertainty ±0.1 °C) connected to a Kaye K-170 ice point reference with stability of ±0.005 °C and accuracy of ±0.005 °C.

A Honeywell Optima Plus propane detector (accuracy ±1% f.s., response time T50 < 3 s) was installed on the center of the box ceiling. It was calibrated by the manufacturer and the full scale was set equal

to the propane LFL (Lower Flammability Limit), which is equal to 2.05±0.05%, as stated by Cashdollar et al. [149]. Its measurement sensor is a cylinder 5 cm high and with a 3 cm diameter. So, it records the average propane concentration inside that volume.

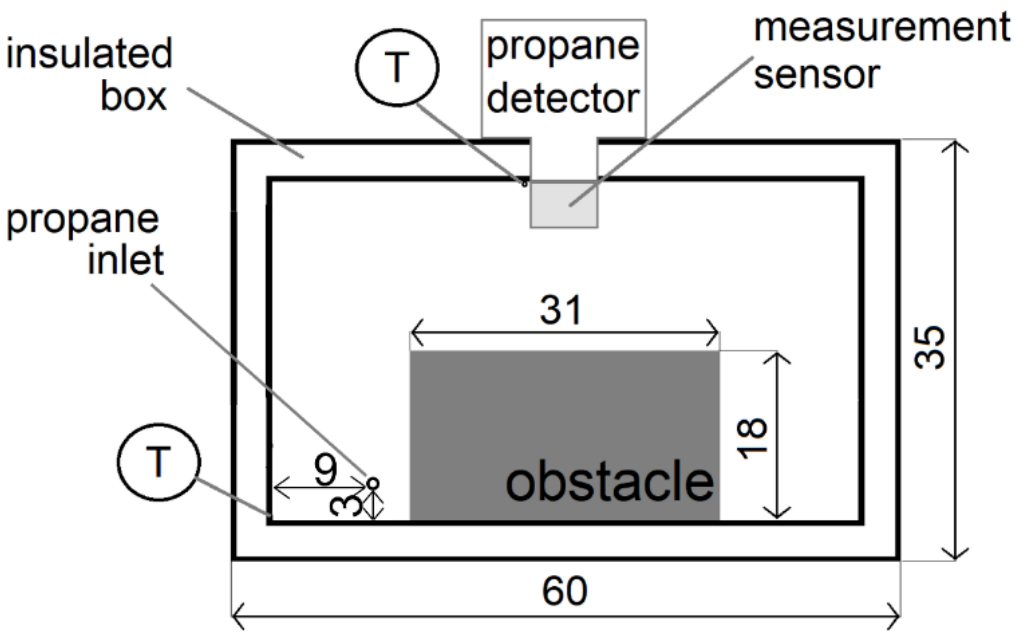

Figure 5.2 A scheme of the experimental set up

By means of a Keysight 34970A data acquisition system, all the data were recorded at a 1 Hz frequency.

5.2 CFD Numerical Model

As shown in Figure 5.3, the fluid domain for the numerical analyses was modelled based on the experimental setup. In particular, the main box was firstly designed and then, by the subtraction Boolean operations, the smaller box representing the obstacle and a cylinder representing the volume occupied by the propane detector were subtracted from the domain. Two inlet positions were investigated, sketched as a 1.6 mm hole. The first one (Figure 5.3, left) was placed as in the experimental set up, the other one (Figure 5.3, right) was positioned at 25 cm from the ground, in the center of the face. They represent two significant potential gas leakage positions along the innovative LTES panel.

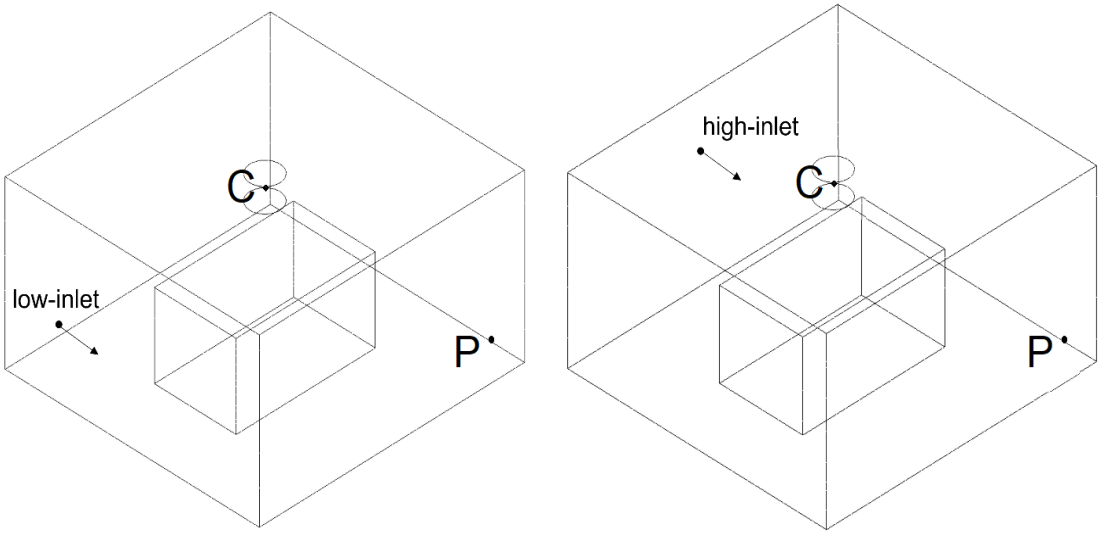

Figure 5.3 Numerical model: geometry and boundary conditions. Low-inlet case (left), high-inlet case (right)

Additionally, the propane concentration at two distinct points was detected: at the middle of the ceiling (denoted as "C" in Fig. 5.3) and at the lower corner opposite to the propane inlet (denoted as "P"). To simulate the propane diffusion inside the room, the Species-Transport Model (Ansys Fluent, 2018) was adopted. No volumetric reactions were considered for the analyses and the system was set isothermal at 20 °C. The fluid domain consisted of a mixture "propane-air", imported from the Fluent database, whose main properties are listed in Table 5.1.

At the "inlet", a "mass-flow-inlet" condition with 100% propane mole fraction was applied, while the room was initialized with only air. After the first 7 seconds in which all the propane amount was released in the room, the "inlet" boundary condition was switched to "wall" in order to stop the propane entrance and let the gas diffusion inside the closed environment to develop.

Table 5.1 "Propane-air" mixrure properties

Density ($kg\ m^{-3}$)	**Heat Capacity** ($J\ kg^{-1}\ K^{-1}$)	**Thermal Conductivity** ($W\ m^{-1}\ K^{-1}$)	**Viscosity** ($kg\ m^{-1}\ s^{-1}$)	**Mass Diffusivity** ($mm^2\ s^{-1}$)
Incompressible-ideal gas	Mixing law	0.0454	$1.72 \cdot 10^{-5}$	$2.88 \cdot 10^{-5}$

Since the experimental setup was assumed to be completely airtight, no outlet conditions were set, and the entire domain was considered as a "wall".

The numerical model was developed and validated on the low-inlet case. Then, the high-inlet case was studied, and the results were compared.

5.2.1 Governing equations

The equations involved in the solution of the developed numerical model relate to the "Species Transport" problem (Ansys Fluent, 2018). In particular, when the conservation equation is solved for chemical species, the solution of a convection-diffusion equation (Eq. (5.1)) for the i-th species is solved and the local mass Y_i is calculated:

$$\frac{\partial}{\partial t}(\rho Y_i) + \nabla(\rho \boldsymbol{u} Y_i) = -\nabla \cdot \boldsymbol{J_i} \qquad \text{Eq. (5.1)}$$

Where, $\boldsymbol{J_i}$ is the diffusion flux of i-th species, considered as a function of gradients of concentration and temperature. The dilute approximation is adopted to model the mass diffusion due to concentration gradients, resulting in the following Fick's law (Eq. (5.2)) for turbulent flows:

$$\boldsymbol{J_i} = -\left(\rho D_{i.m} + {}^{\mu_t}/_{Sc_t}\right)\nabla Y_i - D_{T,i}\frac{\nabla T}{T} \qquad \text{Eq. (5.2)}$$

Where, $D_{i,m}$ is the mass diffusion coefficient of the i-th species in the mixture, $D_{T,i}$ is the thermal diffusion coefficient, Sc_t is the turbulent Schmidt number which is usually equal to 0.7.
The turbulence is solved by adopting the RNG (ReNormalization Group) k-ε model, which solves two transport equations (Eqns. (5.3-4)):

$$\frac{\partial}{\partial t}(\rho k) + \frac{\partial}{\partial x_i}(\rho k u_i) = \frac{\partial}{\partial x_j}\left(\alpha_k \mu_{eff}\frac{\partial k}{\partial x_j}\right) + G_k + G_b - \rho\varepsilon - Y_M \qquad \text{Eq. (5.3)}$$

$$\frac{\partial}{\partial t}(\rho \varepsilon) + \frac{\partial}{\partial x_i}(\rho \varepsilon u_i) = \frac{\partial}{\partial x_j}\left(\alpha_\varepsilon \mu_{eff}\frac{\partial \varepsilon}{\partial x_j}\right) + C_{1\varepsilon}\frac{\varepsilon}{k}(G_k + C_{3\varepsilon}G_b) - C_{2\varepsilon}\rho\frac{\varepsilon^2}{k} - R_\varepsilon \qquad \text{Eq. (5.4)}$$

For the sake of brevity, not all of the involved parameters are explained here. Nevertheless, the following two equations (Eqns. (5.5-6)) refer on how to model the effective viscosity, μ_{eff}, and R_ε, respectively.

$$d\left(\frac{\rho^2 k}{\sqrt{\varepsilon\mu}}\right) = 1.72\frac{{}^{\mu_{eff}}/_{\mu}}{\sqrt{{}^{\mu_{eff}}/_{\mu}{}^3 - 1 + C_v}}d({}^{\mu_{eff}}/_{\mu}) \qquad \text{Eq. (5.5)}$$

$$R_\varepsilon = \frac{C_\mu \rho \eta^3 (1 - {}^{\eta}/_{\eta_0})\varepsilon^2}{(1 + \beta\eta^3)k} \qquad \text{Eq. (5.6)}$$

The second order upwind scheme was adopted to linearize the convective terms with first order derivatives, while the diffusive terms with second order derivatives were linearized by a second order differencing scheme. The SIMPLE scheme was used to solve the pressure-velocity coupling.

5.2.2 Numerical model validation

The experimental results were selected as reference case for the model validation. In Figure 5.4, the experimental results in terms of propane concentration read by the propane detector are plotted as a function of time. Time 0 s is the beginning of the leakage, when in the box there is only air. Both the numerical simulation and the propane detector used in the experiments detected the propane arrival after about 3 s. Then, they both reached an almost asymptotic behavior after about 20 s, suggesting that the leaked gas is approaching a homogeneous concentration. Nevertheless, the numerical model predicted some propane concentration oscillations in the early instants. These are attributed by the authors to minor turbulence motions inside the system, generated as a consequence of the propane entrance. They probably had not been acquired during the experiments because of the time-constant of the propane detector led to a non-negligible inertia.

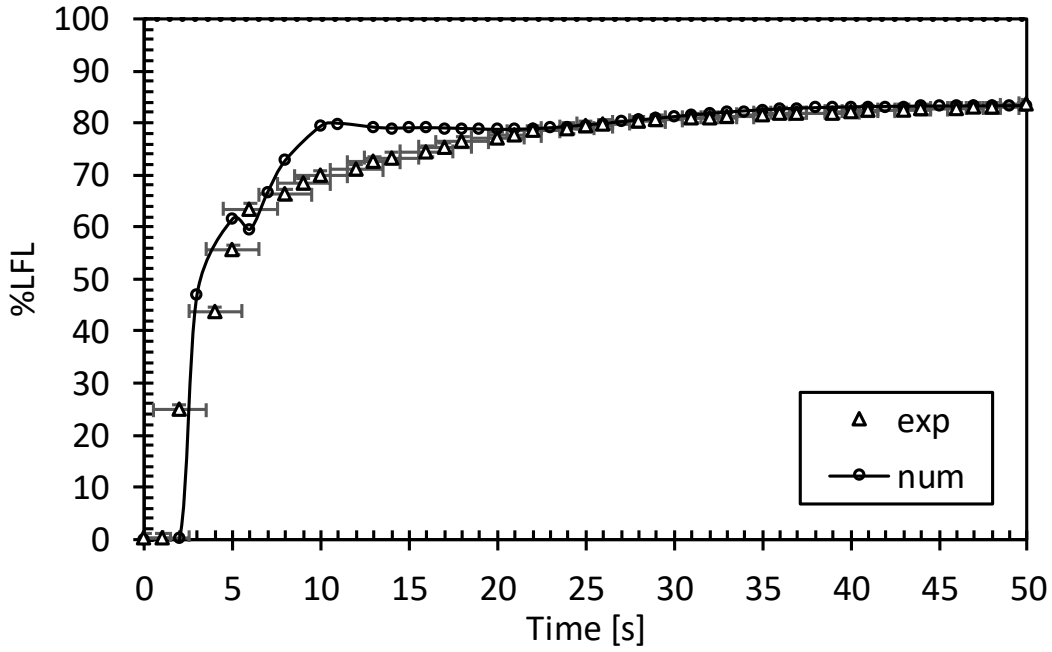

Figure 5.4 Numerical model validation

A mesh sensitivity analysis was run to study the independence of the solution from the grid. As shown in Table 5.2, four different meshes were tested. Among the diverse cases, the Mesh-C (Figure 5.5) was considered the best trade-off between solution accuracy and computational efforts,

and therefore selected for the subsequent simulations. Moreover, a time step sensitivity analysis was conducted. The time step size of 0.01 s was found to be the best compromise.

Table 5.2 Mesh sensitivity analysis

Mesh$_x$	**No. of elements** (10^6)	**Exp %LFL at 50 s**	**Sim %LFL at 50 s**	**Deviation** [%]	**TTF_x/TTF_D** *
A	0.625	83.1	-	-	diverged
B	1.433	83.1	80.3	3.3	0.88
C	2.021	83.1	82.8	0.4	0.92
D	3.362	83.1	83.0	0.1	1
*TTF = Time-To-Finish					

5.3 Results

Figures 5.5 and 5.6 present the propane diffusion inside the closed environment in the low-inlet and high-inlet cases, respectively. The red color refers to the LFL (low flammability level). It can be easily noticed that the propane enters the room from the inlet and starts immediately to diffuse. In particular, in Figure 5.5 (low inlet) the propane leaking, took a preferred path along the side wall close to the inlet: in facts, it is clear that in this area between the wall and the obstacle there was a higher propane concentration, suggesting that some zones have to be carefully managed in order to ensure the safety in a closed room. Then, the propane rebounds against the opposite wall to the inlet and started spreading toward the ceiling. The core of the room remained at a propane concentration of some of 50% of LFL, still in a safety zone. It is interesting to notice what happened at about 12 s from the test start; the gas had diffused almost homogenously, but some potentially dangerous zones could still be remarkably, for instance close to the opposite corners from the leakage inlet. Then, the propane diffusion evolved and at 50 s the room presented a uniform propane distribution, where no risky zones can be identified.

Besides, in the high-inlet case (Figure 5.6), the leaked propane tended to distribute more rapidly inside the environment due to the symmetry of the system, the higher propane density (with respect to the air one) which causes propane to fall and mix quicker with the air, and the absence of obstacles close to the inlet. After 7 s the gas had already reached the entire domain, forming large areas where the

concentration is greater than 100%LEL, and after 12 s only the wall just opposite to the inlet presents some risky zones.

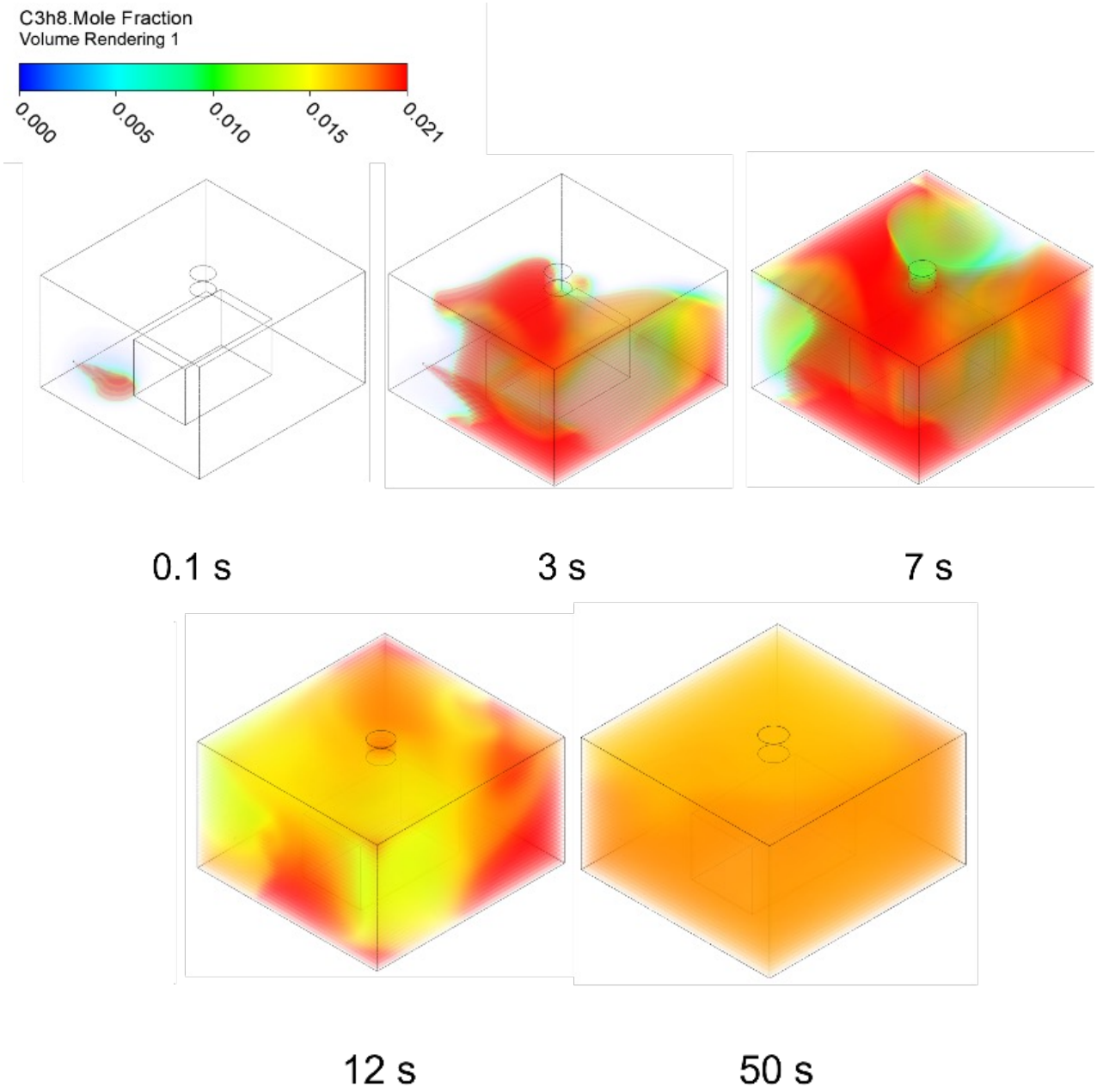

Figure 5.5 Propane diffusion at different instants: low-inlet case

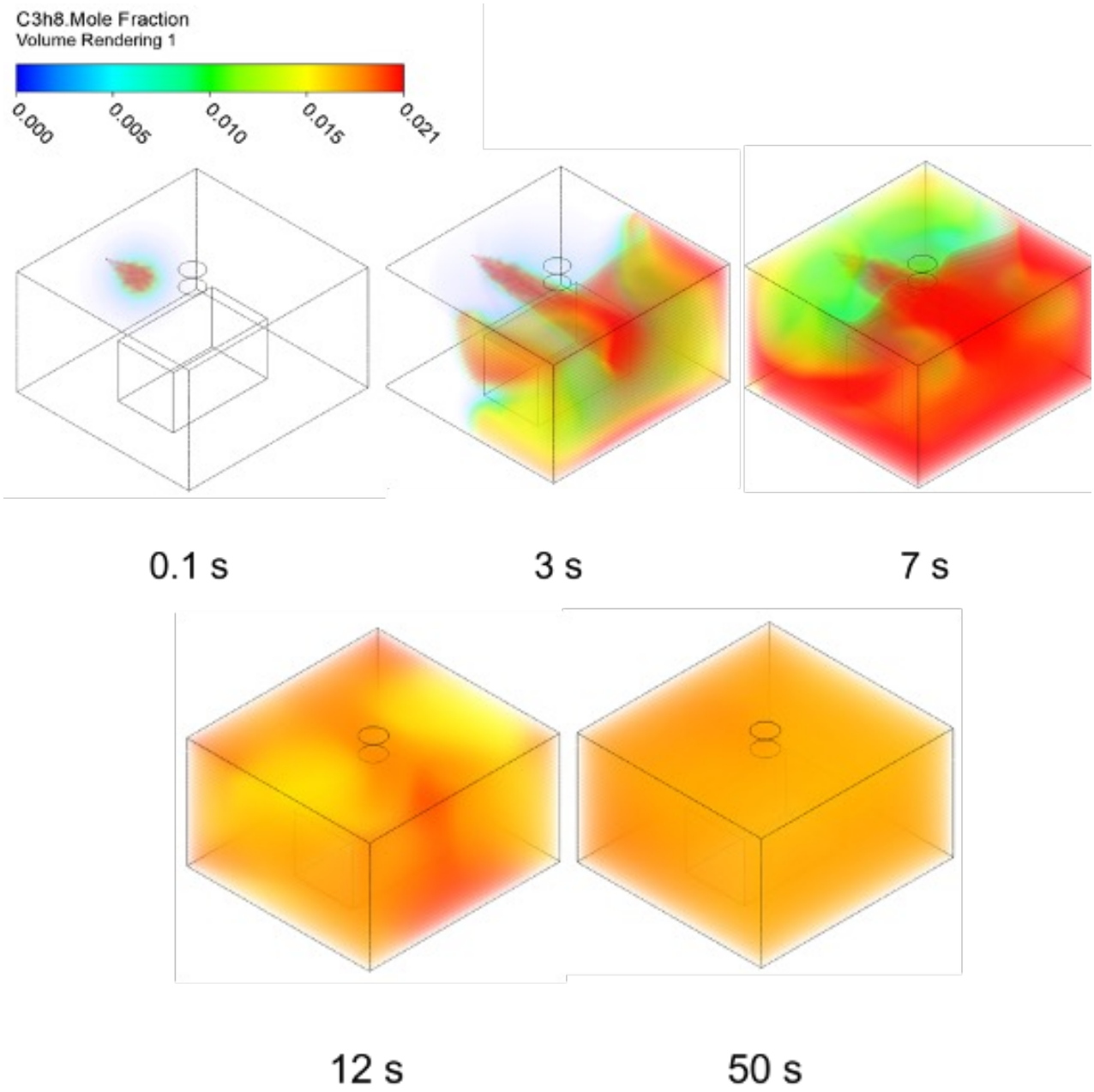

Figure 5.6 Propane diffusion at different instants: high-inlet case

Next, propane concentration was compared in the high-inlet case and the low-inlet case at some particular locations. In detail, Figure 5.7 shows the propane concentration near the propane detector (in the middle of the ceiling, denoted as “C”) while Figure 5.8 in the opposite corner (“P”) to the inlet, where a difference between the two cases has already been highlighted (compare Figures 5.5 and 5.6). Points C and D are highlighted in Figure 5.3.

In area “C” close to the ceiling (Figure 5.7), the presence of propane is detected earlier in terms of time in the high-inlet case. In this case, it also recorded an higher average concentration. This fact was to be expected as the leakage inlet is located close to this measurement point. On the contrary

(the graph has not been reported for space reasons) close the floor the presence of propane is detected earlier and its concentration is higher in the low-inlet case.

It is interesting to compare the two configurations in the "P" location (Figure 5.8). It clearly appears that in the high-inlet case, when the propane reached this area, it was already more mixed with air and internal motions allowed it to diffuse more gradually. In contrast, in the low-inlet case, the lower turbulence limited the mixing with air process. Because of this, more propane remained trapped in the corner, creating a potentially risky condition for a longer time span.

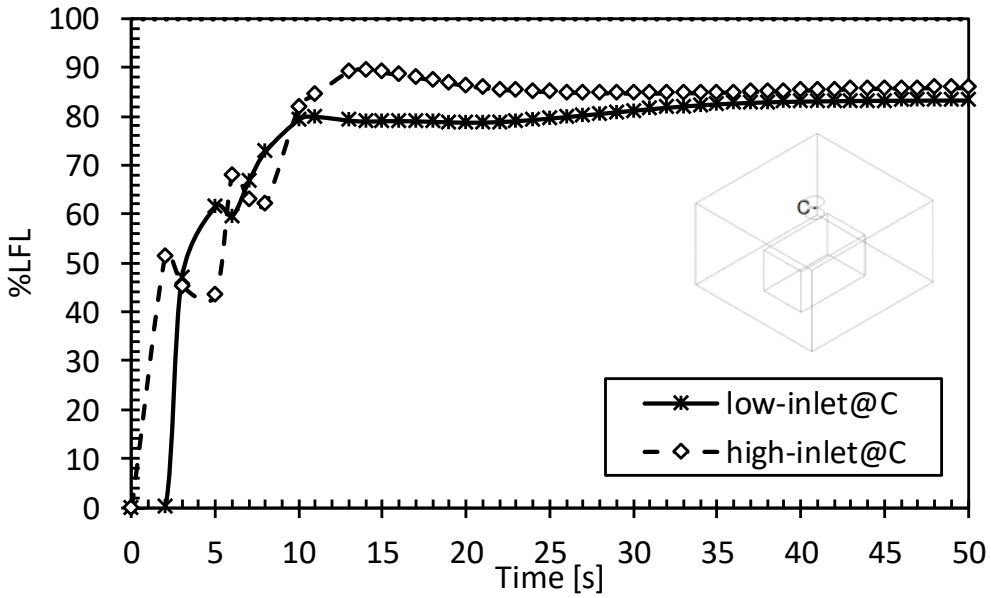

Figure 5.7 Comparison between low-inlet and high-inlet cases: ceiling "C"

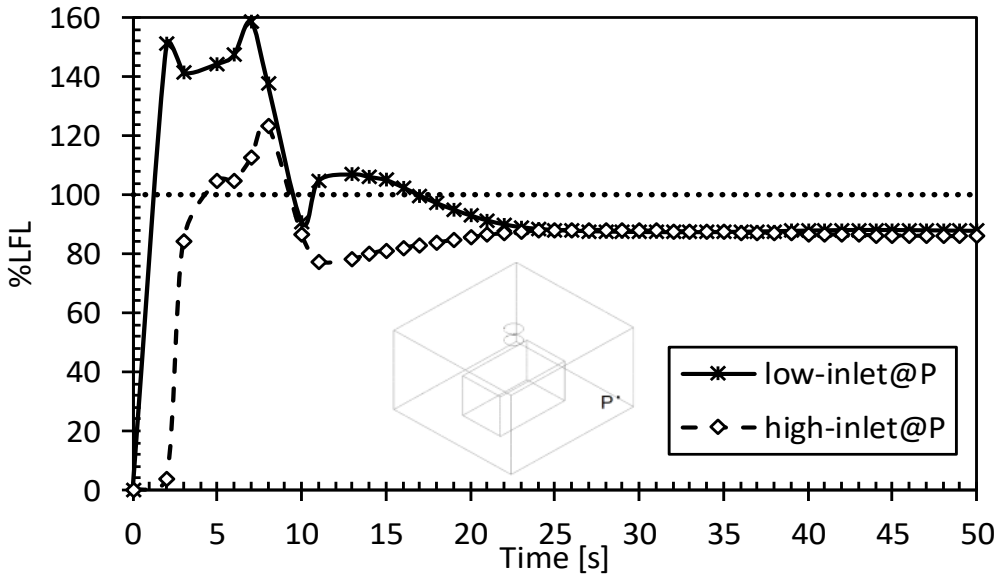

Figure 5.8 Comparison between low-inlet and high-inlet cases: opposite corner "P"

What obtained suggests that, when all other parameters are equal, the refrigeration unit position can have a not-negligible effect on the gas diffusion dynamics inside a closed environment. Therefore, the location must be accurately selected in order to minimize the risks for the human safety in case of flammable refrigerant gas leakage. Based on the results obtained, especially if there are objects in the room, it is recommended to place the air conditioning unit near the ceiling. In this way, a possible flammable gas leakage will not find direct obstacles to the diffusion that will be further helped by the force of gravity.

6. Conclusions

In the first part of this thesis, the works retrieved from the literature involving the adoption of PCM in applications along the cold chain were presented and discussed.

From the surveyed works, it is clear that different solutions have been investigated, so far.

Focusing on the refrigerated transportation, two important macro-categories were identified, the modification of the insulation layer by the insertion of the PCM, or the designing of a novel refrigeration system which exploits the PCM. Moreover, the studies involved the possibility of designing a complete (or almost complete) passive cooling system or an active one. When the PCM is added to the insulation walls, it was found that two different goals might be achieved: reducing the heat load peak and the heat transferred into the refrigerated space or acting as a cooling source. In the first scenario, a PCM having a melting temperature close to the outer temperature (usually ranging between 18 °C (summer night) and 35 °C (summer day)) has been reported to be the best solution, since, by exploiting the latent heat, the incoming heat is absorbed during the critical hours and released after a certain period, under more favorable conditions for the cooling unit (for example, during the evening, if a complete summer day is considered, when the external temperature is lower). It is clear that such idea requires an active system, even if energy consumption emissions reductions, compared with the traditional solutions, have been stated to be achievable. The great advantage is, therefore, the possibility to cool down the PCM of the developed LTES system during the night, without requiring the employment of an additional refrigeration unit.

On the contrary, if the direction goes to the design of an insulation wall incorporating PCM to act as cold source, it has been suggested to locate the PCM in the internal side of the insulated wall, that is facing the cold space. The temperature of the PCM is, in this case, close to the carriage targeted temperature. Therefore, it usually ranges between -20 °C to 5 °C, depending on the cargo typology (frozen or fresh products). The PCM on the wall acting as cold source may take to the development of a complete passive refrigerated vehicle. The PCM, being refrigerated when the vehicle is stationary in depot, releases the cold during the operation. This solution may conduct to remarkable savings in terms of reduction of energy consumed and polluting emissions. In fact, it lets to drop out the dependency from fossil fuel-based refrigeration system, since the latent thermal energy storage system may be charged by an electrical and more efficient stationary external refrigeration unit, which can be easily reflected in economic savings. An almost passive system may also be obtained by designing a PCM-based cooling unit, which is cooled down by an external refrigeration unit and act as cold source by means of a heat transfer fluid and appropriate heat exchangers which let to cool the air inside the refrigerated space. Nevertheless, to design a complete passive system, additional

significant studies are necessary. In particular, the refrigeration load needed must be carefully estimated, it must be clearly identified the effects of the cargo inside the refrigerated, how the system reacts to the door openings period, which occurs several times during a normal transportation and distribution activities.

It must be underlined that from the retrieved works, it was not reported if a food precooling is needed before the introduction in the cooling space, and if and how it differs from the precooling level needed for a traditional transport refrigeration system.

Generally, only few works covered the economic advantages deriving from the adoption of a refrigerated system based on PCM. However, significant economic savings reaching values of 80-90% were declared in few works.

Very different external conditions were investigated: such as a real-life profile temperature, constant temperature, single day operating period or a longer one. Additionally, studies covering full-scale applications are extremely needed to demonstrate the practical feasibility and convenience of the novel solutions. Performances close to real conditions, may enhance the confidence of manufacturers to consider the introduction of latent thermal energy storage systems as substitutes of the traditional ones.

To address some of the gaps found in the literature, a novel insulated wall for refrigerated transport consisting of a PU layer and a PCM one was proposed in this Ph.D work thesis. A 2D section of a traditional refrigerated truck was modelled. The hourly solar irradiance profile of an average hot Italian summer day was obtained aiming at estimating and applying the external heat loads on a reference 10 h truck daily route. By means of CFD numerical simulations, the effect of incorporating a PCM layer in a traditional 5 cm polyurethane insulation layer was studied. Specifically, the additional PCM layer ranged between 0.5 cm and 2 cm. Three commercially available paraffin based PCMs were selected: RT2HC, RT4, RT5HC. Their abilities in maintaining the air temperature in the refrigerated space for fresh food transportation at a suitable level without the use of refrigeration systems were analyzed. Three possible scenarios were investigated: stationary truck, urban route (constant 40 km h^{-1}) and interurban route (constant 80 km h^{-1}). It was demonstrated that the stationary case was the worst in terms of heat entered into the refrigerated space. Therefore, all the other simulations were prepared considering that case. The results showed that the temperature glide during the phase change affected the thermal behavior of the LTESs. In particular, the 0.5 cm PCM layer assured an air temperature lower than the *solidus* temperature only for the first four simulated hours. Then, the air temperature stabilized at about 1 °C over the *solidus* temperature and then, when the PCM was almost fully melted, a sudden temperature increase occurred, which would be potentially

detrimental for high-sensible foodstuffs. The 1 cm layer, instead, let the air temperature to be no more than 2 °C higher than the PCM reference melting temperature for the entire 10 h simulated truck journey. Among all the other investigated layers, the thickest one assured the most uniform air temperature during the route. Since, with the 2 cm layer, only some 25% of PCM melted, an extension of the truck journey should be simulated in future numerical investigations.

Besides, in order to find the optimal LTES solution, the presence of cold freight was considered. The ability of the system in counteracting the external heat load gain with a cabin temperature starting at 2 °C, with 0.5 cm RT2HC layer in the insulation wall, was investigated. Four different scenarios were compared: an empty one, and three food loaded cases (25%, 50%, 75% food loaded) representing three different moments of a traditional daily route. It was obtained that, the 50% cargo loaded scenario lets to reach the lowest air temperature inside the refrigerated compartment during the 10 h, since it exploits the double concurrent effect of the air heat exchanged by natural convection and the presence of a significant additional thermal cold mass. Moreover, being this system proposed for temperature-sensitive cargoes, the role of the heat of respiration due to metabolic activities was analyzed. It was found that it has a more impactful role during the final instants of the route when the PCM was almost completely liquid and, so, not able to counteract the heat entrance. Additionaly, the pre-cooling temperature level has been demonstrated to have a significant impact on ensuring the suitable temperature conditions of the LTES system. In fact, when the cargo was inserted at 5 °C, only the 25% food load scenario ensured the final temperature to be contained into a safe level. 75% of food entering at 5 °C lets the air cell to reach a final temperature of about 10 °C. The proposed system could not control or cool down the food because it is only meant to maintain the safe conditions for the entire route. In order to handle different pre-cooling cargoes, a different active solution needs to be considered and adopted, but this does not limit the promising capabilities of the proposed technology in reducing the GHG emissions the energy costs.

It must be underlined that, the proposed system was designed being tuned on the discharging phase, which is, effectively, the most critical phase when dealing with the refrigerated transport. However, in order to push the market to invest in these innovative and more sustainable refrigerated transport solutions, additional analyses regarding the system as a whole (discharging + charging phases) are vital. In fact, it must be clearly demonstrated that the new proposed idea can ensure the desired transport conditions, by ensuring contemporary the system charging in a convenient and cost-effective way, minimizing the negative impacts for the environment. The clear designing of the charging and discharging phases are essential for the development and subsequent spread of a new refrigerated transport application adopting PCMs.

Therefore, focusing on the charging phase, it was proposed to cool down the PCM by the use of the new environmentally friendly refrigerant R290 (Propane) which circulates in a roll-bond evaporator set between the insulation material and the PCM layer. However, before considering the adoption of R290, it must be clearly investigated the possible negative effects, since one of the main drawbacks of this innovative gas is its flammability. Hence, based on experimental results coming from a small-scale apparatus reproducing a close environment (as a refrigerated cell is), in which the propane concentration after a possible leakage was recorded for several seconds, a numerical model implemented in Ansys Fluent 18.2 was developed. It let to estimate the propane diffusion field. Two different gas leakages were studied: at the corner of the wall or in the middle of the wall, by assuming the same amount of R290 leaking. The results revealed that the leakage position can have an impact on the gas diffusion, potentially affecting the safety of the place and the foodstuff, by reaching and overcoming the R290 Lower Flammability Limit.

Finally, it can be concluded that a promising cost effective and environmentally friendly solution for the refrigerated transport sector can be effectively found. The numerical models developed and proposed in this work thesis can be further adopted to study and develop an integrated LTES system by optimizing the charging and discharging phases and evaluating the thermal and risk performances.

The End

References

[1] Food and Agriculture Organization of the United Nations., International Fund for Agricultural Development, UNICEF, World Food Programme, and World Health Organization, *The state of food security and nutrition in the world: safeguarding against economic slowdowns and downturns.* Accessed: Jun. 03, 2022. [Online]. Available: https://www.fao.org/3/ca5162en/ca5162en.pdf

[2] IIR_UN Environment, "Cold Chain Technology Brief: Transport Refrigeration," 2018. Accessed: Jun. 03, 2022. [Online]. Available: https://wedocs.unep.org/bitstream/handle/20.500.11822/32571/8142Transpor_Ref_EN.pdf?sequence=1&isAllowed=y

[3] Jenny. Gustavsson, Food and Agriculture Organization of the United Nations., and N. ASME/Pacific Rim Technical Conference and Exhibition on Integration and Packaging of MEMS, *Global food losses and food waste : extent, causes and prevention : study conducted for the International Congress "Save Food!" at Interpack 2011 Düsseldorf, Germany*. Accessed: Jun. 03, 2022. [Online]. Available: https://www.fao.org/3/mb060e/mb060e00.htm

[4] UN-environment programme, "Sustainable Cold Chain and Food Loss Reduction," 2019. Accessed: Jun. 03, 2022. [Online]. Available: https://ozone.unep.org/system/files/documents/MOP31-Sustainable-HL_Briefing_Note.pdf

[5] Food and Agriculture Organization of the United Nations and Food Wastage Footprint (Project), *Food wastage footprint full-cost accounting : final report.* Accessed: Jun. 03, 2022. [Online]. Available: https://www.fao.org/3/i3991e/i3991e.pdf

[6] J. A. Evans, E. C. Hammond, A. J. Gigiel, L. Reinholdt, K. Fikiin, and C. Zilio, "Assessment of methods to reduce the energy consumption of food cold stores," *Appl Therm Eng*, vol. 62, no. 2, pp. 697–705, 2014, doi: 10.1016/j.applthermaleng.2013.10.023.

[7] M. A. ben Taher, M. Ahachad, M. Mahdaoui, Y. Zeraouli, and T. Kousksou, "A survey of computational and experimental studies on refrigerated trucks," *Journal of Energy Storage*. Elsevier Ltd, Mar. 01, 2021. doi: 10.1016/j.est.2021.103575.

[8] EASE, "Thermal Storage Position Paper," 2017.

[9] H. Jouhara, A. Żabnieńska-Góra, N. Khordehgah, D. Ahmad, and T. Lipinski, "Latent thermal energy storage technologies and applications: A review," *International Journal of Thermofluids*, vol. 5–6, Aug. 2020, doi: 10.1016/j.ijft.2020.100039.

[10] M. Mobedi, K. Hooman, and W.-Q. Tao, *Solid-Liquid Thermal Energy Storage*. Boca Raton: CRC Press, 2022. doi: https://doi.org/10.1201/9781003213260.

[11] Q. Li, X. Ma, X. Zhang, J. Ma, X. Hu, and Y. Lan, “Microencapsulation of Al-Zn alloy as phase change materials for high-temperature thermal storage application,” *Mater Lett*, vol. 308, Feb. 2022, doi: 10.1016/j.matlet.2021.131208.

[12] G. Righetti, L. Doretti, C. Zilio, G. A. Longo, and S. Mancin, “Experimental investigation of phase change of medium/high temperature paraffin wax embedded in 3D periodic structure,” *International Journal of Thermofluids*, vol. 5–6, Aug. 2020, doi: 10.1016/j.ijft.2020.100035.

[13] C. Pagkalos, G. Dogkas, M. K. Koukou, J. Konstantaras, K. Lymperis, and M. G. Vrachopoulos, “Evaluation of water and paraffin PCM as storage media for use in thermal energy storage applications: A numerical approach,” *International Journal of Thermofluids*, vol. 1–2, Feb. 2020, doi: 10.1016/j.ijft.2019.100006.

[14] “https://sunamp.com.” https://sunamp.com

[15] G. Dogkas *et al.*, “Investigating the performance of a thermal energy storage unit with paraffin as phase change material, targeting buildings’ cooling needs: an experimental approach,” *International Journal of Thermofluids*, vol. 3–4, May 2020, doi: 10.1016/j.ijft.2020.100027.

[16] I. Dincer and M. A. Rosen, *Exergy Analysis of Heating, Refrigerating and Air Conditioning*. 2015.

[17] A. Sharma, V. v. Tyagi, C. R. Chen, and D. Buddhi, “Review on thermal energy storage with phase change materials and applications,” *Renewable and Sustainable Energy Reviews*, vol. 13, no. 2. pp. 318–345, Feb. 2009. doi: 10.1016/j.rser.2007.10.005.

[18] Y. Yusufoglu, T. Apaydin, S. Yilmaz, and H. O. Paksoy, “Improving performance of household refrigerators by incorporating phase change materials,” *International Journal of Refrigeration*, vol. 57, pp. 173–185, Jul. 2015, doi: 10.1016/j.ijrefrig.2015.04.020.

[19] M. A. Ezan, E. Ozcan Doganay, F. E. Yavuz, and I. H. Tavman, “A numerical study on the usage of phase change material (PCM) to prolong compressor off period in a beverage cooler,” *Energy Convers Manag*, vol. 142, pp. 95–106, 2017, doi: 10.1016/j.enconman.2017.03.032.

[20] A. Pirvaram, S. M. Sadrameli, and L. Abdolmaleki, “Energy management of a household refrigerator using eutectic environmental friendly PCMs in a cascaded condition,” *Energy*, vol. 181, pp. 321–330, Aug. 2019, doi: 10.1016/j.energy.2019.05.129.

[21] B. Gin, M. M. Farid, and P. K. Bansal, “Effect of door opening and defrost cycle on a freezer with phase change panels,” *Energy Convers Manag*, vol. 51, no. 12, pp. 2698–2706, Dec. 2010, doi: 10.1016/j.enconman.2010.06.005.

[22] Z. Liu, D. Zhao, Q. Wang, Y. Chi, and L. Zhang, “Étude sur la performance d’un réfrigérateur domestique refroidi par air utilisant des matériaux à changement de phase pour l’entreposage frigorifique,” *International Journal of Refrigeration*, vol. 79, pp. 130–142, Jul. 2017, doi: 10.1016/j.ijrefrig.2017.04.009.

[23] E. Oró, L. Miró, M. M. Farid, V. Martin, and L. F. Cabeza, “Energy management and CO2 mitigation using phase change materials (PCM) for thermal energy storage (TES) in cold storage and transport,” *International Journal of Refrigeration*, vol. 42, pp. 26–35, 2014, doi: 10.1016/j.ijrefrig.2014.03.002.

[24] “https://www.vikingcold.com/.” https://www.vikingcold.com/ (accessed Jun. 03, 2022).

[25] P. Schalbart, D. Leducq, and G. Alvarez, “Ice-cream storage energy efficiency with model predictive control of a refrigeration system coupled to a PCM tank,” *International Journal of Refrigeration*, vol. 52, pp. 140–150, Apr. 2015, doi: 10.1016/j.ijrefrig.2014.08.001.

[26] M. Liu, W. Saman, and F. Bruno, “Development of a novel refrigeration system for refrigerated trucks incorporating phase change material,” *Appl Energy*, vol. 92, pp. 336–342, 2012, doi: 10.1016/j.apenergy.2011.10.015.

[27] B. Michel, P. Glouannec, A. Fuentes, and P. Chauvelon, “Experimental and numerical study of insulation walls containing a composite layer of PU-PCM and dedicated to refrigerated vehicle,” *Appl Therm Eng*, vol. 116, pp. 382–391, 2017, doi: 10.1016/j.applthermaleng.2016.12.117.

[28] T. Lafaye De Micheaux, M. Ducoulombier, J. Moureh, V. Sartre, and J. Bonjour, “Experimental and numerical investigation of the infiltration heat load during the opening of a refrigerated truck body,” *International Journal of Refrigeration*, vol. 54, pp. 170–189, Jun. 2015, doi: 10.1016/j.ijrefrig.2015.02.009.

[29] United Nations. Economic Commission for Europe. Inland Transport Committee, *Agreement on the International Carriage of Perishable Foodstuffs and on the Special Equipment to Be Used for Such Carriage (ATP).*

[30] S. A. Tassou, G. De-Lille, and Y. T. Ge, “Food transport refrigeration - Approaches to reduce energy consumption and environmental impacts of road transport,” *Appl Therm Eng*, vol. 29, no. 8–9, pp. 1467–1477, Jun. 2009, doi: 10.1016/j.applthermaleng.2008.06.027.

[31] G. Li, “Comprehensive investigation of transport refrigeration life cycle climate performance,” *Sustainable Energy Technologies and Assessments*, vol. 21, pp. 33–49, Jun. 2017, doi: 10.1016/j.seta.2017.04.002.

[32] A. P. Simard and M. Lacroix, “Study of the thermal behavior of a latent heat cold storage unit operating under frosting conditions.” [Online]. Available: www.elsevier.com/locate/enconman

[33] X. Li, S. Yang, and D. Zhou, “Study of new cool storage materials for refrigerated vehicle in cold chain,” in *2010 International Conference on Logistics Systems and Intelligent Management, ICLSIM 2010*, 2010, vol. 2, pp. 637–640. doi: 10.1109/ICLSIM.2010.5461341.

[34] L. Melone, L. Altomare, A. Cigada, and L. de Nardo, “Phase change material cellulosic composites for the cold storage of perishable products: From material preparation to computational evaluation,” *Appl Energy*, vol. 89, no. 1, pp. 339–346, 2012, doi: 10.1016/j.apenergy.2011.07.039.

[35] W. Lu and S. A. Tassou, “Characterization and experimental investigation of phase change materials for chilled food refrigerated cabinet applications,” *Appl Energy*, vol. 112, pp. 1376–1382, 2013, doi: 10.1016/j.apenergy.2013.01.071.

[36] A. Sari, A. Karaipekli, R. Eroğlu, and A. Biçer, “Erythritol tetra myristate and erythritol tetra laurate as novel phase change materials for low temperature thermal energy storage,” *Energy Sources, Part A: Recovery, Utilization and Environmental Effects*, vol. 35, no. 14, pp. 1285–1295, Jul. 2013, doi: 10.1080/15567036.2010.516323.

[37] R. Pérez-Masiá, A. López-Rubio, M. J. Fabra, and J. M. Lagaron, “Use of electrohydrodynamic processing to develop nanostructured materials for the preservation of the cold chain,” *Innovative Food Science and Emerging Technologies*, vol. 26, pp. 415–423, Dec. 2014, doi: 10.1016/j.ifset.2014.10.010.

[38] P. Han, L. Lu, X. Qiu, Y. Tang, and J. Wang, “Preparation and characterization of macrocapsules containing microencapsulated PCMs (phase change materials) for thermal energy storage,” *Energy*, vol. 91, pp. 531–539, Nov. 2015, doi: 10.1016/j.energy.2015.08.001.

[39] J. Chen and P. Zhang, “Preparation and characterization of nano-sized phase change emulsions as thermal energy storage and transport media,” *Appl Energy*, vol. 190, pp. 868–879, 2017, doi: 10.1016/j.apenergy.2017.01.012.

[40] A. Coca-Ortegón, V. Torres-Toledo, J. Müller, and A. Coronas, “PAPER ID 10796 Assessment of a Solar Powered Refrigerator Equipped with Thermal Storage for a Dairy Application,” in *ISES Solar World Congress 2017 - IEA SHC International Conference on Solar Heating and Cooling for Buildings and Industry 2017, Proceedings*, 2017, pp. 1655–1666. doi: 10.18086/swc.2017.28.02.

[41] D. W. Lee, “Experimental Study On Performance Characteristics Of Cold Storage Heat Exchanger For Isg Vehicle” *International Journal of Automotive Technology*, vol. 18, no. 1, pp. 41–48, 2017, doi: 10.1007/s12239−017−0004−x.

[42] F. Ma, P. Zhang, and X. J. Shi, “Investigation of thermo-fluidic performance of phase change material slurry and energy transport characteristics,” *Appl Energy*, vol. 227, pp. 643–654, Oct. 2018, doi: 10.1016/j.apenergy.2017.08.146.

[43] L. R. Soenksen, D. A. Martínez-Corona, S. I. de Gante, P. S. Phabmixay, and M. J. M. Maggi, “Low-cost thermal shield for rapid diagnostic tests using phase change materials,” *Journal of Medical Devices, Transactions of the ASME*, vol. 12, no. 1, Mar. 2018, doi: 10.1115/1.4038898.

[44] L. Cong, X. She, G. Leng, G. Qiao, C. Li, and Y. Ding, “Formulation and characterisation of ternary salt based solutions as phase change materials for cold chain applications,” in *Energy Procedia*, 2019, vol. 158, pp. 5103–5108. doi: 10.1016/j.egypro.2019.01.690.

[45] Y. Li, X. Zhang, J. M. Munyalo, Z. Tian, and J. Ji, “Preparation and thermophysical properties of low temperature composite phase change material octanoic-lauric acid/expanded graphite,” *J Mol Liq*, vol. 277, pp. 577–583, Mar. 2019, doi: 10.1016/j.molliq.2018.12.111.

[46] Y. Song, N. Zhang, Y. Jing, X. Cao, Y. Yuan, and F. Haghighat, “Experimental and numerical investigation on dodecane/expanded graphite shape-stabilized phase change material for cold energy storage,” *Energy*, vol. 189, Dec. 2019, doi: 10.1016/j.energy.2019.116175.

[47] Y. Wang *et al.*, “Thermal conductivity modification of n-octanoic acid-myristic acid composite phase change material,” *J Mol Liq*, vol. 288, Aug. 2019, doi: 10.1016/j.molliq.2019.111092.

[48] V. J. Reddy, J. S. Yadav, and S. Chattopadhyay, “Phase change material loaded form-stable composites for low temperature thermal buffering application,” *Mater Chem Phys*, vol. 247, Jun. 2020, doi: 10.1016/j.matchemphys.2020.122859.

[49] T. Wu *et al.*, “Preparation of a low-temperature nanofluid phase change material: MgCl2–H2O eutectic salt solution system with multi-walled carbon nanotubes (MWCNTs),” *International Journal of Refrigeration*, vol. 113, pp. 136–144, May 2020, doi: 10.1016/j.ijrefrig.2020.02.008.

[50] N. Xie, Z. Li, X. Gao, Y. Fang, and Z. Zhang, “Preparation and performance of modified expanded graphite/eutectic salt composite phase change cold storage material,” *International*

Journal of Refrigeration, vol. 110, pp. 178–186, Feb. 2020, doi: 10.1016/j.ijrefrig.2019.10.008.

[51] S. Zhang, X. Zhang, X. Xu, and Y. Zhao, "Experimental study on the storage and release characteristics of phase change materials with different nanomaterials as addictives", doi: 10.1007/s00231-020-02882-1/Published.

[52] S. Zhang, X. Zhang, X. Xu, and Y. Zhao, "Preparation and properties of decyl–myristyl alcohol/expanded graphite low temperature composite phase change material," *Phase Transitions*, vol. 93, no. 5, pp. 491–503, May 2020, doi: 10.1080/01411594.2020.1758319.

[53] J. Zhao *et al.*, "Recyclable low-temperature phase change microcapsules for cold storage," *J Colloid Interface Sci*, vol. 564, pp. 286–295, Mar. 2020, doi: 10.1016/j.jcis.2019.12.037.

[54] M. Berdja, J. Hu, A. Hamid, and O. Sari, "Investigation on the anti-supercooling effect of sodium polyacrylate as an additive in phase change materials for the applications of latent heat thermal energy storage," *J Energy Storage*, vol. 36, Apr. 2021, doi: 10.1016/j.est.2021.102397.

[55] W. Beyne, K. Couvreur, S. Lecompte, and M. de Paepe, "A technical, financial and CO2 emission analysis of the implementation of metal foam in a thermal battery for cold chain transport," *J Energy Storage*, vol. 35, Mar. 2021, doi: 10.1016/j.est.2021.102324.

[56] J. Ji, Y. Wang, X. Lin, B. Liu, and X. Zhang, "Fabrication of highly thermal conductive and shape-stabilized phase change materials," *J Energy Storage*, vol. 44, Dec. 2021, doi: 10.1016/j.est.2021.103256.

[57] N. Lin, C. Li, D. Zhang, Y. Li, and J. Chen, "Enhanced cold storage performance of Na2SO4·10H2O/expanded graphite composite phase change materials," *Sustainable Energy Technologies and Assessments*, vol. 48, Dec. 2021, doi: 10.1016/j.seta.2021.101596.

[58] X. Qiu and L. Lu, "Microencapsulated paraffin as a phase change material with polyurea/polyurethane/poly(lauryl methacrylate) hybrid shells for thermal energy storage applications," *Journal of Renewable and Sustainable Energy*, vol. 13, no. 1, Jan. 2021, doi: 10.1063/5.0025731.

[59] C. E. Tas and H. Unal, "Thermally buffering polyethylene/halloysite/phase change material nanocomposite packaging films for cold storage of foods," *J Food Eng*, vol. 292, Mar. 2021, doi: 10.1016/j.jfoodeng.2020.110351.

[60] D. Zhan *et al.*, "Phase change material for the cold storage of perishable products: From material preparation to material evaluation," *J Mol Liq*, vol. 342, Nov. 2021, doi: 10.1016/j.molliq.2021.117455.

[61] L. Zhao *et al.*, “Preparation and thermal properties of low-temperature composite phase-change materials based on a binary eutectic mixture with expanded graphite: Effect of particle size and mass fraction,” *J Energy Storage*, vol. 40, Aug. 2021, doi: 10.1016/j.est.2021.102778.

[62] Y. Zhao, X. Zhang, and X. Xu, “Application and research progress of cold storage technology in cold chain transportation and distribution,” *Journal of Thermal Analysis and Calorimetry*, vol. 139, no. 2. Springer Netherlands, pp. 1419–1434, Jan. 01, 2020. doi: 10.1007/s10973-019-08400-8.

[63] N. Lin, C. Li, D. Zhang, Y. Li, and J. Chen, “Emerging phase change cold storage materials derived from sodium sulfate decahydrate,” *Energy*, vol. 245, p. 123294, Apr. 2022, doi: 10.1016/j.energy.2022.123294.

[64] L. Liu, X. Zhang, and X. Lin, “Experimental investigations on the thermal performance and phase change hysteresis of low-temperature paraffin/MWCNTs/SDBS nanocomposite via dynamic DSC method,” *Renew Energy*, vol. 187, pp. 572–585, Mar. 2022, doi: 10.1016/j.renene.2022.01.098.

[65] H. H. MERT, B. KEKEVİ, E. H. MERT, and M. S. MERT, “Development of composite phase change materials based on n-tetradecane and β-myrcene based foams for cold thermal energy storage applications,” *Thermochim Acta*, vol. 707, Jan. 2022, doi: 10.1016/j.tca.2021.179116.

[66] Y. Pu, J. Fang, and Y. Du, “Preparation and characterization of reusable water/ethylcellulose phase change cold storage microcapsules with high latent heat,” *Colloids Surf A Physicochem Eng Asp*, vol. 633, Jan. 2022, doi: 10.1016/j.colsurfa.2021.127833.

[67] M. Ahmed, O. Meade, and M. A. Medina, “Reducing heat transfer across the insulated walls of refrigerated truck trailers by the application of phase change materials,” *Energy Convers Manag*, vol. 51, no. 3, pp. 383–392, Mar. 2010, doi: 10.1016/j.enconman.2009.09.003.

[68] H. Tan, Y. Li, H. Tuo, M. Zhou, and B. Tian, “Experimental study on liquid/solid phase change for cold energy storage of Liquefied Natural Gas (LNG) refrigerated vehicle,” *Energy*, vol. 35, no. 5, pp. 1927–1935, 2010, doi: 10.1016/j.energy.2010.01.006.

[69] E. Oró, L. Miró, M. M. Farid, and L. F. Cabeza, “Thermal analysis of a low temperature storage unit using phase change materials without refrigeration system,” in *International Journal of Refrigeration*, Sep. 2012, vol. 35, no. 6, pp. 1709–1714. doi: 10.1016/j.ijrefrig.2012.05.004.

[70] P. Glouannec, B. Michel, G. Delamarre, and Y. Grohens, “Experimental and numerical study of heat transfer across insulation wall of a refrigerated integral panel van,” *Appl Therm Eng*, vol. 73, no. 1, pp. 196–204, Dec. 2014, doi: 10.1016/j.applthermaleng.2014.07.044.

[71] M. Liu, W. Saman, and F. Bruno, “Computer simulation with TRNSYS for a mobile refrigeration system incorporating a phase change thermal storage unit,” *Appl Energy*, vol. 132, pp. 226–235, Nov. 2014, doi: 10.1016/j.apenergy.2014.06.066.

[72] A. Tinti, A. Tarzia, A. Passaro, and R. Angiuli, “Thermographic analysis of polyurethane foams integrated with phase change materials designed for dynamic thermal insulation in refrigerated transport,” *Appl Therm Eng*, vol. 70, no. 1, pp. 201–210, Sep. 2014, doi: 10.1016/j.applthermaleng.2014.05.003.

[73] R. Sepe, E. Armentani, and A. Pozzi, “Development and stress behaviour of an innovative refrigerated container with PCM for fresh and frozen goods,” *Multidiscipline Modeling in Materials and Structures*, vol. 11, no. 2, pp. 202–215, Aug. 2015, doi: 10.1108/MMMS-05-2014-0030.

[74] B. Copertaro, P. Principi, and R. Fioretti, “Thermal performance analysis of PCM in refrigerated container envelopes in the Italian context - Numerical modeling and validation,” *Appl Therm Eng*, vol. 102, pp. 873–881, Jun. 2016, doi: 10.1016/j.applthermaleng.2016.04.050.

[75] R. Fioretti, P. Principi, and B. Copertaro, “A refrigerated container envelope with a PCM (Phase Change Material) layer: Experimental and theoretical investigation in a representative town in Central Italy,” *Energy Convers Manag*, vol. 122, pp. 131–141, Aug. 2016, doi: 10.1016/j.enconman.2016.05.071.

[76] R. Chandran, M. Hasanuzzaman, M. Arıcı, and L. Kumar, “Energy, economic and environmental impact analysis of phase change materials for cold chain transportation in Malaysia,” *J Energy Storage*, vol. 55, Nov. 2022, doi: 10.1016/j.est.2022.105481.

[77] P. Principi, R. Fioretti, and B. Copertaro, “Energy saving opportunities in the refrigerated transport sector through Phase Change Materials (PCMs) application,” in *Journal of Physics: Conference Series*, Nov. 2017, vol. 923, no. 1. doi: 10.1088/1742-6596/923/1/012043.

[78] B. Nie *et al.*, “Experimental study of charging a compact PCM energy storage device for transport application with dynamic exergy analysis,” *Energy Convers Manag*, vol. 196, pp. 536–544, Sep. 2019, doi: 10.1016/j.enconman.2019.06.032.

[79] A. Mousazade, R. Rafee, and M. S. Valipour, “Thermal performance of cold panels with phase change materials in a refrigerated truck,” *International Journal of Refrigeration*, vol. 120, pp. 119–126, Dec. 2020, doi: 10.1016/j.ijrefrig.2020.09.003.

[80] M. A. ben Taher, T. Kousksou, Y. Zeraouli, M. Ahachad, and M. Mahdaoui, “Thermal performance investigation of door opening and closing processes in a refrigerated truck equipped with different phase change materials,” *J Energy Storage*, vol. 42, Oct. 2021, doi: 10.1016/j.est.2021.103097.

[81] S. Tong *et al.*, “A phase change material (PCM) based passively cooled container for integrated road-rail cold chain transportation – An experimental study,” *Appl Therm Eng*, vol. 195, Aug. 2021, doi: 10.1016/j.applthermaleng.2021.117204.

[82] J. H. Ahn, H. Kim, Y. Jeon, and K. H. Kwon, “Performance characteristics of mobile cooling system utilizing ice thermal energy storage with direct contact discharging for a refrigerated truck,” *Appl Energy*, vol. 308, Feb. 2022, doi: 10.1016/j.apenergy.2021.118373.

[83] M. Calati, C. Zilio, G. Righetti, G. A. Longo, K. Hooman, and S. Mancin, “Latent thermal energy storage for refrigerated trucks,” *International Journal of Refrigeration*, vol. 136, pp. 124–133, Apr. 2022, doi: 10.1016/j.ijrefrig.2022.01.018.

[84] K. Zdun and T. Uhl, “Improvement of properties of an insulated wall for refrigerated trailer-numerical and experimental study,” *Energies (Basel)*, vol. 15, no. 1, Jan. 2022, doi: 10.3390/en15010051.

[85] Y. Kozak, M. Farid, and G. Ziskind, “Experimental and comprehensive theoretical study of cold storage packages containing PCM,” *Appl Therm Eng*, pp. 899–912, 2017.

[86] L. Huang and U. Piontek, “Improving performance of cold-chain insulated container with phase change material: An experimental investigation,” *Applied Sciences (Switzerland)*, vol. 7, no. 12, Dec. 2017, doi: 10.3390/app7121288.

[87] J. Du, B. Nie, Y. Zhang, Z. Du, li Wang, and Y. Ding, “Cooling performance of a thermal energy storage-based portable box for cold chain applications,” *J Energy Storage*, vol. 28, Apr. 2020, doi: 10.1016/j.est.2020.101238.

[88] B. Nie *et al.*, “Thermal performance enhancement of a phase change material (PCM) based portable box for cold chain applications,” *J Energy Storage*, vol. 40, Aug. 2021, doi: 10.1016/j.est.2021.102707.

[89] Y. Zhao, X. Zhang, X. Xu, and S. Zhang, “Development of composite phase change cold storage material and its application in vaccine cold storage equipment,” *J Energy Storage*, vol. 30, Aug. 2020, doi: 10.1016/j.est.2020.101455.

[90] A. K. Ray, S. Singh, D. Rakshit, and Udayraj, “Comparative study of cooling performance for portable cold storage box using phase change medium,” *Thermal Science and Engineering Progress*, vol. 27, p. 101146, Jan. 2022, doi: 10.1016/j.tsep.2021.101146.

[91] X. Xu, X. Zhang, and S. Liu, “Experimental study on cold storage box with nanocomposite phase change material and vacuum insulation panel,” *Int J Energy Res*, vol. 42, no. 14, pp. 4429–4438, Nov. 2018, doi: 10.1002/er.4187.

[92] X. Xiaofeng and Z. Xuelai, “Simulation and experimental investigation of a multi-temperature insulation box with phase change materials for cold storage,” *J Food Eng*, vol. 292, Mar. 2021, doi: 10.1016/j.jfoodeng.2020.110286.

[93] J. Guo, J. Liu, J. Ren, Z. Zeng, and E. Lü, “Experimental study on thermal storage characteristics of cold storage distribution box,” *J Energy Storage*, vol. 55, Nov. 2022, doi: 10.1016/j.est.2022.105475.

[94] E. Oró, A. de Gracia, and L. F. Cabeza, “Active phase change material package for thermal protection of ice cream containers,” *International Journal of Refrigeration*, vol. 36, no. 1, pp. 102–109, Jan. 2013, doi: 10.1016/j.ijrefrig.2012.09.011.

[95] D. Leducq, F. T. Ndoye, and G. Alvarez, “Phase change material for the thermal protection of ice cream during storage and transportation,” *International Journal of Refrigeration*, vol. 52, pp. 133–139, Apr. 2015, doi: 10.1016/j.ijrefrig.2014.08.012.

[96] G. Liu *et al.*, “Improving system performance of the refrigeration unit using phase change material (PCM) for transport refrigerated vehicles: An experimental investigation in South China,” *J Energy Storage*, vol. 51, Jul. 2022, doi: 10.1016/j.est.2022.104435.

[97] S. Burgess, X. Wang, A. Rahbari, and M. Hangi, “Optimisation of a portable phase-change material (PCM) storage system for emerging cold-chain delivery applications,” *J Energy Storage*, vol. 52, Aug. 2022, doi: 10.1016/j.est.2022.104855.

[98] K. Liu *et al.*, “Highly-efficient cold energy storage enabled by brine phase change material gels towards smart cold chain logistics,” *J Energy Storage*, vol. 52, Aug. 2022, doi: 10.1016/j.est.2022.104828.

[99] Z. Yin, J. Zheng, H. Kim, Y. Seo, and P. Linga, “Hydrates for cold energy storage and transport: A review,” *Advances in Applied Energy*, vol. 2, p. 100022, May 2021, doi: 10.1016/j.adapen.2021.100022.

[100] B. Nie, A. Palacios, B. Zou, J. Liu, T. Zhang, and Y. Li, “Review on phase change materials for cold thermal energy storage applications,” *Renewable and Sustainable Energy Reviews*, vol. 134. Elsevier Ltd, Dec. 01, 2020. doi: 10.1016/j.rser.2020.110340.

[101] Y. Cao *et al.*, “Designing a system for battery thermal management: Cooling LIBs by nano-encapsulated phase change material,” *Case Studies in Thermal Engineering*, vol. 33, p. 101943, May 2022, doi: 10.1016/j.csite.2022.101943.

[102] X. Xiao, P. Zhang, and M. Li, “Preparation and thermal characterization of paraffin/metal foam composite phase change material,” *Appl Energy*, vol. 112, pp. 1357–1366, 2013, doi: 10.1016/j.apenergy.2013.04.050.

[103] S. Yu, X. Wang, and D. Wu, “Microencapsulation of n-octadecane phase change material with calcium carbonate shell for enhancement of thermal conductivity and serving durability: Synthesis, microstructure, and performance evaluation,” *Appl Energy*, vol. 114, pp. 632–643, 2014, doi: 10.1016/j.apenergy.2013.10.029.

[104] G. Liu *et al.*, “Design and assessments on a hybrid pin fin-metal foam structure towards enhancing melting heat transfer: An experimental study,” *International Journal of Thermal Sciences*, vol. 182, Dec. 2022, doi: 10.1016/j.ijthermalsci.2022.107809.

[105] F. Bruno, M. Belusko, M. Liu, and N. H. S. Tay, “Using solid-liquid phase change materials (PCMs) in thermal energy storage systems,” in *Advances in Thermal Energy Storage Systems: Methods and Applications*, Elsevier Inc., 2015, pp. 201–246. doi: 10.1533/9781782420965.2.201.

[106] X. Zhang, J. Niu, and J. Y. Wu, “Development and characterization of novel and stable silicon nanoparticles-embedded PCM-in-water emulsions for thermal energy storage,” *Appl Energy*, vol. 238, pp. 1407–1416, Mar. 2019, doi: 10.1016/j.apenergy.2019.01.159.

[107] F. Wang, C. Zhang, J. Liu, X. Fang, and Z. Zhang, “Highly stable graphite nanoparticle-dispersed phase change emulsions with little supercooling and high thermal conductivity for cold energy storage,” *Appl Energy*, vol. 188, pp. 97–106, 2017, doi: 10.1016/j.apenergy.2016.11.122.

[108] E. Oró, A. de Gracia, A. Castell, M. M. Farid, and L. F. Cabeza, “Review on phase change materials (PCMs) for cold thermal energy storage applications,” *Applied Energy*, vol. 99. Elsevier Ltd, pp. 513–533, 2012. doi: 10.1016/j.apenergy.2012.03.058.

[109] H. Mehling and C. Luisa F, *Heat and Cold Storage with PCM*. 2008.

[110] M. M. Farid, A. M. Khudhair, S. A. K. Razack, and S. Al-Hallaj, “A review on phase change energy storage: Materials and applications,” *Energy Conversion and Management*, vol. 45, no. 9–10. pp. 1597–1615, Jun. 2004. doi: 10.1016/j.enconman.2003.09.015.

[111] L. F. Cabeza, G. Svensson, S. Hiebler, and H. Mehling, “Thermal performance of sodium acetate trihydrate thickened with different materials as phase change energy storage material,” *Appl Therm Eng*, vol. 23, no. 13, pp. 1697–1704, Aug. 2003, doi: 10.1016/S1359-4311(03)00107-8.

[112] Z. Wang *et al.*, “Preparation and properties of caprylic-nonanoic acid mixture/expanded graphite composite as phase change material for thermal energy storage,” *Int J Energy Res*, vol. 41, no. 15, pp. 2555–2564, Dec. 2017, doi: 10.1002/er.3830.

[113] E. Oró, L. Miró, C. Barreneche, I. Martorell, M. M. Farid, and L. F. Cabeza, “Corrosion of metal and polymer containers for use in PCM cold storage,” *Appl Energy*, vol. 109, pp. 449–453, 2013, doi: 10.1016/j.apenergy.2012.10.049.

[114] G. Ferrer, A. Solé, C. Barreneche, I. Martorell, and L. F. Cabeza, “Corrosion of metal containers for use in PCM energy storage,” *Renew Energy*, vol. 76, pp. 465–469, Apr. 2015, doi: 10.1016/j.renene.2014.11.036.

[115] A. J. Farrell, B. Norton, and D. M. Kennedy, “Corrosive effects of salt hydrate phase change materials used with aluminium and copper,” *J Mater Process Technol*, vol. 175, no. 1–3, pp. 198–205, Jun. 2006, doi: 10.1016/j.jmatprotec.2005.04.058.

[116] S. S. Chandel and T. Agarwal, “Review of current state of research on energy storage, toxicity, health hazards and commercialization of phase changing materials,” *Renewable and Sustainable Energy Reviews*, vol. 67. Elsevier Ltd, pp. 581–596, Jan. 01, 2017. doi: 10.1016/j.rser.2016.09.070.

[117] “https://www.crodaenergytechnologies.com/en-gb/product-finder/product/1382-CrodaTherm_1_9.5.” https://www.crodaenergytechnologies.com/en-gb/product-finder/product/1382-CrodaTherm_1_9.5 (accessed Jun. 03, 2022).

[118] “https://www.iso.org/standard/37456.html.” https://www.iso.org/standard/37456.html (accessed Jun. 03, 2022).

[119] B. R. David, S. Spencer, J. Miller, S. Almahmoud, and H. Jouhara, “Comparative environmental life cycle assessment of conventional energy storage system and innovative thermal energy storage system,” *International Journal of Thermofluids*, vol. 12, Nov. 2021, doi: 10.1016/j.ijft.2021.100116.

[120] P. Duggal, R. K. Tomar, and N. D. Kaushika, “A Review on life cycle assessment of phase change materials in buildings,” in *Proceedings of 2021 2nd International Conference on Intelligent Engineering and Management, ICIEM 2021*, Apr. 2021, pp. 18–22. doi: 10.1109/ICIEM51511.2021.9445375.

[121] E. Kyriaki, C. Konstantinidou, E. Giama, and A. M. Papadopoulos, “Life cycle analysis (LCA) and life cycle cost analysis (LCCA) of phase change materials (PCM) for thermal applications: A review,” in *International Journal of Energy Research*, Jul. 2018, vol. 42, no. 9, pp. 3068–3077. doi: 10.1002/er.3945.

[122] B. Behdani, Y. Fan, and J. M. Bloemhof, “Cool chain and temperature-controlled transport: An overview of concepts, challenges, and technologies,” in *Sustainable Food Supply Chains: Planning, Design, and Control through Interdisciplinary Methodologies*, Elsevier, 2019, pp. 167–183. doi: 10.1016/B978-0-12-813411-5.00012-0.

[123] American Society of Heating Refrigerating and Air-Conditioning Engineers., *2018 ASHRAE handbook : refrigeration*.

[124] S. Estrada-Flores and A. Eddy, “Thermal performance indicators for refrigerated road vehicles,” *International Journal of Refrigeration*, vol. 29, no. 6. pp. 889–898, Sep. 2006. doi: 10.1016/j.ijrefrig.2006.01.012.

[125] D. Y. Lee, V. M. Thomas, and M. A. Brown, “Electric urban delivery trucks: Energy use, greenhouse gas emissions, and cost-effectiveness,” *Environ Sci Technol*, vol. 47, no. 14, pp. 8022–8030, Jul. 2013, doi: 10.1021/es400179w.

[126] T. B. Radebe, Z. Huan, and J. Baloyi, “Simulation of eutectic plates in medium refrigerated transport,” *Journal of Engineering, Design and Technology*, vol. 19, no. 1, pp. 62–80, Mar. 2021, doi: 10.1108/JEDT-02-2020-0065.

[127] J. Jeong, A. E. Benchikh Le Hocine, S. Croquer, S. Poncet, B. Michel, and J. Bonjour, “Numerical analysis of the thermoaeraulic behavior of air during the opening of the door of a refrigerated truck trailer equipped with cold plates,” *Appl Therm Eng*, vol. 206, p. 118057, Apr. 2022, doi: 10.1016/j.applthermaleng.2022.118057.

[128] “https://fdocumenti.com/document/uni-10349-dati-climatici-56264bcc9c91f.html?page=1.” https://fdocumenti.com/document/uni-10349-dati-climatici-56264bcc9c91f.html?page=1 (accessed Jun. 03, 2022).

[129] M. Calati, L. Doretti, C. Zilio, and S. Mancin, “3D numerical simulation of a novel ventilated roof: thermal performance analysis and fluid flow behavior,” *Sci Technol Built Environ*, vol. 27, no. 6, pp. 819–831, 2021, doi: 10.1080/23744731.2021.1917931.

[130] G. Villi, W. Pasut, and M. de Carli, “CFD modelling and thermal performance analysis of a wooden ventilated roof structure,” *Build Simul*, vol. 2, no. 3, pp. 215–228, Sep. 2009, doi: 10.1007/s12273-009-9414-7.

[131] Y. A. Cengel and A. J. Ghajar, *Heat and Mass Transfer: Fundamentals and Applications*. 2015.

[132] F. P. Incropera, D. P. Dewitt, T. L. Bergman, and A. S. Lavine, *Fundamentals of Heat and Mass Transfer*. 2007.

[133] J. A. Duffie and W. A. Beckman, *Solar Engineering of Thermal Processes*. Hoboken, New Jersey, 2013.

[134] V. R. Voller and C. Prakash, “A fixed grid numerical modelling methodology for convection-diffusion mushy region phase-change problems,” *Int J Heat Mass Transf*, vol. 30, no. 8, pp. 1709–1719, 1987.

[135] C. Zhao, M. Opolot, M. Liu, F. Bruno, S. Mancin, and K. Hooman, “Numerical study of melting performance enhancement for PCM in an annular enclosure with internal-external fins and metal foams,” *Int J Heat Mass Transf*, vol. 150, Apr. 2020, doi: 10.1016/j.ijheatmasstransfer.2020.119348.

[136] “Rubitherm, DE.” https://www.rubitherm.eu (accessed Sep. 27, 2022).

[137] “Ansys Fluent Manual.” https://www.afs.enea.it/project/neptunius/docs/fluent/html/ug/main_pre.htm

[138] C. Zhao *et al.*, “Simulations of melting performance enhancement for a PCM embedded in metal periodic structures,” *Int J Heat Mass Transf*, vol. 168, Apr. 2021, doi: 10.1016/j.ijheatmasstransfer.2020.120853.

[139] “Energain.” http://buildinginnovations.dupont.com/en_GB_energain_contact

[140] UNEP, “Montreal Protocol on Substances that Deplete the Ozone Layer.” 1987.

[141] “European F-gas Regulation (Regulation (EU) No 517/2014 of the European Parliament).” 2014.

[142] A. S. Dalkilic and S. Wongwises, “A performance comparison of vapour-compression refrigeration system using various alternative refrigerants,” *International Communications in Heat and Mass Transfer*, vol. 37, no. 9, pp. 1340–1349, Nov. 2010, doi: 10.1016/j.icheatmasstransfer.2010.07.006.

[143] K. Harby, “Hydrocarbons and their mixtures as alternatives to environmental unfriendly halogenated refrigerants: An updated overview,” *Renewable and Sustainable Energy Reviews*, vol. 73. Elsevier Ltd, pp. 1247–1264, 2017. doi: 10.1016/j.rser.2017.02.039.

[144] L. Jia, W. Jin, and Y. Zhang, “Experimental study on R32 leakage and diffusion characteristic of wall-mounted air conditioners under different operating conditions,” *Appl Energy*, vol. 185, pp. 2127–2133, Jan. 2017, doi: 10.1016/j.apenergy.2016.01.041.

[145] H. Okamoto, T. Hattori, C. Dang, and E. Hihara, “Purdue e-Pubs Leakage of Mildly Flammable Refrigerants into a Room Simulation of leakage of mildly flammable refrigerants.” [Online]. Available: http://docs.lib.purdue.edu/iracc/1496

[146] H. Maojuan, L. Jinbo, L. Zhe, and L. Tingxun, “Experimental and numerical simulation analysis of R-290 air conditioner leak,” *International Journal of Refrigeration*, vol. 90, pp. 163–173, Jun. 2018, doi: 10.1016/j.ijrefrig.2018.03.010.

[147] T. Li, “Indoor leakage test for safety of R-290 split type room air conditioner,” *International Journal of Refrigeration*, vol. 40, pp. 380–389, Apr. 2014, doi: 10.1016/j.ijrefrig.2013.11.023.

[148] W. Zhang *et al.*, “Research on the flammability hazards of an air conditioner using refrigerant R-290,” in *International Journal of Refrigeration*, Aug. 2013, vol. 36, no. 5, pp. 1483–1494. doi: 10.1016/j.ijrefrig.2013.03.015.

[149] K. L. Cashdollar, I. A. Zlochower, G. M. Green, R. A. Thomas, and M. Hertzberg, “Flammability of methane, propane, and hydrogen gases,” 2000. [Online]. Available: www.elsevier.com/locate/jlp